2011

# NUMERICAL MODELLING OF HEAT TRANSFER FROM AN ISOTHERMAL CYLINDER BURIED IN HETEROGENEOUS POROUS MEDIA

Yara M. Elserafy

# NUMERICAL MODELLING OF HEAT TRANSFER FROM AN ISOTHERMAL CYLINDER BURIED IN HETEROGENEOUS POROUS MEDIA

(Spine title: Heat Transfer in Porous Media)

(Thesis format: Monograph)

by

Yara M. Elserafy

Graduate Program in Engineering Science
Department of Civil and Environmental Engineering

A thesis submitted in partial fulfillment
of the requirements for the degree of
Master of Engineering Science

The School of Graduate and Postdoctoral Studies
The University of Western Ontario
London, Ontario, Canada

# ABSTRACT

Heat transfer from an isothermal pipe buried in porous media and superimposed by a fluid layer has been investigated numerically using the commercial software FLUENT (6.3.26). Due to natural and induced heterogeneity, soils have variations in their hydraulic and volumetric properties; these must be considered for accurate design purposes. Two types of porous media have been investigated, sand and clay. For sand media, the study investigates the effects of different flow and geometric conditions on the heat transfer process. The flow parameters are represented by the Rayleigh number, the permeability ratio of the backfill to the seabed and the permeability anisotropy of the backfill, while the geometric parameters are represented by the trench size and shape and the position of the pipe in the trench. For clay media, two states of the backfill were investigated; these are slurried and lumpy clays. The study also shows the impact of the different trenching conditions on insulation of the pipe as opposed to expensive coating. Lowest heat losses were achieved for a sand backfill of a permeability 100 times the permeability of the seabed and permeability anisotropy of ($K_{th}/K_{tv}$=50). Clay slurry backfill gave the lowest heat transfer results as the main mode of heat transfer in this case was conduction. In contrast, the high permeability and intergranular porosity of clay lumps, allowed for pure convection heat transfer. It was also noticed that clay lumps of sizes 5 and 10 cm allowed for more heat losses than for a pipe with no backfill at all.

**Keywords:** FLUENT (6.3.26), porous, permeability, backfill, offshore, pipe, heat transfer

# ACKNOWLEDGMENT

I would like to thank my advisor Dr. Tim Newson, for having given me this opportunity to work with him. His guidance, support and patience were essential to the development of this thesis.

I want to express my deep appreciation to my advisor, Dr. Anthony Straatman, for his valuable guidance, discussions and comments.

Special thanks are given to my parents, brothers and parents-in-law who I owe a lot for accepting our small family's absence during our study period here in Canada; they have been a constant source of patience and encouragement.

I would also like to thank my husband, Islam, whose care and support have made it possible for me to accomplish this work.

Last but not least, I would like to thank my son, Ahmed, for making my life happier and relieving my research stress times with his innocent smiles and laughs.

# CONTENTS

# LIST OF TABLES

# LIST OF FIGURES

# NOMENCLATURE

$A$ Cross section area ($m^2$);

$C_H$ Hazen empirical coefficient;

$C_{KC}$ Kozeny-Carman coefficient;

$c_p$ The specific heat capacity (J/kg.K);

$D$ Diameter of the pipe (m);

$d$ Particle diameter (m);

$e$ Void ratio;

$f$ Darcy friction factor;

$g$ Gravitational acceleration ($m/s^2$);

$h$ Convective heat transfer coefficient ($W/m^2.K$);

$K$ Intrinsic permeability ($m^2$);

$k$ Hydraulic permeability (m/s);

$L$ Length of the pipe. (m);

$\dot{m}$ Mass flow rate. (kg/s.);

$P_p$ Pumping power (W);

$p$ Kinematic pressure (Pa);

$\Delta p$ Pressure loss (Pa);

Q Volumetric flow rate ($m^3/s$).

$q$ Rate of heat transfer from the coating surface to the surrounding (W);

$q''$ Heat flux. ($W/m^2$);

$R$ Resistance to heat transfer (K/W);

$r_K$ Permeability anisotropy ratio;

r radius of the pipe (m);

$S$ Specific surface ($m^2/kg$) ;

$T$ Temperature (K);

$u$ Velocity in the x-direction (m/s);

$v$ Velocity (m/s);

$x$ Tortuosity ratio;

**Non-dimensional variables:**

$Nu$ Nusselt number;

$Pr$ Prandtl number;

$Ra$ Rayleigh number;

**Greek Letters:**

$\alpha$ Thermal diffusivity (J/m$^3$.K);

$\beta$ Coefficient of thermal expansion (1/K);

$\varphi$ Porosity;

$\mu$ Dynamic viscosity (kg/m.s);

$\rho$ Density (kg/m$^3$);

$\lambda$ Thermal conductivity (W/m.K);

$\sigma$ Standard deviation;

**Sub/superscripts:**

$c$ coating;

$eff.$ effective;

$f$ fluid;

$h$ horizontal;

$i$ inner;

$o$ outer;

$s$ solid;

s seabed;

t trench;

$v$ vertical;

$\infty$ free stream;

**Other:**

$\langle\ \rangle$ volume average.

# CHAPTER 1

# INTRODUCTION

## 1.1 General

A number of engineering applications involve buried heated cylinders in porous media, such as groundwater systems used for industrial and agricultural purposes, buried electrical cables, pipelines for oil and gas transport and storage of radioactive waste materials. Although extensive study of heat and mass transfer around these structures buried in porous media has taken place through experiments and numerical simulations in various engineering disciplines much of this work addressed partially saturated soils. In contrast offshore applications involve the presence of a superimposed fluid layer over a saturated porous media. In addition, due to natural and induced heterogeneity, soils can have spatially varying volumetric and hydraulic properties. To date permeability anisotropy and spatial variations have received very little attention in the literature leading to potential errors in design. Buried pipes are usually trenched in the soil, i.e. the soil is excavated, the pipe is laid in the trench and then the pipe is backfilled with the original soil or selected backfill. These trenches can be of different sizes and shapes that need to be considered in design.

Insulation of offshore hydrocarbon carrying pipelines is essential to prevent their blockage that results from waxing and hydration of the flowing fluid as its temperature falls due to heat losses from the pipe. In addition to burying the pipelines in porous

media to help maintain proper temperature of the flowing fluid and minimize pipeline heat losses, different coating techniques are also employed for these purposes, Quenelle and Gunaltun (1987). Several insulation techniques have been developed to overcome this thermal issue by the addition of low conductivity coatings on the outer pipe surface, such as synthetic materials, and also using the pipe-in-pipe technique which involves two pipes concentrically positioned and an insulating material filling the gap between them. In the current study, it is assumed that a single thermal coating has been used to reduce the thermal losses. Figure (1.1) shows the thermal circuit for the problem studied; the focus of the present study is not on the entire circuit but it is only concerned with the last element of the circuit ($R_4$) representing heat transfer from the coating surface to the surrounding porous medium. The rate of heat transfer for this case is, Incropera & Dewitt (2002),

$$q = \frac{(T_c - T_f)}{R_4} \tag{1.1}$$

Where, $q$ is the rate of heat transfer from the coating surface to the surrounding (W);

$T_f$ is the temperature of the fluid in the porous medium (K);

$T_c$ is the temperature of the outer coating of the pipe (K);

$R_4$ is the resistance due to convection in the porous backfill (K/W).

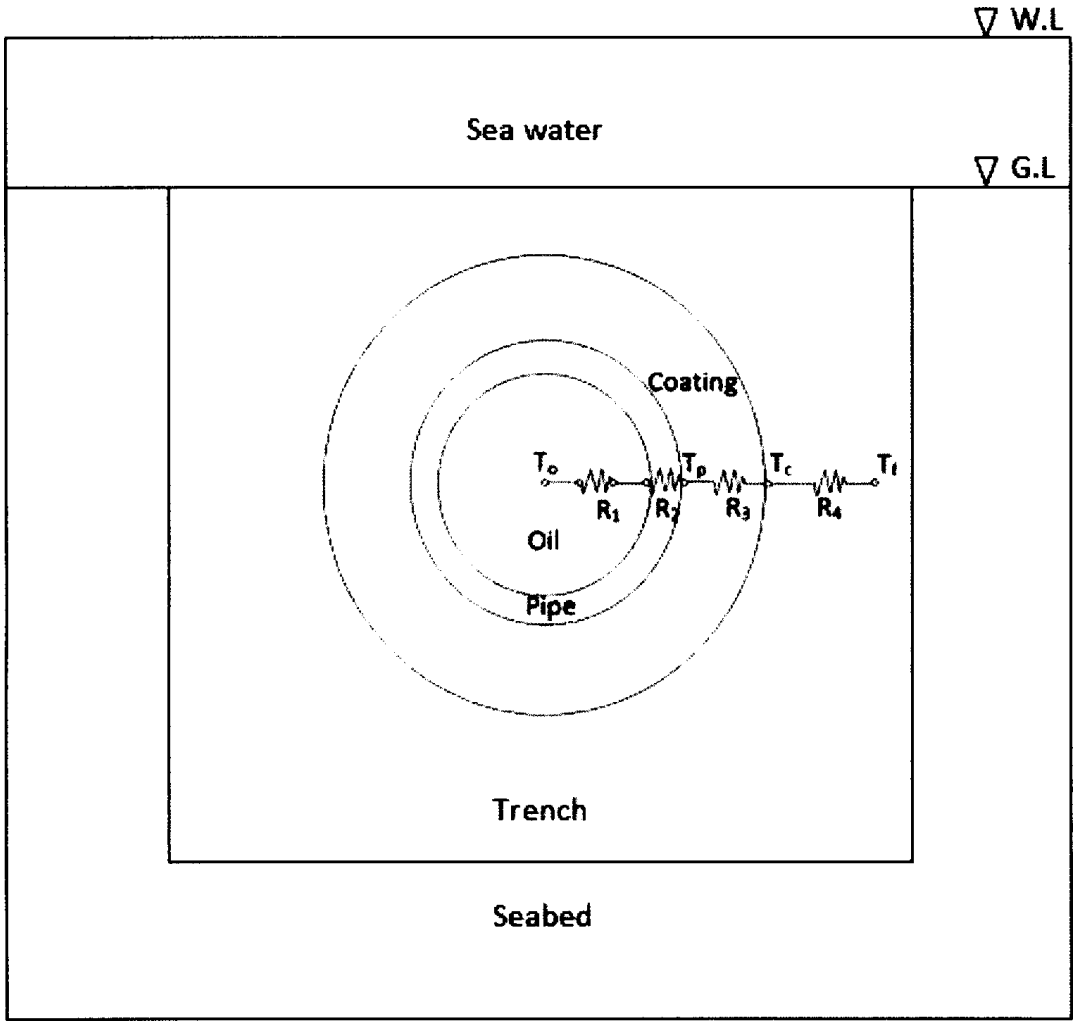


Figure 1.1 Thermal circuit for the present study.

Computational modelling of heat transfer has become increasingly popular as it can provide detailed information about the process to support and validate experimental modelling. The present study is concerned with heat and mass transfer from an offshore heated pipeline buried in porous media. This study is intended to examine the interaction between the porous media and the overlaying fluid layer, the effect of permeability anisotropy of the soil on heat transfer and the effect of varying sizes and shapes of the trench and position of the pipe in the trench on the heat transfer process, to find the optimum conditions to help in minimizing heat losses from these structures.

This investigation has been performed numerically using the commercial software FLUENT (6.3.26).

## 1.2 Background

Offshore pipelines are trenched in the seabed for various purposes, these include protection from upheaval buckling, protection from anchors and fishing activities and the reason this study is concerned with, which is providing thermal insulation. Knowledge of the different properties of the surrounding porous media is obviously of great importance to assess the thermal behaviour of the complete system.

*A porous medium* can be defined as a material consisting of a solid matrix possessing interconnected voids. In addition to offshore pipelines, porous materials are involved in many other engineering applications such as, groundwater systems used for agricultural and industrial purposes, buried electrical cables and storage of radioactive waste materials.

Since fluid flow and heat transfer in porous media are involved in many engineering disciplines, a number of textbooks and handbooks have been published for discussing this subject. Extensive research in this subject was performed by Muskat (1949), Bear (1972), Scheidgger (1974), Kaviany (1995), Nield and Bejan (1999) and Vafai (2005). In the environmental and civil engineering sector, a knowledge of soil structure and its properties is of great importance when studying groundwater flow and contaminant transport. In the chemical engineering sector, porous media are involved in fuel cells, filtering and drying processes. In the mechanical and offshore engineering sector,

porous media are used in applications such as the transportation of crude oil through buried pipelines. These pipes are buried to reduce heat losses to help prevent waxing of the flowing fluid and blockage of the pipeline. Also in the disposal of nuclear waste materials, waste canisters are buried and the process media acts as a barrier to prevent radiation leakage. For buried electrical cables, the porous media absorb extra heat dissipated by these cables to avoid their overheating. The involvement of porous media in many of these applied science and engineering problems can be beneficial or detrimental to the project involved. Engineers must account for the potentially wide range of properties that porous media can have and these can be divided into physical, mechanical and thermal properties, and will be described in the next sections.

### 1.2.1 Fluid Flow through Porous Media

Fluid flow through porous bodies depends on two important properties of the media; these are the porosity and the permeability of the medium. The following is an overview for these two physical properties.

*Porosity "φ"* is a mechanical property of porous media that is defined as the fraction of the total volume of the medium that is occupied by void space.

$$\varphi = \frac{Volume\ of\ voids}{Total\ volume} \tag{1.2}$$

Intrinsic Permeability "K" is a mechanical property of porous media which measures the ease with which fluid is transmitted through that medium. The intrinsic permeability ($m^2$) is independent of the nature of the fluid i.e. independent of the density and

viscosity of the fluid; it is only dependent on the geometry of the medium. However, intrinsic permeability can be calculated based on the properties of the fluid occupying the porous medium through the equation obtained by Carman (1956):

$$K = \frac{k\mu}{\rho g} \tag{1.3}$$

Where, $K$ is the intrinsic permeability ($m^2$);

$k$ is the hydraulic permeability (m/s);

$\mu$ is the dynamic viscosity (kg/m.s);

$\rho$ is the density of the fluid. ($kg/m^3$);

$g$ is the gravitational acceleration ($m/s^2$).

Permeability and porosity of a porous medium are related by the Kozeny-Carman equation, Bear (1972):

$$K = \frac{1}{C_{KC}} \frac{d^2 \varphi^3}{(1-\varphi)^2} \tag{1.4}$$

Where, $K$ is the intrinsic permeability ($m^2$);

$d$ is the mean particle diameter (m);

$\varphi$ is the porosity;

$C_{KC}$ is the Kozeny-Carman constant.

Due to natural and induced heterogeneity, permeability is considered to be an anisotropic property. *Permeability anisotropy* "$r_k$" is the ratio of permeability in the horizontal direction to the permeability in the vertical direction.

$$r_k = \frac{K_h}{K_v} \tag{1.5}$$

Accounting for the permeability anisotropy is important to avoid inefficiencies in design. The literature has reported permeability anisotropy ratios in the range of (0.75 to 4.1) for granular soils and a range of (0.7 to 4.6) for cohesive soils. Permeability anisotropy is caused mainly by consolidation or structure of the soil. *Consolidation* is the time dependent process through which the volume in the porous material decreases by the dissipation of pore water from the voids, in response to the application of a compressive load. It is known in soil mechanics that the particles in the soil media are relatively incompressible and thus the majority of consolidation takes place due to the rearrangement of the soil particles, Terzaghi and Peck (1967).

### 1.2.2 Heat Transfer through Porous Media

Knowledge of the thermal properties of porous media is essential for the effective design of the structures to be buried within these porous media. A comprehensive review of the thermal properties in porous media was presented by Farouki (1981). Three principal properties are typically used to describe heat transfer in a material; these are thermal conductivity, specific heat capacity and thermal diffusivity. A brief description of each of the specific heat capacity and the thermal diffusivity will be presented followed by a detailed explanation of the thermal conductivity as it is

considered to be the most important thermal property of a porous medium and it is the one researched extensively.

*Specific heat capacity "$c_p$"* is an index of a material's ability to store heat. It is the heat capacity per unit mass of that material at constant pressure.

*Thermal diffusivity "$\alpha$"* corresponds to the rate of temperature change for a particular material when a temperature gradient exists. Materials of a small thermal diffusivity will respond slowly to changes in the temperature and take longer time to reach equilibrium condition, while materials of a large thermal diffusivity will respond quickly to changes in the thermal conditions and possess an equilibrium state quickly.

*Thermal conductivity "$\lambda$"* indicates the ability of a material to conduct heat. It is an index of the rate of heat flow. Thermal conductivity values for different materials are provided by different literature sources, Eckert and Drake (1972) and Incropera and DeWitt (1985).

Due to the fact that a porous medium consists of a fluid phase as well as a solid phase, each with its own thermal conductivity, an "effective" thermal conductivity comprising a fraction of each phase has to be considered to efficiently model porous media. The effective thermal conductivity of a porous medium depends on the geometry of the medium. The maximum value of the effective thermal conductivity occurs when the solid and fluid phases are in layers parallel to the heat flow. For this case the effective thermal conductivity may be expressed as:

$$\lambda_{eff} = \varphi\,\lambda_f + (1-\varphi)\lambda_s \tag{1.6}$$

The minimum value of the effective thermal conductivity occurs when the solid and fluid layers are in layers normal to the direction of heat flow. For this case the effective thermal conductivity may be expressed as:

$$\lambda_{eff} = \frac{\lambda_s \lambda_f}{\varphi\lambda_s + (1-\varphi)\lambda_f} \tag{1.7}$$

The weighted geometric mean of the solid and fluid phases assumes random distribution of these phases.

$$\lambda_{eff} = \lambda_f^{\varphi} . \lambda_s^{1-\varphi} \tag{1.8}$$

Where, $\lambda_f$ is the fluid's thermal conductivity (W/m.K);

$\lambda_s$ is the solid's thermal conductivity (W/m.K);

$\varphi$ is the porosity.

There are three different modes in which heat is able to transfer from one point to another in a porous medium, these are,

(a) *Conduction,* it is the process by which heat energy transfers from one point to another in the material body without the movement of the material itself, see Figure (1.2). In a porous medium, heat conduction occurs in all its constituents i.e. in both the fluid and the solid phases. For a fully saturated soil, since water has a very low thermal conductivity, this means that as the soil saturates more, heat transferred by conduction will decrease.

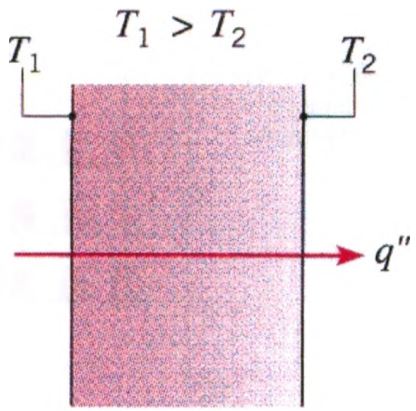


Figure 1.2 Conduction through a solid or a stationary fluid (Incropera & DeWitt 2002).

*(b) Convection,* it is the process by which energy is carried from one place to another by the movement of the heated matter. This mass transfer occurs due to either temperature or pressure difference. There are two types of convection these are forced and natural (free) convection. Forced convection is heat transfer that produces mass transfer of fluid due to pressure difference, an example of forced convection is groundwater flow. On the other hand free convection is heat transfer that produces mass transfer of a fluid due to density differences resulting from a difference in temperatures. See Figure (1.3).

Two primary dimensionless numbers govern the heat flow physics, these are the Rayleigh number (Ra) and the Nusselt number (Nu).

- Rayleigh number is the dimensionless buoyancy driven flow coefficient. It shows the presence and strength of convection within a fluid; when the Rayleigh number is below the critical value for that fluid then conduction is the primary

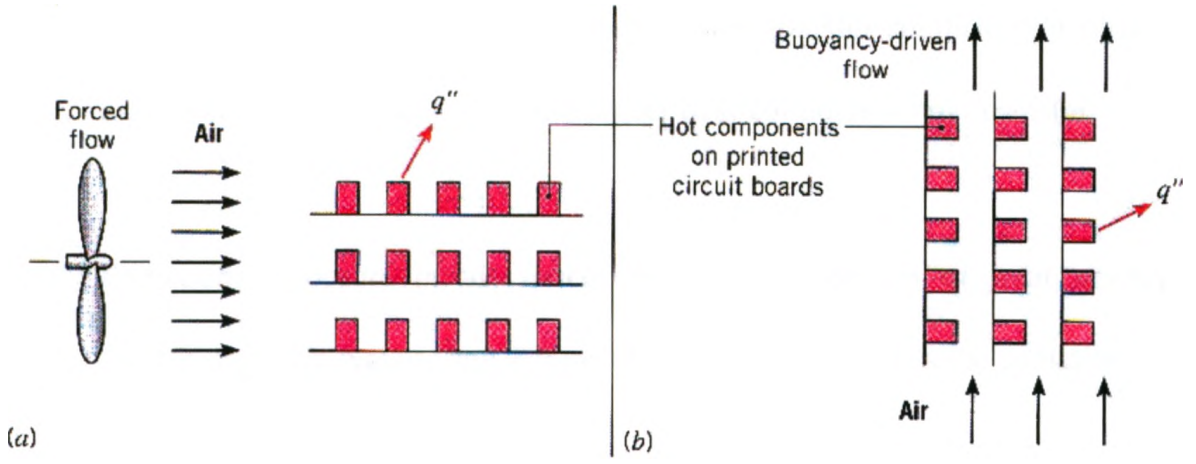


Figure 1.3 (a) Forced convection (b) Natural convection (Incropera & DeWitt 2002).

mode of heat transfer and when it exceeds the critical value, convection becomes the primary mode of heat transfer. Rayleigh number is the ratio of buoyancy forces to viscous forces and is defined as,

$$Ra = \frac{g\,\beta\,D^3\,\Delta T\,\rho^2 c_p}{\lambda\,\mu} \tag{1.9}$$

Where, $g$ is the gravitational acceleration (m/s$^2$);

$\beta$ is the coefficient of thermal expansion (1/K);

D is the diameter of the pipe (m);

$\Delta T$ is the difference in temperature between the pipe's surface and the fluid (K);

$\rho, c_p, \lambda, \mu$ are fluid properties.

- Nusselt number (Nu) is the dimensionless heat transfer coefficient; it shows the enhancement of convection heat transfer over conduction heat transfer.

(c) *Radiation,* it occurs in air spaces by the propagation of heat energy as electromagnetic waves, see Figure (1.4). In the case of soils, radiation has a negligible effect.

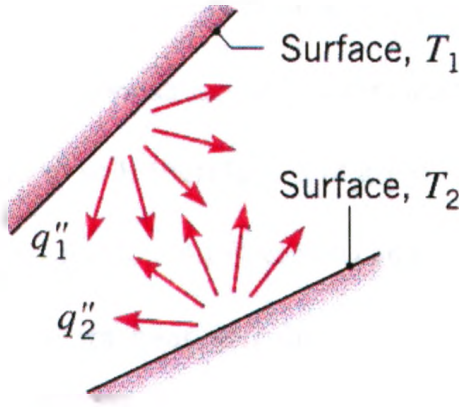


Figure 1.4 Net radiation heat exchange between two surfaces (Incropera & DeWitt 2002).

Where, $q''$ is the heat flux. ($W/m^2$);

$T_1$ is the temperature of surface "1";

$T_2$ is the temperature of surface "2".

## 1.3 Objectives of the Study

Porous media can either be used for suppressing heat transfer or enhancing it. For example, crude oil carrying pipelines are buried in low permeability porous media for reducing heat losses from them to keep the oil temperature above a given value to minimize thickening of the oil and potential blockage in the pipes. The offshore oil and gas industry spend a considerable amount of money on pipeline coatings to ensure thermal stability of the oil and this is currently done without much consideration of the backfill soil in offshore trenches. Optimisation of this pipeline system, allowing for the effects of the thermal insulation of soils therefore is of great interest to the industry. In other engineering applications such as buried electrical cables, high permeability porous media are used for dissipating extra heat generated by these cables to avoid their overheating. The data provided in this study therefore can be used for either suppressing heat transfer or enhancing it, but the data presented herein are used to show how to suppress heat transfer from a buried pipeline in porous media. The aim of the current study is to understand the effect of trench geometric and flow conditions on minimizing heat losses from offshore pipelines. This is achieved numerically using the software FLUENT (6.3.26) by examining the effect of a trench backfill with different permeability compared to the permeability of the seabed, different permeability anisotropy conditions of the trench, different trench size, shape and varying the position of the pipe in the trench on the heat transfer process. It is important to note that the current parametric study does not address exact heat transfer coefficient values, but it shows different heat transfer trends under variable flow and geometric conditions.

## 1.4 Thesis Outline

The chapters of this thesis cover the following aspects:

*Chapter 2* provides a review of published literature that is relevant to the current work. The areas following are presented in this chapter: (a) A background on marine sediments (b) empirical formulae for measuring permeability of a sediment (c) permeability anisotropy (d) thermal conductivity of seabed sediments (e) offshore pipelines and methods of their trenching and (f) heat transfer from isothermal pipes.

*Chapter 3* defines the problem in the study, describes the governing equations and the assumptions adopted. It also outlines the methodology of analysis, which includes creating the grid and meshing using GAMBIT (2.4.6), and heat and mass transfer analysis using FLUENT (6.3.26). Far-Field position and mesh independence tests, and further verification of the modelling approach were also investigated in this chapter.

*Chapter 4* describes and justifies the range of parameters used in the parametric study. It also shows the results of heat and mass transfer from an isothermal pipe buried in porous media overlaid by a fluid layer under different conditions, and discusses these results. Modelling of fluid flow in the pipe under different backfill conditions is also examined to determine the effectiveness of backfilling a pipe over expensive coatings in insulating the pipes.

*Chapter 5* presents a summary of the present study and recommendations for future work.

# CHAPTER 2

# LITERATURE REVIEW

## 2.1 Introduction

This chapter gives a brief background on the formation, classification and distribution of marine sediments. It also reviews empirical formulae reported in the literature for predicting permeability of porous media and shows how these equations were validated and assessed in the literature by comparing the predicted values with measured values. Due to the fact that soils are heterogeneous in nature or due to external effects, ranges of permeability anisotropy for different types of soils measured in the literature have been reviewed, as well as the methods used for measuring this anisotropy. Also factors affecting thermal conductivity of soils and ranges reported in the literature are presented here.

Since this study is concerned with heat transfer from offshore pipelines, a description of these pipes, methods of their trenching and heat transfer mechanisms in different porous media conditions found in the literature are also described herein.

## 2.2 Background on Marine Sediments

Oceans have highly complex seabed sediment mineralogy due to the various environmental and geological processes influencing their formation, especially in the shallow waters of the continental shelves. The extents of the continental shelves around

the world vary depending on whether the continental margin is rising or settling; the average width of the continental shelf is 70 km, Poulos (1988). They are widest in the Arctic Ocean and along the north and west sides of the Pacific Ocean and narrowest near young mountain ranges, Poulos (1988).

### 2.2.1 Formation of Marine Sediments

Most marine sediments are formed in the same way as onshore soils, as part of the end weathering process of rocks. They are composed of rock weathering by-products from land that have been transported into streams by rivers, glaciers and winds. During the transportation of these soils, further breakage and weathering take place. The sediments get deposited in the seafloor, buried and compacted over ages of time, Dean (2010). However, marine sediments become influenced by environmental and geological processes that make them differ from onshore soils, these include, Poulos (1988);

(a) The salinity of the pore water.

(b) The high pressure and low temperature affect the microstructure of the sediments.

(c) The presence of biogenous particles resulting from shells and skeletons of marine organisms.

(d) The low rate of the deposition of the particles.

### 2.2.2 Classification of Marine Sediments

Offshore sediments can be classified according to the particle sizes and the origin of the sediments.

(1) Particle size.

Particle size determines how the particle is transported and how far it has travelled before settling in the seabed. Hamilton (1974) has classified sediments from the continental margin according to their size as shown in table (2.1).

| Sediment type | Number of samples | Mean grain diameter(mm) | Sand (%) | Silt (%) | Clay (%) | Specific gravity |
|---|---|---|---|---|---|---|
| **Sand** | | | | | | |
| **Coarse** | 2 | 0.5285 | 100 | 0 | 0 | 2.71 |
| **Fine** | 18 | 0.1638 | 92.4 | 4.2 | 3.4 | 2.708 |
| **Very fine** | 6 | 0.0915 | 84.2 | 10.1 | 5.7 | 2.693 |
| **Silty sand** | 14 | 0.0679 | 64 | 23.1 | 12.9 | 2.704 |
| **Sandy silt** | 17 | 0.0308 | 26.1 | 60.7 | 13.2 | 2.668 |
| **Silty sand** | 12 | 0.0213 | 6.3 | 80.6 | 13.1 | 2.645 |
| **Sand-silt-clay** | 18 | 0.0183 | 33.3 | 40.2 | 26.5 | 2.705 |
| **Clayey silt** | 54 | 0.0074 | 5.9 | 60.6 | 33.5 | 2.656 |
| **Silty clay** | 19 | 0.0027 | 4.8 | 41.2 | 54 | 2.701 |

Table 2.1 Average sediment size analyses in the continental margin (Hamilton 1974).

(2) Particle origin.

According to Poulos (1988), sediments can be divided to,

(a) Lithogenous sediments.

These are sediments with silica based mineralogy derived from the weathering of terrigenous rocks. These include: (a) sands with very hard, angular or round particles. (b) Clays formed from silica-aluminate minerals. They are overconsolidated due to having been subjected to intense loads

from overburden or glaciers which have been removed lately by erosion or melting. (c) Silts of fluviaglacial origin are found in Arctic and sub-Arctic regions. They show high degree of overconsolidation, even though if there is no geologic history of burial, this has been accounted for by the freeze-thaw cycling in shallow waters.

(b) Biogenous particles.

These include the insoluble remains of marine organisms; they include skeleton, teeth and shells. These form calcareous sediments with calcite minerals. They are commonly found at relatively shallow depths, they are not found in water depth greater than 4000 m as at these high depths, the calcium carbonate dissolves due to the high pressures. High calcium carbonate concentrations are found in sediments existing in the East Pacific Ocean, Australia and the North Indian Ocean.

### 2.2.3 Distribution of Marine Sediments

Rivers are considered to be the largest source of sediments to the ocean, fine sediments such as fine silt and clay travel in suspension while coarse gravel and sand are pushed along the river stream as bed load. The rate of settling of the particles is controlled by the particles diameters, larger particles settle out more rapidly. As the river enters the ocean, and the flow slows down, sands and gravel settle out. Finer particles take longer to settle and so silts are transported considerable distances and clays can be transported even greater distances before getting deposited. Also wind transports sediments from deserts and mountains. Melt water from glaciers can transport clays to great distances

to the ocean. Bjerrum (1973) has shown the distribution of the North Sea sediments as shown in Figure (2.1).

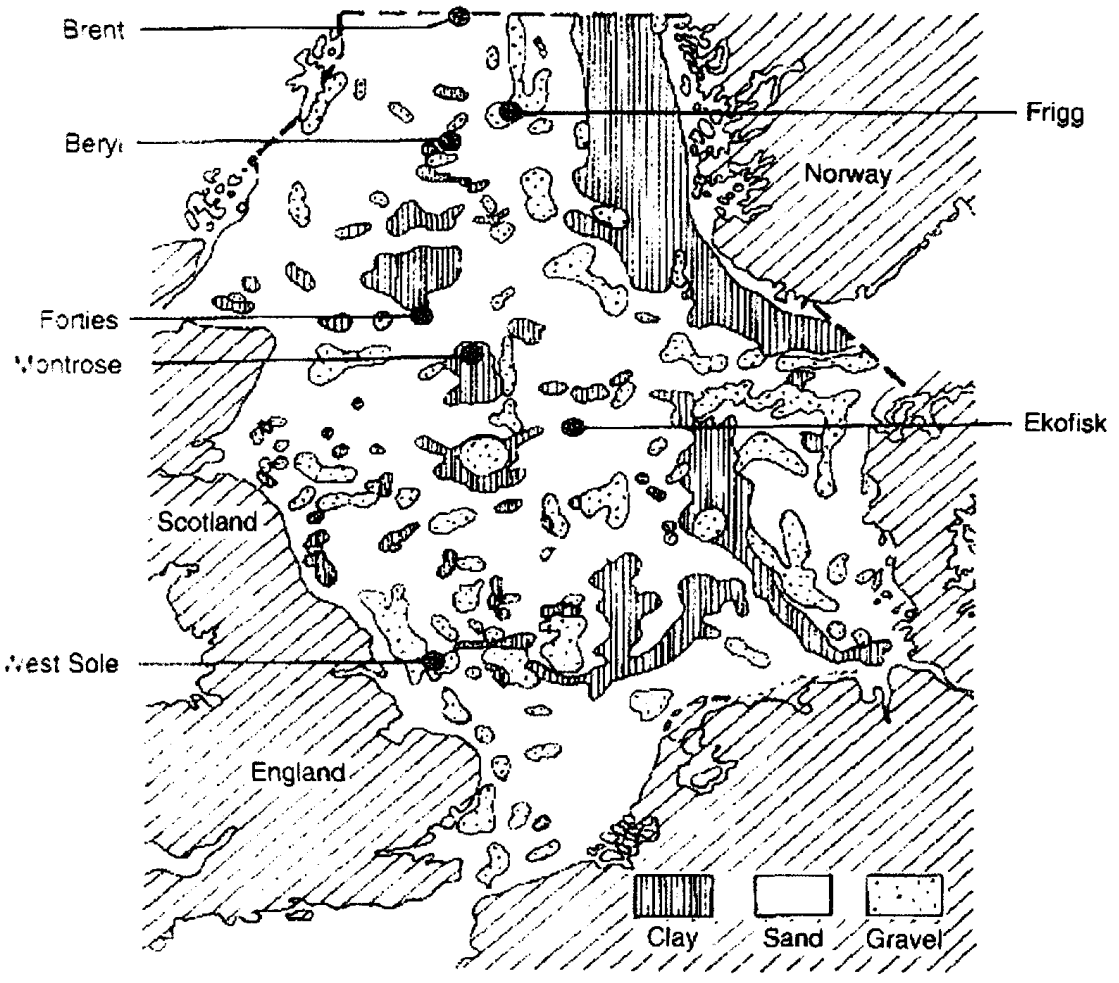


Figure 2.1 Distribution of sediments in the North Sea (Bjerrum 1973).

## 2.3 Permeability of Porous Media

The permeability of a porous medium plays a very important role in the heat transfer process. Permeability can be measured in different ways in-situ, in the laboratory or from empirical relationships. Different empirical formulae relating permeability of a sediment to its properties and geometry were proposed in the literature, these include

Hazen (1911), Kozeny (1927), Carman (1937) and Krumbein and Monk (1942). Hazen (1911) developed an empirical formula for predicting the permeability of saturated sands; it related permeability directly to grain size using the following formula,

$$K = C_H d_{10}^2 \quad (2.1)$$

Where, $C_H$ is Hazen empirical coefficient (In the range of 1 to 1000 according to geotechnical books e.g. Lambe & Whitman (1969), Mansur & Kaufman (1962), Terzaghi & Peck (1967));

$d_{10}$ is the particle size for which 10 % of the soil is finer (the formula is applicable for particles 0.01 cm < $d_{10}$ < 0.3cm).

Although this formula is simple to use and easy to memorize, it can give incorrect permeability values as it is only based on the $d_{10}$ particle size and also the wide range of Hazen coefficients that can be applied can create permeability values that vary by three orders of magnitude.

Kozeny (1927) and Carman (1937) introduced a semi empirical formula which is based on the particle shape, particle size distribution and void ratios for predicting the permeability of porous media; the expression is as follows,

$$K = \frac{1}{C_{KC}} \frac{d^2 e^3}{(1+e)} \quad (2.2)$$

Where, $C_{KC}$ is the Kozeny-Carman empirical coefficient;

$d$ is the particle diameter;

$e$ is the void ratio.

Krumbein and Monk (1942) modified the Hazen formula by using the median of the grain size distribution ($d_{50}$) and the standard deviation of the grain size distribution. The formula is as shown,

$$K = 760\, d_{50}^2\, e^{-1.31\sigma} \tag{2.3}$$

Where, $d_{50}$ is the median of the grain size distribution at the phi logarithmic scale;

$\sigma$ is the standard deviation of the grain size distribution.

Empirical formulae do not predict the exact permeability values of sediments, even if the actual sediment properties were used in the estimation, but they provide a general idea of the range of permeability that can be expected for a certain sediment. A number of investigations were performed in the literature on predicting the permeability of different marine and coastal sediments using empirical formulae and comparison of the results to measured permeabilities.

Millham and Howes (1995) investigated the permeability in upland and offshore aquifer zones of a sandy outwash aquifer located in the water shed of Little Pond, a coastal embayment in Falmouth, Massachusetts. They used five methods for this investigation; these included three insitu field methods (tidal damping, natural gradient tracer test and slug tests) and two laboratory methods (permeameter tests and grain size analysis). The grain size analysis was performed using the Hazen (1911) formula, Equation (2.1) and

the Krumbein and Monk (1942) formula, Equation (2.3). They found that the method which gave best results for the shoreline and the upland regimes was the slug test. The grain size analysis has shown better results in the upland than the shoreline, the results were similar to those obtained by the slug test. In case of shoreline sediments the permeabilities predicted by the grain size analysis were underestimated.

Forster et al. (2003) compared measured vertical permeabilities from superficial sandy sediments from the southern Baltic Sea with permeabilities calculated by two empirical equations; these were the Kozeny-Carman equation, Equation (2.2) and the Krumbein and Monk equation, Equation (2.3). They found that using formulas that depend on sediment properties in calculating the permeability overestimates the measured permeabilities by up to a factor of 2.6. They have also mapped seafloor permeability in the southern Baltic Sea according to their results; their mapping has shown large areas of intermediate permeability ($2.5x10^{-12}$ $m^2 < K < 5x10^{-12}$ $m^2$).

Wislon et al. (2008) examined data from 23 different studies in the literature to determine the range of permeability of marine sands and to determine the applicability of empirical relationships in determining the permeability. They collected data which was concerned with the upper 50 cm of Sublittoral sand deposits; these data included undisturbed cores, disturbed samples and sieved sediments from different locations including the North Sea, Japan, Hawaii and Australia. The database has showed a range of permeability of ($2x10^{-12}$ $m^2 < K < 1x10^{-8}$ $m^2$). Their results have suggested the use of empirical formulae with caution in predicting permeability, but with the knowledge of the depositional environment and grain size data.

Chapuis and Aubertin (2003) evaluated the validity of the Kozeny-Carman equation in predicting the permeability of about 300 laboratory test results taken from the literature, the investigation included different types of soils including sand, gravel, till, clay and silt. They used a different form of the Kozeny-Carman equation in their calculations which is given by,

$$K = \frac{C}{\rho_w} \frac{e^3}{S^2 D_R^2 (1+e)} \tag{2.4}$$

Where, $C$ is a constant (0.2, Carman 1937);

$S$ is the specific surface ($m^2/kg$) ;

$e$ is the void ratio;

$D_R$ is the specific weight ($\rho_s/\rho_w$);

$\rho_w$ is the density of water ($kg/m^3$);

$\rho_s$ is the density of solids ($kg/m^3$).

The publications from which the data was gathered included all information needed for the prediction of the permeability, they either included the complete gradation curve for non-cohesive soils to predict the specific surface or provided the measured value of the specific surface for cohesive soils. The authors have shown that the Kozeny-Carman equation predicts fairly well the permeability of saturated, homogeneous soils as the predicted values were falling in the range of (1/3 to 3) times the measured values;

reasons for the discrepancies in results were suggested to be due to inaccurate value of the provided specific surface, unsaturated soil, inadequate permeability test procedure,

## 2.4 Permeability Anisotropy of Porous Media

Since soils and sedimentary rocks have anisotropic physical and mechanical properties, it is expected that they also possess anisotropic permeability. Knowledge of soil anisotropy is of major interest in many engineering disciplines like geotechnical, chemical, agricultural and environmental engineering. The knowledge of the rate and direction of fluid flow in the soil is important for many sub-surface fluid transport problems such as foundation settlement, Terzaghi and Peck (1967); design of drainage systems for roads and airfields, Cedergen (1974); fluid flow and contaminant transport, Nielsen (1986); and compression dewatering, Clayton et al. (2003) and Clayton et al. (2006).

### 2.4.1 Factors Causing Permeability Anisotropy

Permeability anisotropy occurs either naturally (sedimentation) or due to the application of a compressive force. This results in deformation from compression of the soil skeleton. This leads to the pore configuration in the vertical and horizontal directions becoming different, resulting in a different permeability for the vertical and horizontal flows.

Zaslavsky and Rogowski (1969) suggested that soils consisting of layers parallel to the soil surface will have a horizontal permeability greater than the vertical permeability.

Witt and Brauns (1983) have investigated theoretically and experimentally the permeability anisotropy of an oriented, but randomly packed bed. Their theoretical derivation has shown that the factor of permeability anisotropy is equal to the square of the reciprocal ratio of their tortuosity (tortuosity (T) is the ratio of the length of the actual path of the fluid particles to the shortest path length in the direction of the flow).

$$r_k = \frac{K_h}{K_v} = (\frac{T_v}{T_h})^2 \qquad (2.5)$$

Where, $K_h$ is the hydraulic permeability in the horizontal direction;

$K_v$ is the hydraulic permeability in the vertical direction;

$T_v$ is the vertical tortuosity;

$T_h$ is the horizontal tortuosity.

Their experimental investigation has shown good agreement with their theoretical results proving that due to flatness and orientation of the particles, the permeability anisotropy could not exceed a value of 2.5. The investigations suggested three reasons that would cause permeability anisotropy of sedimentary soils, these are micro-stratification, macro-stratification and flatness and orientation of particles.

Investigation of the upper layers of soils by Selim (1987) has shown an opposite effect, where the vertical permeability proved to be higher than the horizontal permeability, due to the presence of worm holes and vertical shrinkage cracks. He also suggested that for lower subsoil layers, that the horizontal permeability is often higher than the vertical permeability.

Kiyama et al. (1996) have reported the results of triaxial tests on granite. These results have proven that directional fracture is another cause of permeability anisotropy.

Wong (2003) proposed a model that accounts for permeability anisotropy induced by shear deformation in a deformable porous medium. The model stated that the permeability changes are anisotropic and dependent on the induced strains. He validated the results of the proposed model by performing experimental tests to determine the permeability of idealized regularly packed and random assemblies. The model yielded reasonable and consistent results in predicting the experimental results.

### 2.4.2 Measurement of Permeability Anisotropy

Investigators interested in the determination of the permeability anisotropy have developed various models and experiments for determining the horizontal and vertical components of the permeability.

Childs et al. (1957) used the two well pumping method, Childs (1952) and the tube method, Kirkham (1945) for determining the horizontal and vertical components of the hydraulic permeability. The two well pumping method was used to obtain the horizontal hydraulic permeability and the tube method was used to obtain the geometric mean of the vertical and horizontal hydraulic permeabilities.

Bouma and Dekker (1981) presented a field method for determining the permeability anisotropy ratio; called the cube method. In this method, a gypsum covered cube of soil, with dimensions of 25 cm for all sides was carved out in situ. Water was shallowly added on top of the sample, creating a hydraulic gradient across it and the vertical hydraulic

permeability was measured, the experiment was repeated on the other direction to determine the horizontal hydraulic permeability.

Al-Tabaa and Wood (1987) used the falling head permeability test for measuring the horizontal and vertical components of Speswhite kaolin clay during consolidation. The kaolin clay samples were tested in the normally consolidated and over consolidated states. The sample was first prepared as isotropic slurry with void ratio of 3.1, steady vertical effective stress was applied incrementally and the void ratio was steadily falling due to the one-dimensional consolidation taking place. The measurements have shown that at high void ratio, the clay structure is random and permeability isotropy essentially exists, but as the sample was compressed vertically, the vertical permeability decreased and therefore the permeability anisotropy increased up to 2.8.

Chapuis et al. (1989) have shown that the hydraulic permeability anisotropy does not only depend on the void ratio alone, but also on the sample preparation method. They performed densification tests using two different compaction modes for determining the hydraulic anisotropy of clean sand. The samples were compacted in the first series statically and in the second series dynamically. For the static compaction the hydraulic permeability anisotropy result was higher than one and for the dynamic compaction, the hydraulic anisotropy ratio was less than one.

Leroueil et al. (1990) performed seven series of tests from five soft clay sites, three of these samples were for marine soft clays and the two other samples were for Swedish clay and varved clay; varved clay is clay with visible annual layers formed in proglacial

lakes due to differences in organic content. In the summer, light grey silt settles and accumulates and in the winter, when the lake is frozen, dark grey in color clay settles and accumulates. The horizontal permeability was measured in a radial-flow permeameter and the vertical permeability was measured in triaxial and odeometer cells. For the results of marine clays, it was proved that the permeability anisotropy did not vary significantly for compressions up to strains of 25%. However, for the varved clay samples, the vertical permeability decreased significantly compared to the horizontal permeability when compressed vertically.

Scholes et al. (2006) proposed a model that predicts permeability anisotropy as a function of sample compression or void ratio. Two assumptions were adopted when forming the model these are, deformation was due to compression of the particles and not due to particle rearrangement and flow in different directions occurred within the same network of pores. The developed model is,

$$r_K = \left(\frac{1+e_o}{1+e}\right)^x \tag{2.6}$$

Where, $r_K$ is the permeability anisotropy ratio;

$e_o$ is the initial void ratio where isotropy existed;

$x$ is the tortuosity ratio.

The model predicts the vertical permeability if data or a suitable expression for the horizontal permeability exists, and vice versa is correct. A lignite sample from the Loy Yang Lignite mine in Victoria, Australia, was tested experimentally using compression

permeability cells to predict the permeability ratio. The model predicted the experimental permeability ratio accurately for lignite and for other materials including sand, clay and kaolin.

### 2.4.3 Ranges of Permeability Anisotropy Reported in the Literature

A number of studies have estimated the range of permeability anisotropy ratio for different types of soils. These results have shown values in the range of (0.75 to 4.1) for granular soils, and range of (0.7 to 4.6) for cohesive soils. There exist few exceptions for both sand and clay samples where their anisotropy ratios either exceeded or were lower than in the mentioned ranges, e.g. varved clays have shown permeability ratios of up to 40.

#### 2.4.3.1 Non-cohesive Soils

Mansur and Dietrich (1965) tested granular soil in the field using the pumping test for determining the permeability ratio. Their results have shown a permeability ratio in the range of (1.4 to 4.1).

Latini (1967) reported values for quartz sand in the range of (1.04 to 1.06)

Fontugne (1969) reported values in the range of (0.93 to 1.36) for quartz sand.

Chapuis et al. (1989) tested the effect of densification on the permeability anisotropy results for sand samples using two different compaction modes. The sand samples had a uniformity coefficient, $C_u$ of 3.5, fine content in the range of (2%-3%), specific gravity of solids, $G_s$ of 2.69 and water content of 10.3 %. Statically compacted samples showed

permeability anisotropy results more than unity (1.33 to 1.83) while dynamically compacted samples showed permeability anisotropy results less than unity (0.87 to 1).

#### 2.4.3.2 Cohesive Soils

De Boodt and Kirkham (1952) collected "clods" of moist soil samples of Clarion Loam and Ida silt loam for measuring their air permeability. "Clods" are fragments of soil of 5-7.6 cm size, broken from the natural body of the soil in place; these were used rather than core samples as they are believed to be more representative of soil in place. They reported permeability anisotropy values in the range of (1.13 to 2.09) for these loam samples.

Olsen (1962) reported permeability anisotropy ratios of (0.9 to 4) for illite and Boston blue clay, and a range of (1.3 to 1.7) for kaolinite consolidated one dimensionally.

Basak (1971) performed an experimental study on different structures of kaolinite samples; these are ordinary, flocculated and dispersed structures. The aim of the study was to determine the effect of the void ratio on the vertical and horizontal permeabilities and therefore on the permeability anisotropy ratio. The results have shown that the permeability anisotropy ratio is inversely proportional to the void ratio; permeability anisotropy ratio in the range of (1 to 1.6) was obtained for void ratio in the range of (0.655 to 0.85) depending on the percentage of dispersing or flocculating particles in the sample.

Chan and Kenny (1973) tested varved clay soil near New Liskeard, Ontario that consists of: (a) a zone of silty clay (b) a zone of a thin layer of grey varved soil and (c) a zone of

thick layer varved soil. They reported values of permeability anisotropy in the range of (1.5 to 3.5).

Tavenas et al. (1983) tested soft clays from Quebec, USA and Sweden; these were samples of Champlain sea clays, Tyrell sea clays, Lacstrine varved clay, Matagami clay, Atchafalaya clay and Backebol and Lilla Mellosa Swedish clays. These samples had clay fractions of (31% to 91%), placticity indices of (6% to 73%), liquidity indices of (0.5% to 2.9%) and preconsoildation pressures of (40 to 300 KPa). They reported values of (0.9 to 2.5) for these marine clays.

Chason and Siegel (1986) reported permeability ratios in the range of (1 to 2) for peat cores in Northern Minnesota.

Al-Tabaa and Wood (1987) examined the horizontal and vertical permeabilities for kaolin clay samples. The initial isotropic slurry sample had an anisotropy ratio of 1 and when it was compressed, the anisotropy ratio reached 2.8.

Tests on Kaolin clay performed by Znidarcic and Aiban (1988) gave permeability anisotropy ratio of 1.75.

Garga (1987) performed experimental investigation on undisturbed block samples of fissured blue London clay with liquid limit of 72%, plastic limit of 29%, and clay fraction of 57%; the clay samples were heavily overconsolidated. The anisotropy ratio determined for the samples was in the range of (0.7 to 4.6).

Mitchell (1993) reported an average anisotropy ratio of 2 for many types of clays.

Scholes et al. (2006) reported permeability anisotropy ratio values up to 8 for lignite dewatered from void ratio of 2.2 to 0.65.

An excellent review on the permeability anisotropy ratios values reported in the literature for cohesive, non-cohesive and rocks was reported by Chapuis and Gill (1989).

## 2.5 Thermal Conductivity of Porous Media

Heat transfer occurs in soils due to a combination of the various heat transfer mechanisms mentioned in Section (1.2.2), but the predominant mode of heat transfer is conduction as shown in Figure (2.2) which shows the various conditions under which the different mechanisms of heat transfer occur in different types of soils, Johansesn (1975). Since conductive heat transfer depends on the effective thermal conductivity of the soil, knowledge of the ranges of these values for different soil types and locations would be of great importance.

Factors affecting thermal conductivity:

(1) Porosity.

As explained before in Section (1.2.1), porosity is the volume of voids per total volume; for soils as voids increase, the proportion containing pore water will also increase and since the thermal conductivity of water is lower than the thermal conductivity of the soil solids so an increase in porosity would mean a decrease in the effective thermal conductivity of the sediment. Hadley et al. (1984) performed laboratory measurements of thermal conductivity on samples of reconsolidated, surficial, and fine grained illite and

smectite obtained by dredging and coring operations in the North Pacific Ocean. Their laboratory measurements were performed at a pore pressure of 60 MPa and temperatures ranging from room temperature to 420 C° as to represent soil conditions around a buried waste canister at a depth of 6120 m. The samples were homogenised and reconsolidated to the desired overburden stresses. The thermal conductivities of the sediments were measured using the line probe method. They reported values in the range of (0.65 to 0.95 W/m.K) for a porosity range of (0.15 to 0.95).

(2) Water Content.

An increase in the water content results in a decrease in the effective thermal conductivity as explained previously. Newson et al. (2002) performed laboratory tests on grey slightly sandy clayey sediment from the North Sea to find the coupled compressibility-thermal conductivity relation of the undisturbed and fluidised states. The undisturbed samples were characterised using the standard odeometer while the fluidised samples were characterised using a one dimensional consolidometer. Thermal conductivity of the samples was measured periodically during the loading process using a transient thermal probe. The reported thermal conductivity range for the undisturbed samples was (0.97 to 1.119 W/m.K) for moisture content decreasing from (63 to 46 %). For the fluidised samples, the thermal conductivity range obtained was (0.8 to 1.15 W/m.K) for a range of moisture content of (95 to 35 %).

(3) Density.

As the water content decreases, the bulk density of seabed sediment increases and therefore its effective thermal conductivity increases. Ratcliffe (1960) reported the change in effective thermal conductivity with respect to the change in the bulk density; he measured the thermal conductivities of sediments collected from the Mediterranean, Atlantic and mid- Pacific in the laboratory using the steady state method, the divided bar apparatus. He reported values of effective thermal conductivity in the range of (0.57 to 1.05 W/m.K) for bulk density in the range of (1.1 to 1.65 gm/cm$^3$).

(4) Depth below the Seabed Surface.

As the depth below the seabed surface increases, the porosity of the seabed sediment decreases; a decrease in porosity results in an increase in the effective thermal conductivity. This trend has been proved by Brereton (1992) who measured the thermal conductivities of Quaternary and lower Cretaceous sediments obtained from the Indian Ocean. He examined the variation of the sediments thermal conductivity with respect to depth below the seabed. The values reported for thermal conductivity were in the range of (0.8 to 2.15 W/m.K) for depths below the seabed of (0 to 700 m).

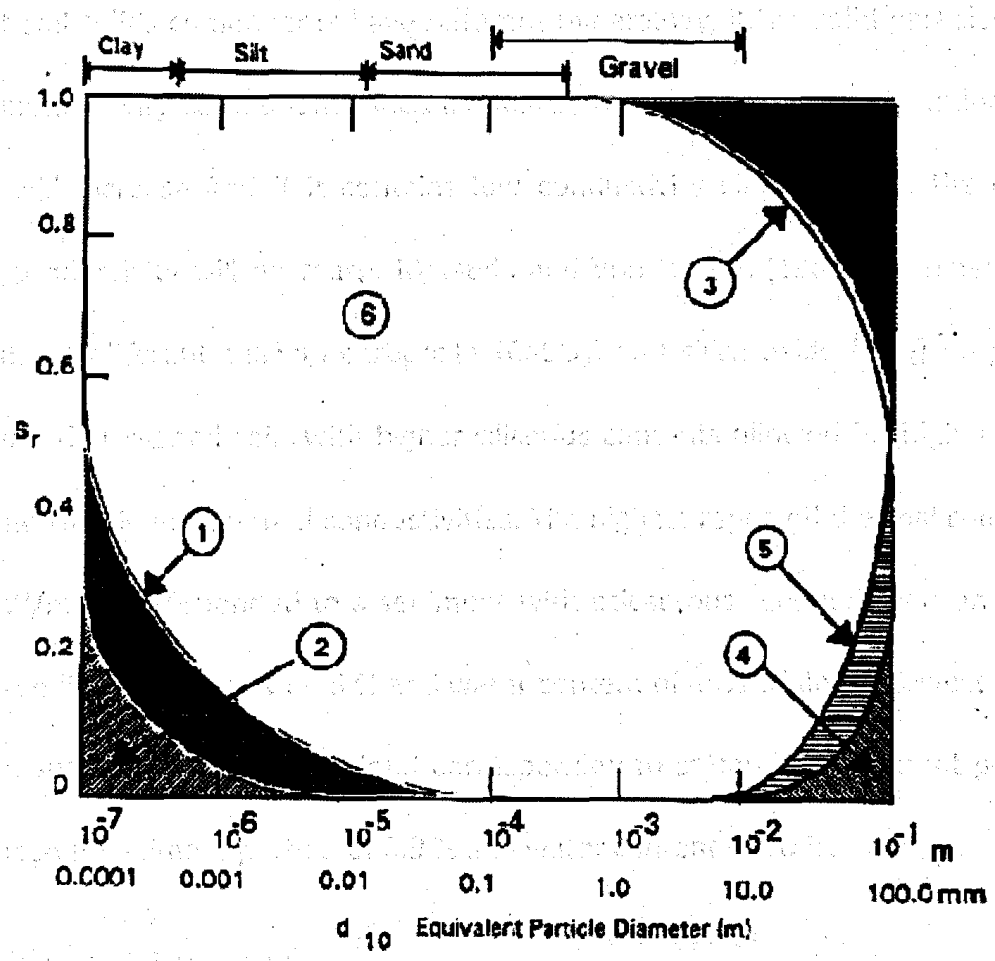


Figure 2.2 Regions of the predominant influence of the different heat transfer mechanisms for sediments of different sizes and moisture content (Johansen 1975).

(5) Mineral Composition.

Different soil solids components have different mineralogy, if the solid particles consist of high conductivity components such as quartz, the effective thermal conductivity of the soil will increase and if it contains low conductivity clay minerals, the effective thermal conductivity will decrease. Matsuda and Von Herzen (1986) examined seabed sediments of different calcium carbonate ($CaCO_3$) and silica oxide ($SiO_2$) proportions, they found that seabed soils with higher siliceous contents allowed for higher porosity values and thus lower thermal conductivities. The highest reported thermal conductivity of 0.94 W/m.K corresponded to a sediment with calcareous sediment portion of 43 %, siliceous sediment portion of 4.5 % and water content of 49% while the lowest reported thermal conductivity of 0.682 W/m.K corresponded to calcareous sediment portion of 16 %, siliceous sediment portion of 8.9 % and water content of 70 %.

## 2.6 Offshore Pipelines

In the last few decades, small diameter (< 0.5 m) offshore pipelines and flowlines have become more widespread for transporting oil, gas, water and other chemicals. The need for offshore pipelines and flowlines has arisen due to the greater number of shallow offshore sites in use and more exploration of marginal oil reservoirs in mature fields e.g. North Sea and Gulf of Mexico. Smaller pipelines can therefore be used in these cases, connecting with existing infrastructure and eventually major pipelines. There are different types of offshore pipelines that are involved with the process of hydrocarbons transportation and these can be classified as shown in Figure (2.3), Bai & Bai (2005) and discussed below:

(a) Flowlines transporting oil or gas from satellite wells to subsea manifolds.

(b) Flowlines transporting oil or gas from subsea manifolds to an offshore platform facility.

(c) Infield flowlines transporting oil or gas between offshore platform facilities.

(d) Export pipelines transporting oil or gas from an offshore platform facility to an onshore platform facility.

In addition to offshore pipelines, offshore cables are also involved in the process of hydrocarbons transport. Offshore cables carry electrical power, between platforms and also carry telephone and internet traffic across seas/oceans.

Offshore pipelines or cables can either be laid directly on the seabed or more common trenched below it. The process by which the seabed is excavated for the pipelines to be installed is called trenching. Several textbooks have discussed the process of offshore trenching; these include textbooks by Bai, Y. (2001), Braestrup, M. & Anderson, J. (2005), Guo, B. (2005) and Dean, E. (2010). The need for trenching pipelines has arisen for the following reasons:

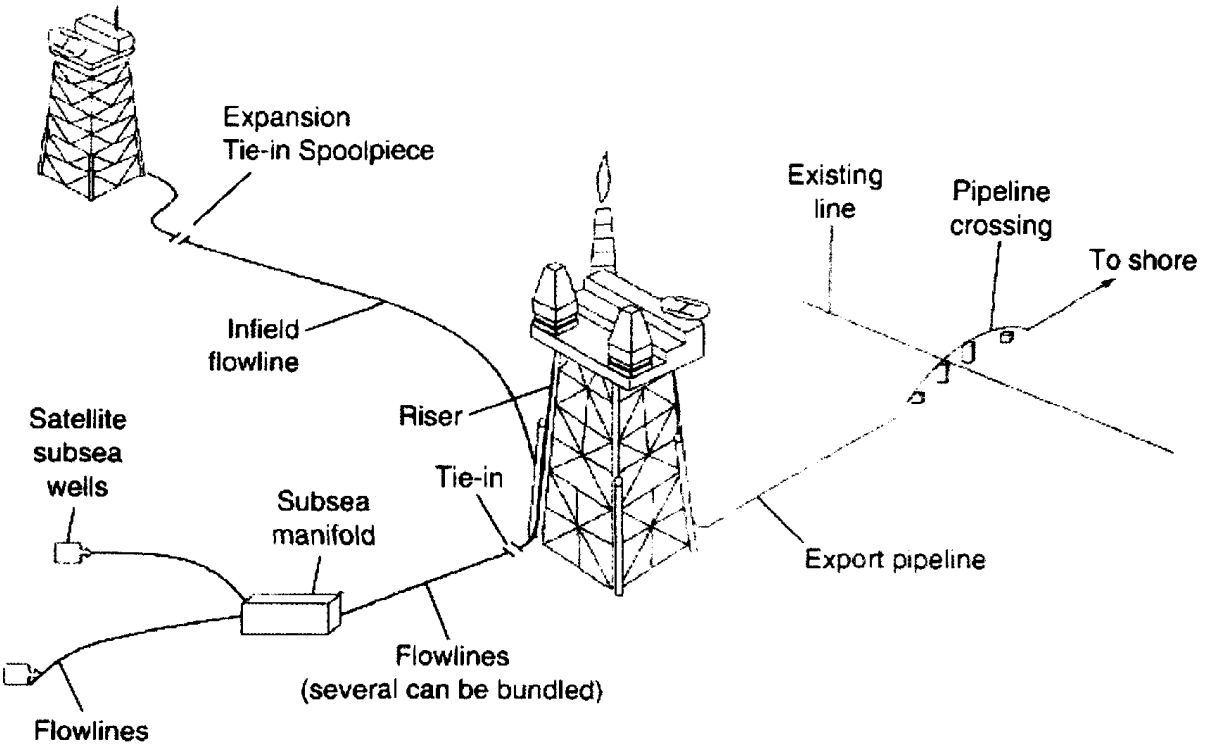


Figure 2.3 Types of offshore pipelines and flowlines (Bai & Bai 2005).

(a) To avoid thermal upheaval buckling of the pipes that may result if the pipeline is operated at higher than ambient temperatures or pressures or due to unevenness of the seabed profile.

(b) To protect the pipelines from mechanical damage that may result from fishing activities or ship anchors.

(c) To provide a thermally stable environment; if the pipeline temperature cools sufficiently, the hydrocarbons will become more viscous and may even cause pipe blockage.

(d) To provide protection for the pipeline against hydrodynamic forces.

Offshore trenching include three methods, these are:

(1) Water Jetting.

In this process, a jet sled rides on the pipeline and high pressure water jets from nozzles fluidize the seabed soil and then air lifts are used to disperse the soil away from the pipeline allowing it to sink into the formed trench, see Figure (2.4). Large jet sleds can trench through dense sand, stiff clay, silt and sandstone, while small jet sleds can trench through loose sand, silt and soft clay.

(2) Ploughing.

In this process, the pipeline rests on top of a "share", the pipeline is pulled along and as the plough moves forward, the pipeline settles in the trench, see Figure (2.5). This allows for backfilling in the same operation by pushing spoil into the trench. Ploughing is suitable for all soil types.

(3) Mechanical cutters.

Mechanical diggers move along the seabed digging the seabed to form a trench for the pipeline to be laid. These mechanical diggers are controlled from a surface vessel through umbilical power, see Figure (2.6). This method is suitable for reasonably firm soil; it cannot be used for very soft clay or very hard clay.

Backfilling of the trench can be done in the same operation of trenching as in the case of ploughing, or the trench could be left open and backfilling occurs naturally by sedimentation or a backfilling device could be used for backfilling the trench either with the spoil resulting from the trenching process or by external backfilling material. The

resulting trenches from these operations are typically (1.5 to 2 m) deep, with side walls that vary between vertical and the angle of repose of the soil (30° to 45°). Pipelines will be embedded between (1 - 4) diameters below the original seabed. Depending on the soil type, the backfill material will either completely fluidize or will break into large pieces (5 to 20 cm in diameter). Once fluidized the soil will consolidate/settle and densify; the time required will depend on the compressibility and permeability of the material. In clay this may take up to (6 – 9) months. Ploughing has been found to create a lumpy clay backfill with a dual porosity structure; high porosity in between the large clay blocks (intergranular porosity) and low permeability within a single block (intragranular porosity). Whilst some consolidation occurs with this lumpy clay structure, the volume change will be less than for fluidized clay.

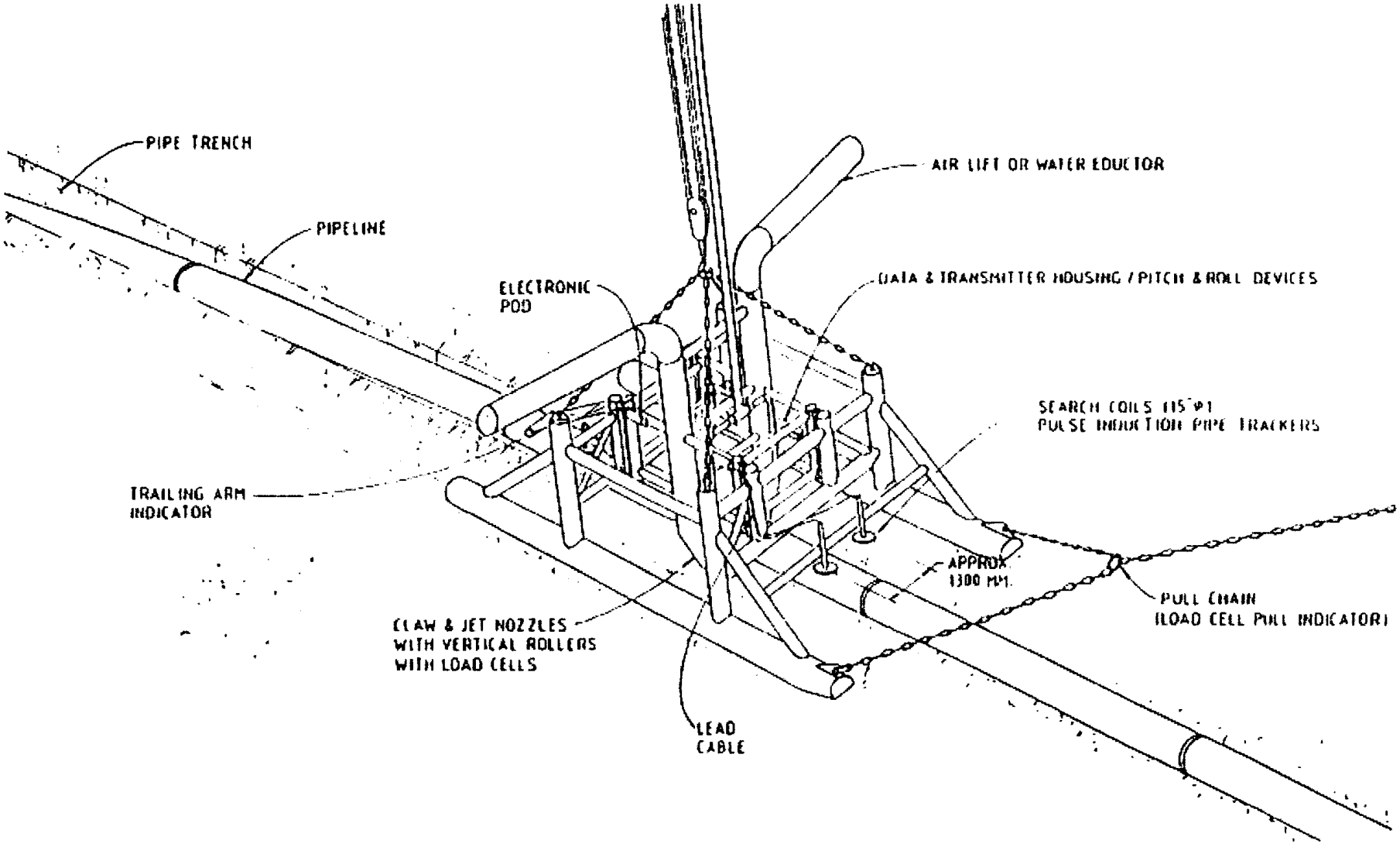


Figure 2.4 Jet trenching system (Bai 2001).

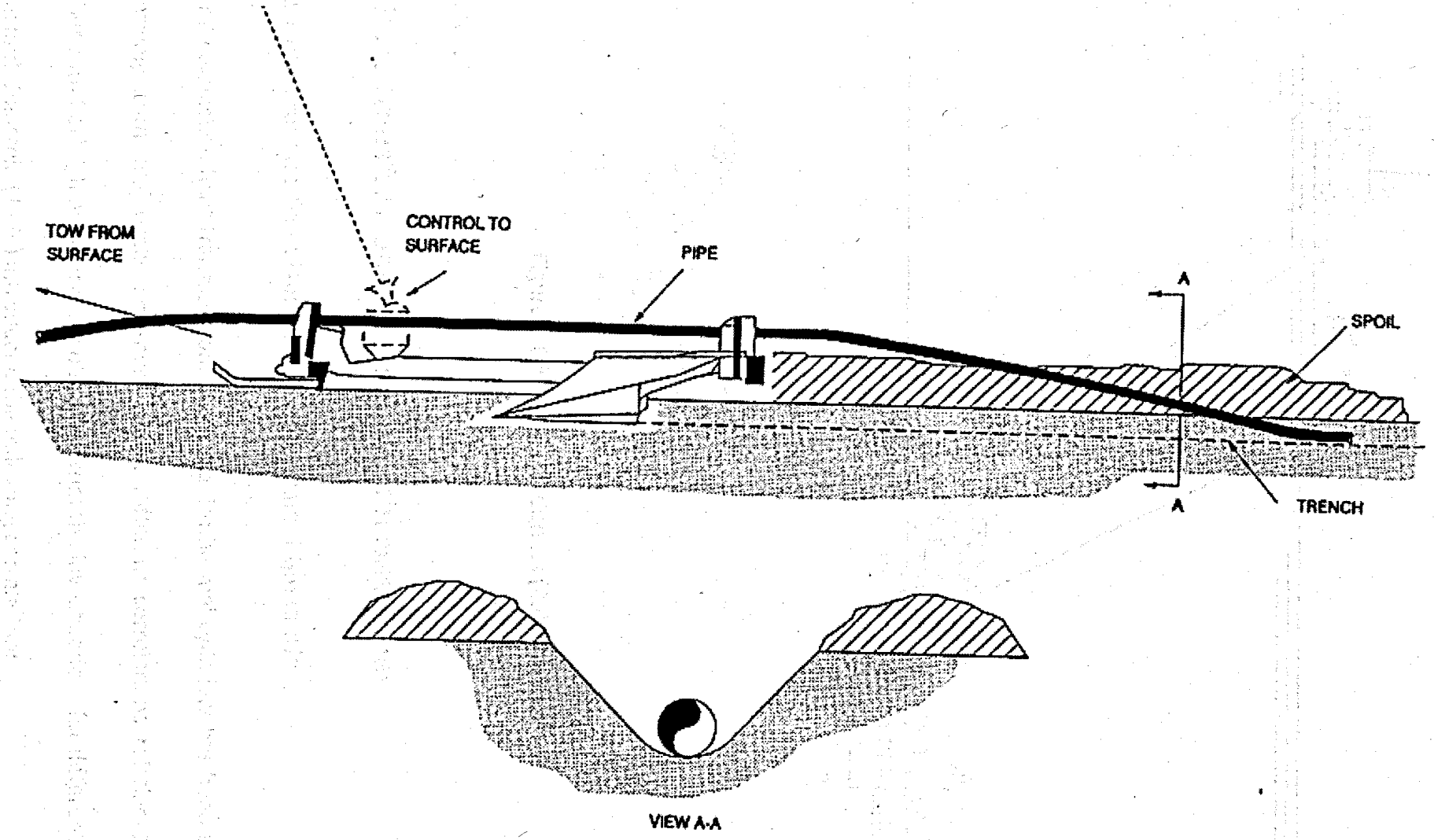


Figure 2.5 Offshore plough trenching systems (Bai 2001).

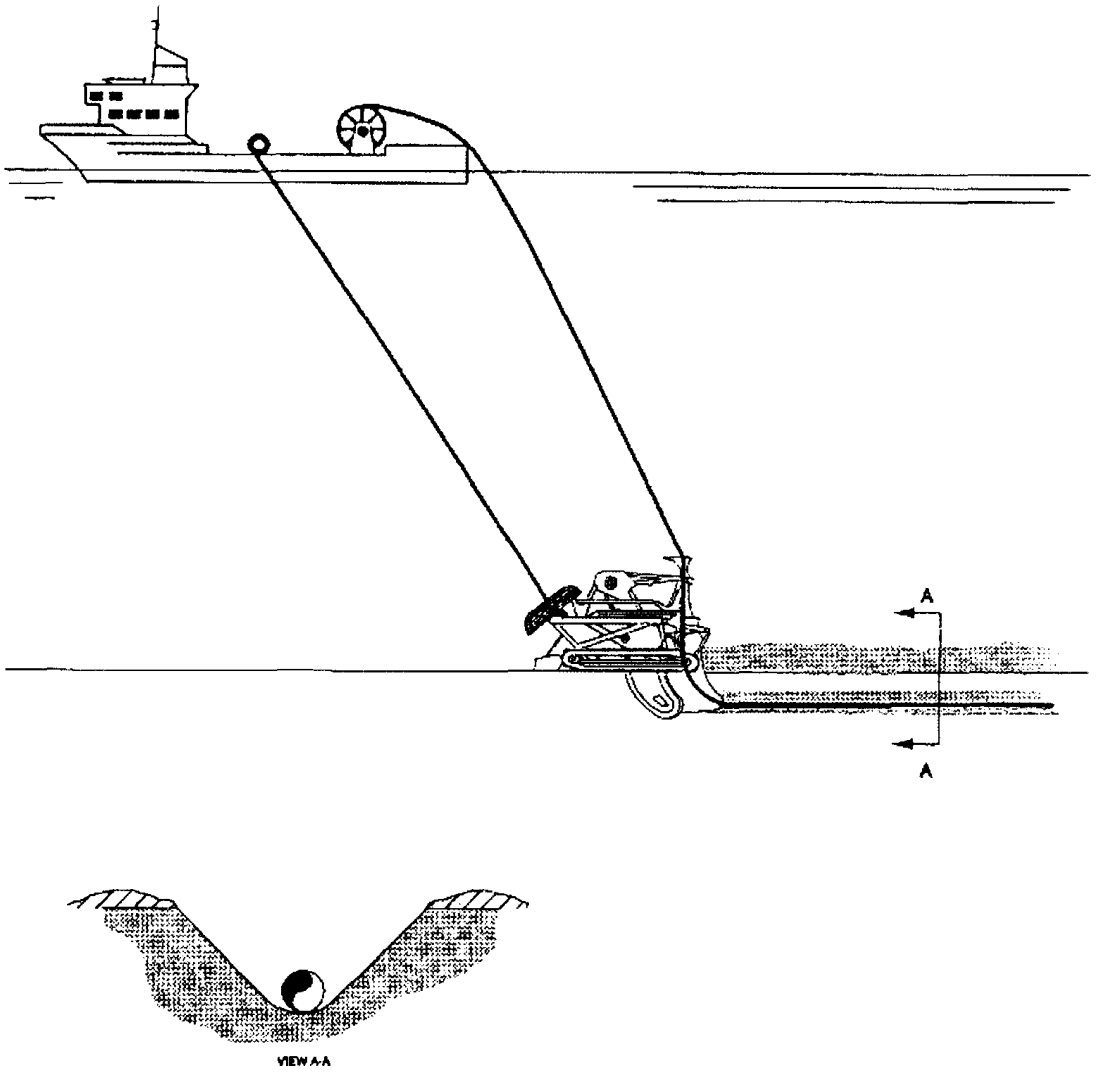


Figure 2.6 Mechanical Cutters (Bai 2001).

## 2.7 Heat Transfer from Horizontal Isothermal Pipes

### 2.7.1 Heat Transfer from Horizontal Isothermal Pipe in Air

Natural convection heat transfer from horizontal isothermal cylinders has been studied extensively both analytically and numerically. Different correlations relating Nusselt number with Rayleigh number were obtained from the investigations for different fluids. Kuehn and Goldstein (1976) introduced the following correlation:

$$Nu = \frac{2}{Y} \tag{2.7}$$

$$\text{Where, } Y = ln\left\{\frac{2}{\left[\left[0.518\, Ra^{\frac{1}{4}} \times \left(1+\left(\frac{0.559}{Pr}\right)^{\frac{3}{5}}\right)^{-\frac{5}{2}}\right]^{15} + \left(0.1\, Ra^{1/3}\right)^{15}\right]^{1/15}}\right\} \tag{2.8}$$

$Nu$ is the Nusselt number;

$Ra$ is the Rayleigh number;

$Pr$ is the Prandtl number, defined as the ratio of the kinematic viscosity to the thermal diffusivity, $(Pr = \frac{\upsilon}{\alpha})$.

This correlation is applicable for any Rayleigh number and Prandtl number. More than 24 correlations have been published in the literature. An excellent review by Morgan (1997) summarized the results for 34 experimental studies and 23 analytical and numerical studies in air for a Prandtl number of 0.7 and Rayleigh number in the range of (10 to $10^8$). A comparison between the mean Nusselt numbers obtained from each of the experimental, analytical and numerical results were obtained for the range of the Rayleigh number studied. A discrepancy between the mean values of the results for a given Rayleigh number was noticed. The mean Nusselt number results agreed within 3.5% between the experimental and analytical and numerical results for the range ($10 \leq Ra \leq 10^4$). At higher Rayleigh numbers, the mean analytical and numerical results were lower than the experimental results with a percentage difference of (7.86% to

11.3%) as Rayleigh number increased. This discrepancy in results was explained by experimental errors and measurement uncertainties.

### 2.7.2 Heat Transfer from Horizontal Isothermal Pipe Buried in a Homogeneous Porous Medium

The first work related to convective heat transfer from an isothermal cylinder in a porous medium was done by Wooding (1963). Convective heat transfer from a point heat source in a saturated porous medium was the subject studied in this case. This study was valid for highly convective flows as a high Rayleigh number range was investigated. He employed the boundary layer approximations equivalent to the classical viscous theory to simplify the study as this means that the vertical gradients of temperature and velocity were neglected. He showed that in this high Rayleigh number range, flow and temperature fields far away from the heat source are described by a solution similar to the solution obtained by Schlichting (1960) for a laminar round jet.

Later on, in the same subject of heat transfer from a heat source embedded in an infinite porous medium, Bejan (1978) examined low Rayleigh number behaviour expressing weak convective flows. He assumed that the fluid flow in the porous medium was governed by Darcy's approximation and a perturbation analysis was performed for deriving the solution. Both transient and steady flows were investigated analytically. The transient investigation was accurate for Rayleigh numbers $\leq 10$ and the steady state analysis was valid for Rayleigh numbers $\leq 20$. Temperature and flow distributions around the heat source were obtained for both the transient and steady state analyses.

Hickox and Watts (1980) investigated heat transfer from a concentrated heat source in an infinite porous medium for a wide range of Rayleigh number (0.1 to 100) numerically. Their results have shown temperature fields indicating conduction heat transfer at low Rayleigh numbers, while for high Rayleigh numbers, convective heat transfer was indicated by the plume above the heat source in the temperature field. It is important to note that their results are applicable for deeply buried heat sources.

Ingham and Pop (1987) investigated natural convection from a heated circular cylinder embedded in an unbounded porous medium for a range of Rayleigh number of ($10^{-2}$ to 400). The investigation was performed numerically using the expanded exponential method and the standard central differences for finite Rayleigh numbers. The numerical results agreed reasonably with the experimental results obtained by Fand et al. (1986) for Rayleigh numbers $\leq$ 10, but as the Rayleigh number increases to $10^2$, the numerical results no longer matched the experimental results and the reason for this was that Darcy's approximation was no longer applicable. Streamlines and isotherms in the vicinity of the cylinder for Rayleigh= 10, 40 and 200 were presented in the study. It was observed that as the Rayleigh number increases, the temperature approaches zero everywhere except in the vicinity of the pipe and in the plume.

Natural convection around a heated cylinder embedded in a box filled with porous materials representing a semi-infinite porous medium has been investigated by Himasekhar and Bau (1988). It was discovered from the experimental and numerical investigations that Rayleigh number dominated the process of heat transfer. The results have shown that at small Rayleigh numbers, conduction dominates the heat transfer

process. At medium values of Rayleigh number, convection dominates the heat transfer process and the flow was described to be two dimensional. At high Rayleigh numbers, the flow becomes three dimensional and fluctuating.

Britto et al. (1989) analysed the coupled heat transfer-consolidation problem in fully saturated kaolin clay within which heated cylinders were installed. Two states of kaolin clay were investigated, normally consolidated and lightly over consolidated; each state was measured experimentally in the centrifuge test and numerically using the finite element formulation HOT CRISP. In the case of cylinders buried in normally consolidated kaolin, both the experimental and numerical analyses have shown that the excess pore water pressures generated due to the high temperature of the cylinders generating conduction heat transfer, reach peak values and dissipate long time before maximum temperatures were reached. In the case of cylinders buried in slightly over consolidated clay, the excess pore water pressure was under predicted by the numerical model. However, in the centrifuge test, horizontal cracks from the end of the heated cylinder were observed.

Pop et al. (1993) investigated transient free convection from a horizontal circular cylinder embedded in a porous medium. Large and finite Rayleigh numbers were investigated analytically using the method of matched asymptotic expansions. The development of the plume regime near the top of the cylinder occurred in stages as follows; heat was initially transferred by conduction to the adjacent porous medium. As Rayleigh number increased, the upward flow of the fluid in the porous medium along the surface of the cylinder forming a distinct temperature front between the heated

fluid and the adjacent unheated fluid. Finally when the steady state was reached, the convection plume was formed by the heated fluid. This work was extended considering a constant surface flux, Pop et al. (1996).

Bradean (1997) reinvestigated the work done by Pop et al. (1993) numerically and analytically and the results agreed well for small and large values of Rayleigh numbers and at small times. Numerical solutions for large times have shown a good agreement with the vicinity of the cylinder with the steady state solution obtained by Ingham and Pop (1987).

### 2.7.3 Heat Transfer from Horizontal Isothermal Pipe Buried in a Heterogeneous Porous Medium

A homogeneous porous medium does not occur frequently in nature; ignoring the heterogeneity of a porous medium that would occur either naturally or enforced by a mechanical process can lead to inaccurate results. Very few reports in the literature have considered the heterogeneity of a porous medium. Muralidhar et al. (1986) examined heat transfer in a horizontal annulus numerically and experimentally. Their numerical results have agreed well with the experimental results except for some cases where divergence in the results was observed, this was explained to have occurred due to non-Darcy effects.

For buried pipes, the structure of the backfill soil is different from the surrounding soil due to the changes caused from the excavation process. Change in the permeability of the soil is considered to be the most important to be studied. Ngo and Lai (2005) have

examined numerically the effect of backfill permeability on heat transfer from a buried pipe. They have examined a wide range of Rayleigh number ($10 \leq Ra \leq 500$) and permeability ratios of the backfill to the hosting soil ($0.1 \leq \frac{K_1}{K_2} \leq 10$) and also the thickness of the backfill material ($0.5 \leq \frac{t}{r} \leq 2$) ,where "r" is the radius of the pipe. The top surface was assumed to be impermeable with a constant temperature "$T_c$" and the pipe's surface at a higher temperature "$T_h$" while assuming a sufficiently large domain to omit heat and fluid flow far away from the pipe. Due to the complexity of the geometry, an elliptic grid generating system was adopted for generating the grid. The governing equations and the boundary conditions were solved using the finite difference method. The results included different isotherms and flow fields for the different conditions studied and it suggested that a backfill more permeable than the hosting soil can minimize heat loss from the pipe.

### 2.7.4 Heat Transfer from Horizontal Isothermal Pipe Buried in a Porous Medium Superimposed by a Fluid Layer

For simplification, many of these studies have assumed an impermeable interface between the fluid layer and the porous layer neglecting the convection effect that occurs in the fluid layer. These studies include, Farouk and Shayer (1988), Christopher and Wang (1993) and Oosthuizen and Naylor (1996). A recent study by Ngo and Lai (2009) has considered the interaction between the fluid layer and the porous medium within which the pipe was buried. They studied heat transfer from a pipe in a soil heating system numerically. The effect of the Rayleigh number, Darcy number and the

air layer thickness on the flow patterns and the heat transfer rate represented by the values of the Nusselt number were examined. The study has shown that the critical air layer thickness required for minimizing heat losses from the pipe should be greater than what was predicted by Oosthuizen and Naylor (1996); this was explained to have happened due to the difference in the boundary condition specified for the interface. The study also suggested that the critical air layer thickness should increase as the permeability of the porous medium decreases for a given Rayleigh number.

## 2.8 Summary

The major properties which affect the process of heat and mass transfer in a porous medium are permeability, permeability anisotropy and thermal conductivity of the medium. This chapter has shown different empirical formulas in the literature used for predicting the permeability of a sediment from the knowledge of it properties. Assessment of this method in predicting permeability in the literature has also been shown. Factors causing permeability anisotropy, methods of measuring it and range of permeability anisotropy reported in the literature for different sediments were also discussed. A summary of some of the factors affecting thermal conductivity of offshores soils was introduced in this chapter.

A brief discussion on the types of offshore pipelines, the need for them, methods of their trenching and need for this trenching were introduced. Finally heat transfer results from isothermal pipes in air and buried in porous media reported in the literature have been summarized.

# CHAPTER 3

# PROBLEM FORMULATION AND METHODOLOGY

## 3.1 Introduction

This chapter describes the mathematical formulation used to model heat transfer from an isothermal pipe embedded in porous media, with a superimposed fluid layer. The governing equations, theoretical assumptions, parameters used in the simulations and the numerical procedure are described in this chapter. The commercial software FLUENT (6.3.26) was used to solve the governing equations.

Two test cases were run to verify the accuracy of the computational software in modelling heat transfer from an isothermal pipe, by comparing the predicted results to numerical and experimental data found in the literature. The first test case was heat transfer by natural convection from a horizontal isothermal circular cylinder in air, Morgan (1997) and the second test case was convective heat transfer from a pipe buried in porous media, Ngo & Lai (2005). Only laminar free convection was investigated, since the study described in this dissertation concerns only the laminar region.

## 3.2 Problem Description

In this study, heat transfer from an isothermal, two dimensional pipe of radius (r) embedded in the seabed has been analyzed under different geometric and flow conditions. The geometric parameters are represented by the trench size (W, H) which was varied from (2.5rx2.5r) to (6rx6r), the trench shape with slope angles (θ) of 45° (B) and 90° (A), and the position of the pipe, which was placed either in the middle of the trench or at the bottom of the trench. The operating conditions were imposed by specifying, the permeability of the backfill material to the permeability of the seabed, the anisotropic permeability ratio of the backfill, the pipe wall temperature and the surface water layer temperature. A schematic of the problem is shown in Figure (3.1).

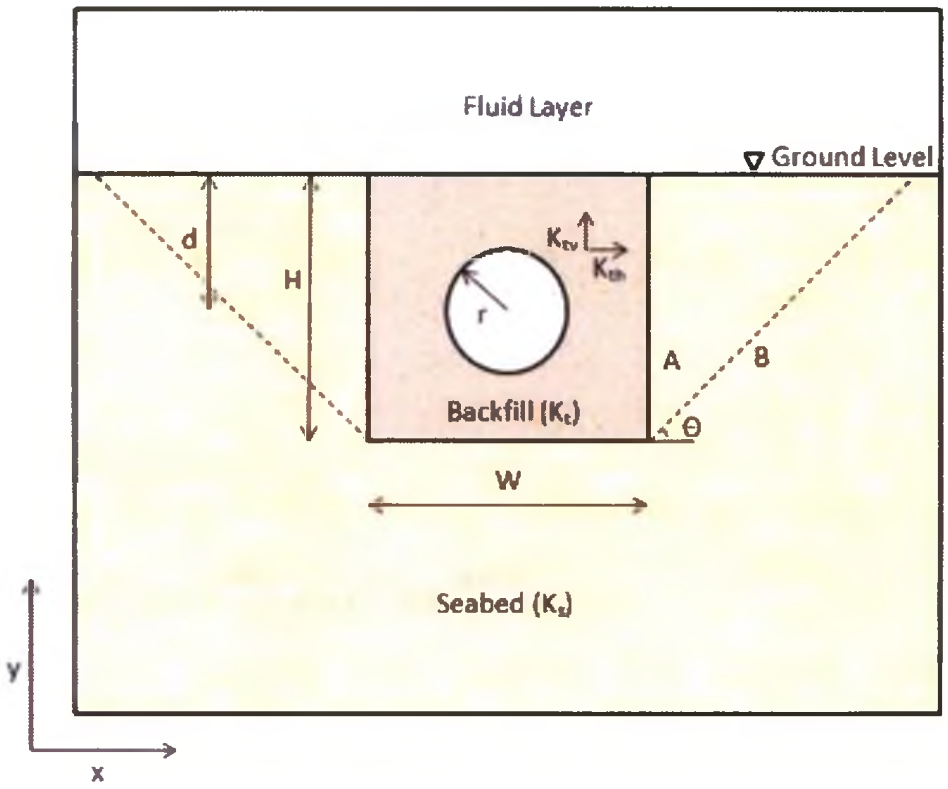


Figure 3.1 Schematic of the problem.

Heat transfer in two different porous media was investigated in this study. The first one was sand, which has a fairly high permeability and the other porous medium studied was clay. For the clay two different forms of backfill were investigated; slurry backfill, which is considered to be of a low permeability and lumps of clay backfill, which represents higher porosity and permeability.

## 3.3 Governing Equations

The problem is reduced to that of a laminar, two-dimensional convective heat transfer problem with steady state boundary conditions. The formulation of the problem involves simultaneous solutions of sets of transport equations for the fluid and porous regions, coupled via the interfaces that separate the different zones.

### 3.3.1 Fluid Zone

In the fluid zone, the following equations are solved;

Mass conservation equation:

$$\frac{\partial u_f}{\partial x} + \frac{\partial v_f}{\partial y} = 0 \tag{3.1}$$

U-Momentum equation:

$$\rho_f \left( u_f \frac{\partial u_f}{\partial x} + v_f \frac{\partial u_f}{\partial y} \right) = -\frac{\partial p_f}{\partial x} + \mu \left( \frac{\partial^2 u_f}{\partial x^2} + \frac{\partial^2 u_f}{\partial y^2} \right) \tag{3.2}$$

V-Momentum equation:

$$\rho_f \left( u_f \frac{\partial v_f}{\partial x} + v_f \frac{\partial v_f}{\partial y} \right) = -\frac{\partial p_f}{\partial y} + \mu \left( \frac{\partial^2 v_f}{\partial x^2} + \frac{\partial^2 v_f}{\partial y^2} \right) + \rho_f g \beta \, (T - T_o) \tag{3.3}$$

Energy equation:

$$\rho_f c_p \left(u_f \frac{\partial T_f}{\partial x} + v_f \frac{\partial T_f}{\partial y}\right) = \lambda_f \left(\frac{\partial^2 T_f}{\partial x^2} + \frac{\partial^2 T_f}{\partial y^2}\right) \quad (3.4)$$

Where,

$u$ is the velocity in the x-direction (m/s);

$v$ is the velocity in the y-direction (m/s);

$\mu$ is the dynamic viscosity (kg/m.s);

$p_f$ is the kinematic pressure (Pa).

The last term in the V-momentum equation is the Boussinesq approximation, it combines the hydrostatic component of the total pressure with the gravity term to produce a force that relies on local temperature differences; using the Boussinesq approximation density is assumed constant except where it is modelled in this term.

$\rho$ is the density of the fluid (kg/m$^3$);

$g$ is the gravitational acceleration (m/s$^2$);

$\beta$ is the thermal expansion coefficient,(1/K);

$T$ is the temperature (K);

$T_o$ is the operating temperature (K);

$c_p$ is the specific heat capacity (J/kg.K);

$\lambda$ is the thermal conductivity (W/m.K);

$f$ is a subscript denoting for fluid phase.

### 3.3.2 Porous Zone

Since the porous medium contains both solid and fluid phases then the governing equations have to be locally averaged over volume elements. This method of volume averaging was developed by Slattery (1967) and Whitaker (1967). The Representative Elementary Volume (REV) is the averaged volume which should not be too small to ensure that it contains both the fluid and the solid phases and should not be too large to ensure that macroscopic changes can take place within it.

Volume averaged mass conservation equation:

$$\frac{\partial\langle u\rangle}{\partial x}+\frac{\partial\langle v\rangle}{\partial y}=0 \tag{3.5}$$

Volume averaged U-Momentum equation:

$$\frac{\rho_f}{\varphi^2}\left(\langle u\rangle\frac{\partial\langle u\rangle}{\partial x}+\langle v\rangle\frac{\partial\langle u\rangle}{\partial y}\right)=-\frac{\partial\langle p\rangle}{\partial x}+\mu\left(\frac{\partial^2\langle u\rangle}{\partial x^2}+\frac{\partial^2\langle u\rangle}{\partial y^2}\right)-\frac{\mu}{K}\langle u\rangle \tag{3.6}$$

Volume averaged V-Momentum equation:

$$\frac{\rho_f}{\varphi^2}\left(\langle u\rangle\frac{\partial\langle v\rangle}{\partial x}+\langle v\rangle\frac{\partial\langle v\rangle}{\partial y}\right)=-\frac{\partial\langle p\rangle}{\partial y}+\mu\left(\frac{\partial^2\langle v\rangle}{\partial x^2}+\frac{\partial^2\langle v\rangle}{\partial y^2}\right)+\rho_f g\beta(\langle T\rangle-T_o)-\frac{\mu}{K}\langle v\rangle \tag{3.7}$$

(Advection) = (Pressure) + (Diffusion) + (Buoyancy force) – (Viscous resistance)

Volume averaged energy equation:

$$\rho_f c_p \left( \langle u \rangle \frac{\partial \langle T \rangle}{\partial x} + \langle v \rangle \frac{\partial \langle T \rangle}{\partial y} \right) = \lambda_{eff} \left( \frac{\partial^2 \langle T \rangle}{\partial x^2} + \frac{\partial^2 \langle T \rangle}{\partial y^2} \right) \quad (3.8)$$

Where, The effective thermal conductivity:

$$\lambda_{eff} = \varphi \lambda_f + (1 - \varphi) \lambda_s \quad (3.9)$$

$K$ is the permeability of the porous medium, ($m^2$).

$s$ is a subscript denoting for solid phase.

## 3.4 Assumptions

To facilitate the solution of the governing equations for the problem of heat transfer from an isothermal pipe backfilled in the seabed, a number of assumptions were made; these are:

- The water flow is assumed to be steady and laminar;
- The solid matrix and fluid both have constant physical properties;
- The solid matrix and the fluid in the porous media are in thermal equilibrium with each other i.e. the solid and fluid phases temperatures are equal ($T_s$=$T_f$=T);
- The interface between the fluid layer and the porous layer is permeable and water is the common fluid for heat transfer;
- The Boussinesq approximation is valid for entire range of parameters explored;
- The porous medium consists of identical spherical particles;
- Isotropic porosity and single phase flow in each porous medium;

- Inertial loss in the porous media was ignored as the porosity and permeability values in the porous medium are very small and have negligible effect for natural convection.

The aforementioned assumptions are applicable for the current study for the following reasons:

- Since the timescale required for the soil settling process is very long compared to the timescale required for heat transfer to take place, and so a transient analysis is not strictly necessary. Hence a number of steady state analyses representing different stages of the settling process were carried out.
- The low permeability and porosity of the porous media provide high resistance to fluid flow, suppressing its velocity and so the flow is laminar.
- The difference in temperatures between the solid and fluid phases comprising the porous media is not significant since the ratio between their thermal conductivities is small. Also local thermal equilibrium applies for cases where no internal heat generation takes place which occurs in the current study.
- The Boussinesq approximation is valid for buoyancy driven flows, where the variation in temperatures in the domain does not produce significant variations in the fluid density; this holds true for the current study as sea water's coefficient of thermal expansion is very small, i.e. its tendency to change in dimensions in correspondence to change in temperature is very low.

## 3.5 Numerical Procedure

The commercial software GAMBIT (2.4.6) was used for grid creation and mesh generation. Due to symmetry, only half of the domain was discretized and analyzed. An unstructured, triangular mesh was generated to efficiently model the 2-dimensional grid involving a circular geometry which represents the pipe. Also, setting up for the boundary conditions for modelling the problem was done using GAMBIT (2.4.6). The mesh was exported to FLUENT (6.3.26) for simulation by selecting the suitable solver conditions and iterating the model until a converged solution was reached.

### 3.5.1 Discretization Scheme in FLUENT

FLUENT (6.3.26), a commercial CFD software based on a finite volume technique was used for solving the current problem of heat transfer as it has proved to be one of the most powerful packages of existing commercial software for solving heat transfer and fluid flow problems. This finite volume method consists of dividing the domain into discrete control volumes using a computational grid and then integrating the governing equations over each control volume, yielding discrete equations that conserve the dependent variables on a control volume basis. Although the scalar quantities are stored at the cell centres, an upwind scheme can be used to interpolate these quantities from the cell centres to get the face values if required. An upwind scheme derives the face values of the required quantities from quantities in the cell upstream, relative to the direction of the normal velocity. A second order upwind scheme was used in solving

momentum and energy equations using the cell values of two adjacent cells to compute the face value of the current cell.

The segregated solver which is a solution algorithm by which the governing equations are solved sequentially (i.e. segregated from one another) was adopted. The SIMPLE (Semi-Implicit Method for Linked Equations) was used to calculate the pressure field and enforce mass conservation using the relationship between velocity and pressure. Also the PRESTO discretization method was used for solving for pressure as it is recommended by ANSYS Fluent User's Guide (2010) in case of natural convection simulations.

### 3.5.2 Operating and Boundary Conditions

The operating conditions that drive the heat transfer process are; a specified pipe wall temperature and operating temperature equal to the temperature of the fluid (minimum temperature in the domain). This renders the buoyancy term to be non-zero, thereby driving the flow in the convective heat transfer problem.

Boundary conditions are critical for obtaining appropriate solutions to the governing equations as they represent the operating conditions for fluid flow and heat transfer. These boundary conditions should be defined correctly in to get accurate results; the boundary conditions specified for the current problem are shown in Figure (3.2) and explained below.

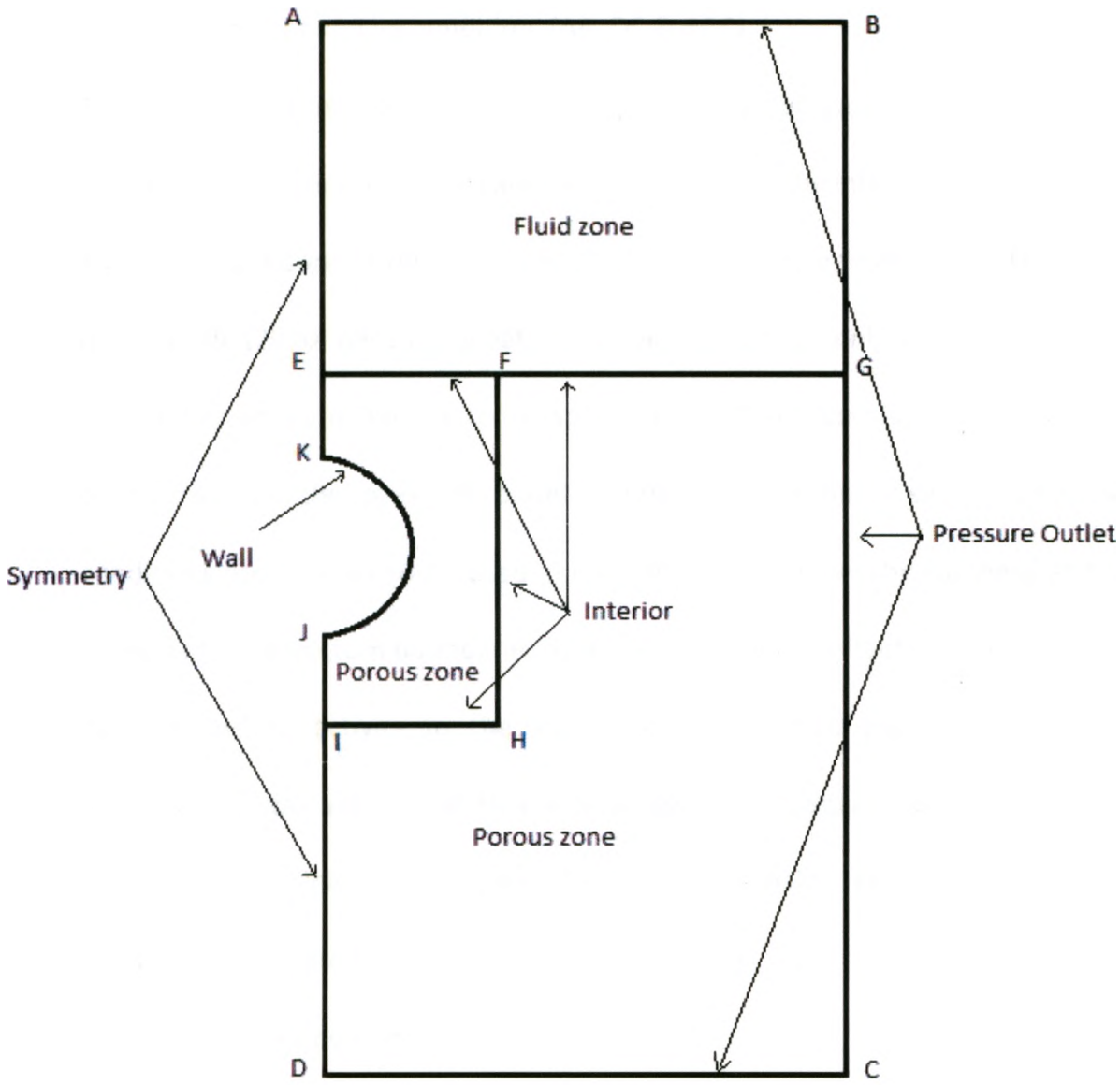


Figure 3.2 Modelled boundary Conditions.

- Symmetry Boundary Condition, (AEK & JID).

  Since the physical geometry and the expected pattern of flow are symmetric, only half of the domain was studied to save computational time. At a symmetry boundary condition all the normal gradients are set to zero and also FLUENT assumes zero flux of all quantities, $\left[u = 0,\ \frac{\partial T}{\partial x} = 0\right]$

- Pressure outlet boundary condition, (AB, DC & BGC).

  This boundary condition requires the specification of gauge pressure at the outlet while all other quantities are extrapolated from the interior of the domain. The gauge pressure in this case was set to zero as recommended by FLUENT's user's guide (2010) because in natural convection we are only interested in flow due to buoyancy and not due to the specification of a differential pressure across boundaries. At the pressure outlet boundary condition a set of backflow conditions are also set to be used in case of reversed flow; this happens at the vertical and the bottom boundaries as at these boundaries fluid is drawn into the domain due to activity in the vicinity of the heated pipe. The backflow temperature was set normal to the boundary with a value equal to the fluid temperature (minimum temperature in the domain) and this was fixed throughout the parametric study, $[P_s = 0,\ T = T_o]$

- Wall Boundary Condition, (KJ)

  A wall boundary condition was used for the surface of the pipe. At a wall boundary condition, horizontal and vertical velocities are set to zero. Since the current problem is one of heat transfer and so the energy equation has to be solved, thermal boundary condition has to be set at the wall boundary. The Rayleigh number for the parametric study was changed by changing the temperature of the wall (pipe), $[T = T_h,\ u = 0,\ v = 0]$

- Fluid Zone, (ABGE).

  The superimposed fluid layer was defined as a fluid zone and the only required input in this case is to define the type of fluid which is water, with properties to be defined; these are density, dynamic viscosity, thermal conductivity and specific heat capacity.

- Porous Zone, (EFHIJK & FGCDIH).

  Each of the backfill and the seabed were defined as porous zones. A porous zone is treated as a special type of a fluid zone and the inputs required for each zone were,

  - Define the porous zone in the fluid region.
  - Select the fluid flowing in the porous zone which in this case was water.
  - Define the viscous resistance coefficient in the horizontal and vertical directions. The viscous resistance coefficient is the inverse of permeability i.e. it indicates how easy a fluid can flow in the porous zone.
  - Define the porosity of the porous zone.
  - Select the solid material composing the porous medium.

- Interface Boundary Condition, (EFG).

  This represents the interfaces between the two porous zones and the interface between the porous zones and the fluid layer. Nothing has to be specified at this boundary. It allows free fluid flow between zones,$[P_f = P_p,\ T_f = T_p,\ u_f = u_p,\ v_f = v_p]$ where "$f$" denotes for fluid and "$p$" denotes for porous.

### 3.5.3 Far-Field Boundary Position and Mesh Dependency Tests

A far-field boundary position test was performed for each trench size and shape studied in this thesis to assure that the physical domain size does not interfere with the heat transfer results. Also a mesh dependency investigation was performed to examine the solution sensitivity to changes in mesh refinement and then the optimal mesh for the problem simulation was selected.

#### 3.5.3.1 Far-Field Boundary Study.

As mentioned before, the far-field boundary test was performed for every change in the trench size or shape. Only the results for a (4rx4r) square trench which is considered to be a median representative will be shown here to explain this test. For a (4rx4r) square trench several grid sizes were investigated, these are, (8rx8r), (10rx10r), (12rx12r) and (14rx14r), these were run for one of the case studies which represents the worst case scenario, where the permeabilities of the backfill and the seabed are at their lowest values. At these very low permeabilities, heat transfer is by mixed convection; for pure convection only a small grid would be enough for the formation of the thermal plume, but for the case of mixed convection, a bigger grid is required as the plume can be very broad. Table (3.1) shows the percentage difference in results between the four grid sizes. A (12rx12) grid was selected since the percentage difference between the Nusselt number result produced from it and a (14rx14r) is only 1.85%. Hence to reduce the computational time, the (12rx12r) grid was selected. For all trench sizes and shapes, a

grid that produces a percentage difference in results that does not exceed 2% was selected.

| Grid Size | Nu | % difference |
|---|---|---|
| 8rx8r | 14.4 | - |
| 10rx10r | 13.76 | 4.4 |
| 12rx12r | 13.35 | 3 |
| 14rx14r | 13.1 | 1.85 |

Table 3.1 Far-Field Boundary investigation for a (4rx4r) square trench.

3.5.3.2 Mesh Independence Study.

In addition, the mesh independence test was performed on all grid sizes that resulted from the different trench sizes and shapes, but only results for a (4rx4r) trench size are shown here. A suitable mesh was selected when further refinement of the mesh did not produce a significant improvement in the heat transfer results represented by the Nusselt number. The mesh was created to be fine near the pipe surface and gets coarser as on moving away from the pipe. Three mesh types were investigated; these are fine mesh consisting of 28057 triangular cells, an intermediate mesh consisting of 10798 triangular cells and a coarse mesh consisting of 8186 triangular cells. The results of the percentage difference in the Nusselt number results are shown in Table (3.2). Since refinement of the mesh from 10798 to 28057 triangular cells produced a percentage difference in the results of only 1.2%, then the mesh consisting of 10798 triangular cells was selected to reduce computational time. The mesh for the (4rx4r) square trench is

shown in Figure (3.3) and a close up near the pipe to show the meshing style is shown in Figure (3.4).

| Number of cells | Nu | % difference |
|---|---|---|
| 8186 | 13.01 | - |
| 10798 | 13.35 | 2.6 |
| 28057 | 13.51 | 1.2 |

Table 3.2 Mesh Independence investigation for a (4rx4r) trench size.

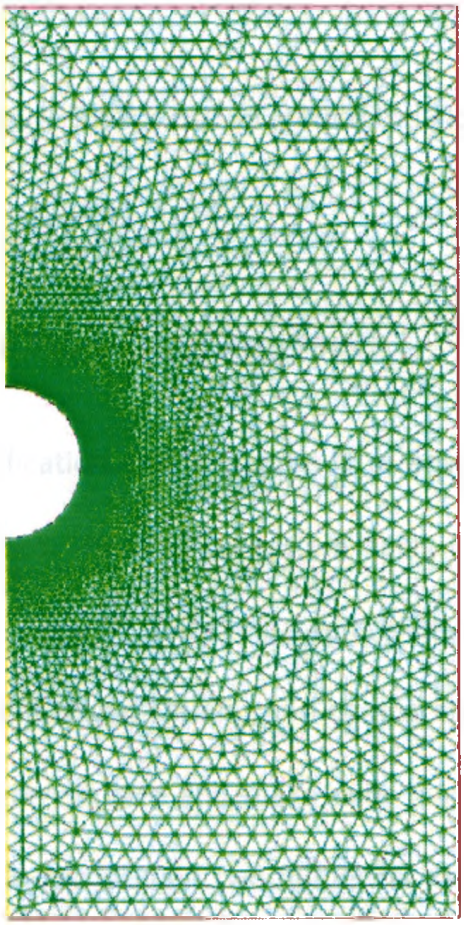

Figure 3.3 Mesh for a 4rx4r square trench.

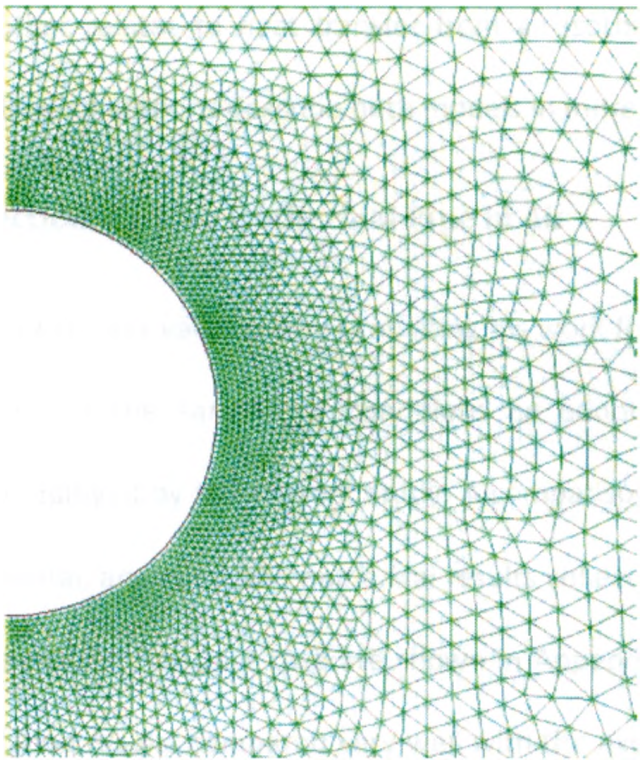

Figure 3.4 A close up around the pipe.

## 3.6 Verification of the Modelling Approach

The purpose of model verification and validation is to ensure that the model and the boundary conditions represent the physical system being modeled to ensure accurate results. The verification was done by modelling a reference model in the literature using the software employed in this study, FLUENT and comparing the predicted results from the software with the reference data and make sure that both behave similarly and produce the same output. In this section two numerical models found in the literature were run using FLUENT; one is a problem of convective heat transfer from an isothermal

pipe in air and the other relates to heat transfer from an isothermal pipe buried in porous media. The following sections describe both models in more detail.

### 3.6.1 Natural Convection from an Isothermal Pipe in Air

The work of Morgan (1997) was validated by simulating his work for the specified range of Rayleigh number under the same flow conditions he adopted, using the same boundary conditions employed by the present study. A comparison between the mean results of the experimental, analytical and numerical results collected by Morgan (1997) and the results obtained from the test case are shown in Appendix A. As shown from Figure (A.1), the validation results compared very well with the experimental, analytical and numerical results as they all follow the same trend.

### 3.6.2 Heat Transfer from a Pipe Buried in Porous Media

The work of Ngo & Lai (2005) was also validated using FLUENT modelling approach. It was validated twice, one time using the boundary conditions used by Ngo & Lai (2005) and another time using the boundary conditions adopted by the current study. In both cases the finite volume approach followed by FLUENT and also a mesh with triangular cells was used for the simulations. The heat transfer results represented by the Rayleigh-Nusselt relation for Ngo & Lai (2005) and the two validation test results are shown in the Appendix, Figures (A.2) and (A.3) respectively. Also shown in Appendix A are comparisons of the isotherms for the cases when ($K_1/K_2$= 0.1), Figure (A.4) and ($K_1/K_2$= 10), Figure (A.5) between those obtained by Ngo & Lai (2005) and the test cases where the boundary conditions in the current study were employed. The isotherms obtained by

the test case where the same boundary conditions used by Ngo & Lai (2005) were employed were similar to his results.

## 3.7 Summary

This chapter has presented a description of the problem of heat transfer from an isothermal pipe trenched in the seabed superimposed by sea water layer. The governing equations describing the two dimensional, steady, laminar flow in the fluid zone and the porous zones were also presented noting that for the porous zones, the governing equations were averaged over volume elements as these zones consist of solid and fluid phases. The discretization scheme, operating and boundary conditions used to solve the problem numerically using the software FLUENT were described. Verification of the modelling approach was also shown in the chapter for two different bench-mark problems.

# CHAPTER 4

# RESULTS AND DISCUSSION

## 4.1 Introduction

In this chapter the numerical results of heat transfer from a trenched pipe are presented for different soil types, flow conditions and geometric conditions. Assuming that the trenched pipe is transporting hydrocarbons, it is important to reduce heat losses from the pipe, to ensure the oil temperature is high enough to avoid thickening or waxing of the oil and, thus, blockage of the pipe.

Therefore, the objective of this chapter is to examine numerically the interaction between the porous media and the overlaying fluid layer, the effect of anisotropic soil variation and the effect of varying the permeability of the backfill with respect to that of the seabed, on the heat transfer results, and also the effect of varying sizes and shapes of the trench and position of the pipe in the trench.

Also analytical modelling of fluid flow in the pipe is performed to show the impact of the different backfill conditions investigated on reducing heat losses from the oil in the pipe and, thus, saving on the pumping power costs that can be achieved.

## 4.2 Material Properties

This section describes the rationale for the range of material properties used in the simulations performed for the current study. Material thermophysical properties can be

divided into two types, thermodynamic and heat transport properties. The thermodynamic properties remain unchanged with time i.e. they represent the equilibrium state of the material. These include density (ρ) ($kg/m^3$) which is the ratio of mass to volume of a specific material.

The heat transport properties include dynamic viscosity (μ), thermal conductivity (λ) and the coefficient of thermal expansion (β). Dynamic viscosity ($N/m^2.s$) is a measure of the resistance of fluid flow due to an applied force. Thermal conductivity (W/m.K) is the property of a material that characterizes its ability to conduct heat. The coefficient of thermal expansion (1/K) is the tendency of a material to change its dimensions in response to a change in temperature.

The modelled fluid is sea water with properties at a temperature of 7 C° (280.16 K), which is an upper bound temperature representing deep offshore (i.e. 800 m depth) conditions as shown in Figure (4.1). These properties are listed in Table (4.1), after Sharqawy et al. (2010).

The soil solid properties for both sand and clay are also listed in Table (4.1); these are typical particle densities obtained from Incropera & DeWitt (2002); they are not used in the calculations.

It is important to note that the thermal conductivity for sand and clay listed in Table (4.1) is the particle solid thermal conductivity ($\lambda_s$) for the sand and clay and not the effective thermal conductivity ($\lambda_{eff}$) for the soil body, as FLUENT calculates the effective

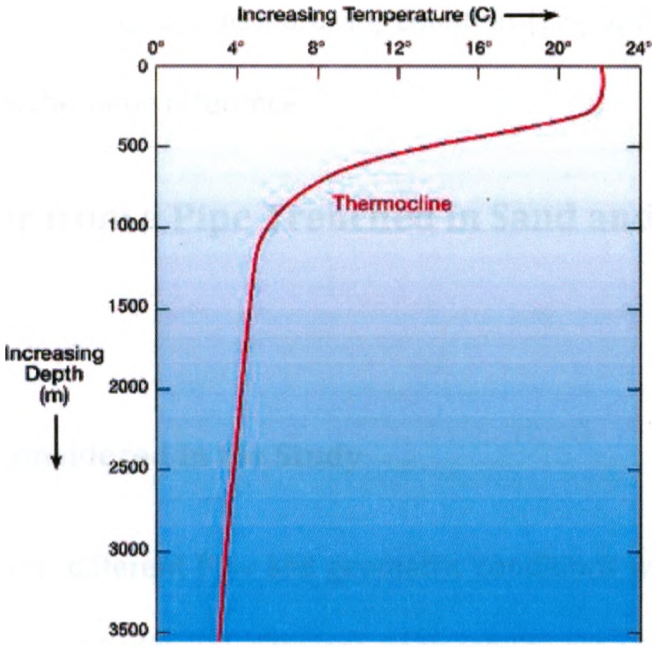


Figure 4.1 Temperature-depth ocean water profile.

| Material | ρ (Kg/m3) | λ (W/m.K) | μ (Kg/m.s) | β (1/K) |
|---|---|---|---|---|
| Water | 1025 | 0.58 | 0.001422 | $4.6*10^{-6}$ |
| Sand | 2000 | 7.69 | - | - |
| Clay | 1750 | 1.54 | - | - |

Table 4.1 Generic material properties employed in the present study.

thermal conductivity as the volume average of the fluid thermal conductivity and the solid thermal conductivity using Equation (1.6). For sand, the solid particle thermal conductivity was that of quartz. For clay, the solid particle thermal conductivity was calculated from Newson et al. (2002) who reported a range of effective thermal conductivities for typical clayey offshore soils. An average value of the given range of effective thermal conductivity (0.8 to 1.15 W/m.K) was estimated and the solid particle

thermal conductivity was back calculated using Equation (1.6) with the porosity of the seabed obtained from the same reference.

## 4.3 Heat Transfer from a Pipe Trenched in Sand and overlain by a Fluid Layer

### 4.3.1 Parameters Considered in the Study

In this part of the study, different flow and geometric conditions were considered. Flow conditions were represented by: (a) different permeability ratios between the trench backfill and the intact seabed ($K_t/K_s$), (b) different anisotropic permeability ratios ($K_{th}/K_{tv}$) of the trench backfill; these were chosen with respect to the literature survey study on the permeability anisotropy of soils (Section 2.4) and (c) different Rayleigh numbers, accounted for by varying the temperature of the outer coating of the pipe covering a possible range of pipe surface temperatures, from a bare pipe case to various representations of thickness or effectiveness of the pipe coatings. These are listed in Table (4.2). The permeability ratios ($K_t/K_s$) and anisotropy ratios ($K_{th}/K_{tv}$) represent a range of conditions of the trench compared to the seabed after backfilling. For instance, when the trench is excavated, pipe laid in the trench and the trench is backfilled with lumps, then the permeability ratio will be as high as ($K_t$= 1000 $K_s$), and the anisotropy ratio could fall in the range of ($K_{th}/K_{tv}$= 1, 10 or 50), it could be ($K_{th}/K_{tv}$= 1) when the soil is first backfilled into the trench and then increases to ($K_{th}/K_{tv}$= 10 or 50) after it is allowed to settle and the vertical permeability falls. A permeability ratio of ($K_t$= $K_s$) occurs when the backfill in the trench completely settles and becomes similar to the

sand in the surrounding seabed; if the stress history is similar, this takes place after a long time after backfilling.

| Parameter | Range |
|---|---|
| Permeability ratio ($K_t/K_s$) | 1, 10, 100, 1000 |
| Anisotropy ratio ($K_{th}/K_{tv}$) | 1, 10, 50 |
| Temp. at the pipe surface ($T_h$) (K) | 320,330,340,350,360 |

Table 4.2 Range of flow parameters considered in the modelling of heat transfer from a buried pipe in sand.

The geometric parameters studied include the trench shape; size and the position of the pipe in the trench, Howard (1996). The ranges of these parameters are listed in Table (4.3).

| Parameter | Range |
|---|---|
| Shape of the trench | 45° & 90° |
| Size of the trench | 2.5rx2.5r, 3rx3r, 4rx4r, 5rx5r and 6rx6r |
| Position of the pipe in the trench | Middle, Bottom |

Table 4.3 Range of geometric parameters considered in the modelling of heat transfer from a buried pipe in sand.

### 4.3.2 Calculation of the Permeability and the Porosity of the Backfill

The excavation of the trench to bury the pipe produces changes in the structure and properties of the excavated soil. Jetting or ploughing this soil back into the trench for bedding and backfill for the pipe produces even more changes in the heterogeneity and spatial conditions of the backfill soil. These changes include variations in the permeability and the porosity of the backfill soil. The relation used to correlate permeability and porosity in this study was the Kozeny-Carman equation, Bear (1972), shown previously as Equation (1.4).

The sand seabed properties were kept spatially uniform; these are an intrinsic permeability of $1.24*10^{-10}$ $m^2$, anisotropy ratio ($K_{th}/K_{tv}$) of 1 and a porosity of 0.372, these properties were estimated by Schock (2004) for well sorted marine, medium sand sediment.

The permeability of the trench backfill was related to that of the seabed by ratios of 1, 10, 100 and 1000. The porosity for each case was back-calculated using the Kozeny-Carman equation, Equation (1.4). For the cases when the anisotropy ratio of the backfill is 10 and 50, an average porosity was obtained from the back-calculated porosities using each of the horizontal and vertical permeabilities. The horizontal permeability, vertical permeability and porosity of the backfill for different conditions are listed in Table (4.4).

These flow conditions were run for all trench sizes and shapes, and for the different positions of the buried pipe in the trench.

| | $K_{th}/K_{tv}$ =1 | | | $K_{th}/K_{tv}$ =10 | | | $K_{th}/K_{tv}$ =50 | | |
|---|---|---|---|---|---|---|---|---|---|
| | $K_{th}$ ($m^2$) | $K_{tv}$ ($m^2$) | φ | $K_{th}$ ($m^2$) | $K_{tv}$ ($m^2$) | φ | $K_{th}$ ($m^2$) | $K_{tv}$ ($m^2$) | φ |
| $K_t=K_s$ | $1.24*10^{-10}$ | $1.24*10^{-10}$ | 0.372 | $1.24*10^{-10}$ | $1.24*10^{-11}$ | 0.29 | $1.24*10^{-10}$ | $2.48*10^{-12}$ | 0.253 |
| $K_t=10K_s$ | $1.24*10^{-9}$ | $1.24*10^{-9}$ | 0.44 | $1.24*10^{-9}$ | $1.24*10^{-10}$ | 0.345 | $1.24*10^{-9}$ | $2.48*10^{-11}$ | 0.3 |
| $K_t=100K_s$ | $1.24*10^{-8}$ | $1.24*10^{-8}$ | 0.613 | $1.24*10^{-8}$ | $1.24*10^{-9}$ | 0.5 | $1.24*10^{-8}$ | $2.48*10^{-10}$ | 0.436 |
| $K_t=1000\ K_s$ | $1.24*10^{-7}$ | $1.24*10^{-7}$ | 0.78 | $1.24*10^{-7}$ | $1.24*10^{-8}$ | 0.675 | $1.24*10^{-7}$ | $2.48*10^{-9}$ | 0.6 |

Table 4.4 Range of horizontal and vertical permeabilities and the porosities of the backfill.

### 4.3.3 Discussion of the Results

In this section the results are shown with respect to the influence of:

(a) The anisotropy ratio of the backfill;

(b) The permeability ratio of the backfill with respect to the seabed;

(c) The effect of trench size;

(d) The effect of trench shape;

(e) The effect of the position of the pipe in the trench.

It is important to note the following:

- Varying the permeability and anisotropy ratio of the backfill; both have significant effects on heat transfer from the pipe surface. Table (4.5) simplifies the relationship between the horizontal and vertical permeabilities of the backfill with respect to the permeability of the seabed for different anisotropy ratios.

| | $K_{th}/K_{tv}=1$ | | $K_{th}/K_{tv}=10$ | | $K_{th}/K_{tv}=50$ | |
|---|---|---|---|---|---|---|
| **Permeability ratio** | $K_{th}$ | $K_{tv}$ | $K_{th}$ | $K_{tv}$ | $K_{th}$ | $K_{tv}$ |
| $K_t=K_s$ | $K_s$ | $K_s$ | $K_s$ | $0.1\ K_s$ | $K_s$ | $0.02\ K_s$ |
| $K_t=10\ K_s$ | $10\ K_s$ | $10\ K_s$ | $10\ K_s$ | $K_s$ | $10\ K_s$ | $0.2\ K_s$ |
| $K_t=100\ K_s$ | $100\ K_s$ | $100\ K_s$ | $100\ K_s$ | $10\ K_s$ | $100\ K_s$ | $2\ K_s$ |
| $K_t=1000\ K_s$ | $1000\ K_s$ | $1000\ K_s$ | $1000\ K_s$ | $100\ K_s$ | $1000\ K_s$ | $20\ K_s$ |

Table 4.5 Horizontal and vertical permeabilities of the backfill with respect to the permeability of the seabed at different anisotropic ratios.

- The distance "d" shown in Figure (3.1) representing the position of the pipe center from the top surface was not kept constant as the trench size changed, as the pipe was always placed in either the middle (d=H/2) or the bottom (d=H-r) of the trench, (H/d was kept constant for each case).

#### 4.3.3.1 Backfill with different Anisotropic Conditions

The results for a (4rx4r) square trench, where the pipe is in the middle of the trench has been chosen to be presented in this section of the study as they represent a median case. Figure (4.2) shows the isotherms when the permeability ratio of the backfill to the seabed is 1000 ($K_t$= 1000 $K_s$) for different anisotropic ratios and Rayleigh numbers represented by the pipe temperature. The following can be noticed from the figure:

- For a given anisotropy ratio, as the temperature of the pipe increases and thus the Rayleigh number increases, the isotherms are clustered near the pipe indicating a region of high temperature gradients and high buoyancy.
- When the trench is isotropic ($K_{th}/K_{tv}$=1), more heat is lost from the pipe surface as convection dominated heat transfer is produced. This represents a case where the soil was just poured in the trench and did not settle yet so the vertical permeability was still high as well as the porosity of the soil giving a higher chance for flow in the vertical direction and thus more heat losses result.
- As the anisotropic ratio increases, the plume weakens because when the vertical permeability decreases as can be noted from Table (4.5), this provides resistance to the warm fluid flow vertically. This phenomenon happens because the flow

escaping from the voids in the vertical direction due to buoyancy effect resulting from the temperature difference between the pipe's surface and the surrounding fluid in the porous media.

- As the anisotropic ratio increases and, thus, the vertical permeability decreases, the plume is forced to spread laterally. This is because it becomes more difficult for the pore water flowing from the voids to move vertically as the resistance to flow increased in this direction and so it spreads out laterally thus reducing heat losses.

Figure (4.3) shows the heat transfer results in terms of the Rayleigh- Nusselt relation. The following is observed from the graph:

- For a given anisotropy ratio, as the temperature of the pipe increases and thus the Rayleigh number (Ra) increases, more heat is lost to the surrounding soil giving rise to higher heat transfer. The higher temperature difference results in a higher density difference between the fluid in the porous medium adjacent to the pipe and the surrounding stagnant fluid and so more buoyancy force is generated, inducing more fluid motion and higher convective heat transfer.
- Nusselt number (Nu) decreases as the anisotropic ratio decreases as heat losses decrease; as explained before for Figure (4.2).

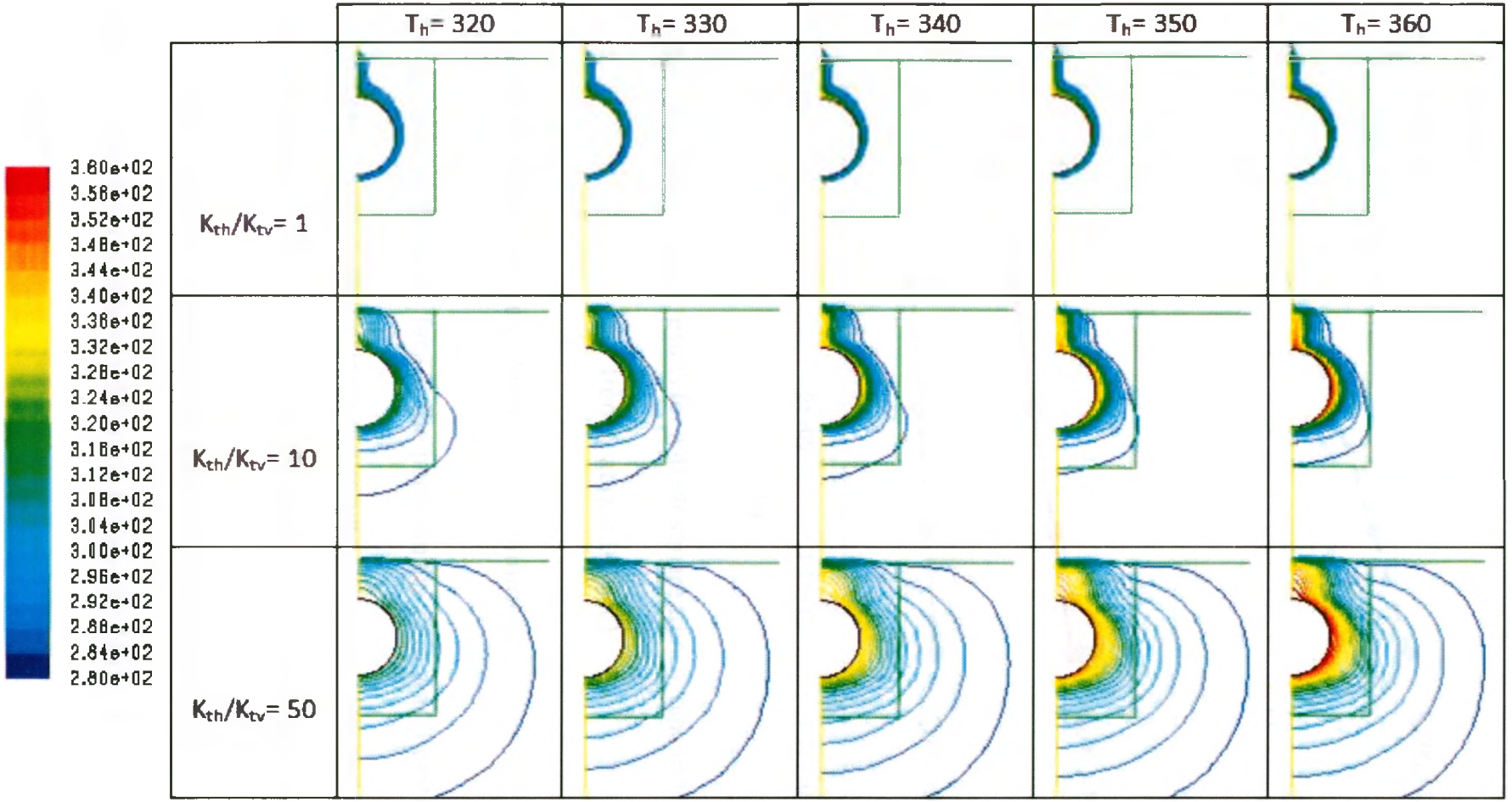


Figure 4.2 Isotherms for a 4rx4r square trench at different anisotropic ratios and $T_h$ values for ($K_t$= 1000 $K_s$).

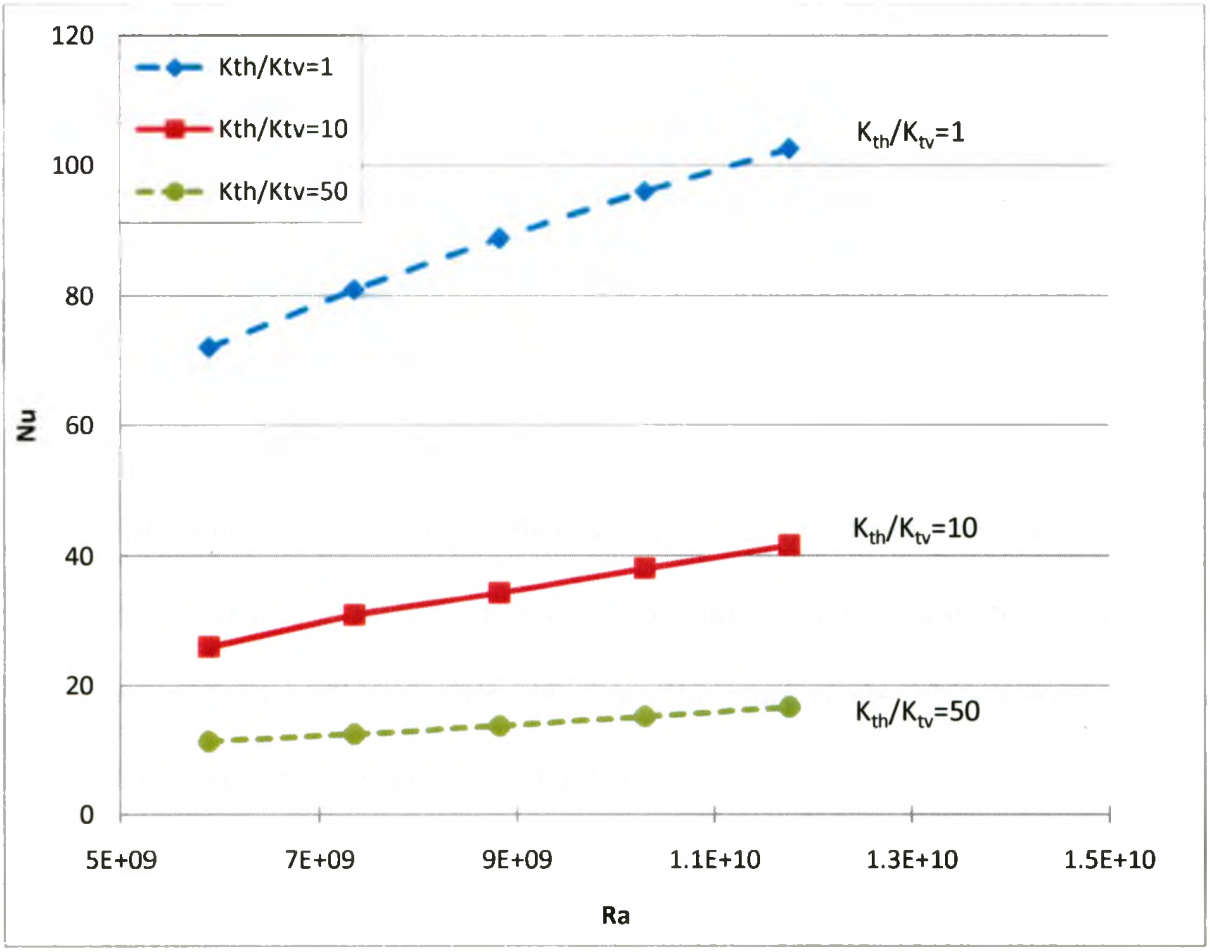


Figure 4.3 Heat transfer results for a 4rx4r square trench, pipe in the middle of the trench, at ($K_t$= 1000 $K_s$).

### 4.3.3.2 Backfill with Different Permeability Conditions

In the present study, the effect of the permeability ratio was investigated for all other flow and geometric conditions only the results for a pipe trenched in a (4rx4r) square trench, when the pipe is placed in the middle of the trench will be shown.

Figure (4.4) shows the isotherms for different permeability ratios of the backfill with respect to that of the seabed at different anisotropic ratios. The following can be seen from the figure:

- For a given permeability ratio, when the vertical permeability decreases, it becomes difficult for water to flow vertically as the resistance to flow increases in this direction and so the plume is forced to spread laterally.
- For a given anisotropic ratio, for the case when the pipe is first backfilled and the ratio between the backfill's permeability and the seabed permeability is really high ($K_t$= 1000 $K_s$) and the porosity is also high, it becomes easy for water to flow from the voids due to its high velocity resulting from the lower hydraulic resistance and so higher convected heat is produced compared to that produced by conduction. This is noticeable from the more clustered isotherms near the pipe indicating a region of high buoyancy.

  For the case representing complete settlement of the backfill until its permeability becomes equal to the permeability of the seabed ($K_t$= $K_s$) as both are of the same porous material, it becomes more difficult for water to flow from the voids and so conduction heat transfer is the predominant mode of heat transfer. This is noticeable from the more spread out isotherms at ($K_t$= $K_s$).

Figure (4.5) shows the Rayleigh-Nusselt relation for the case when the backfill is isotropic ($K_{th}/K_{tv}$=1), the higher the permeability and the porosity of the backfill, the higher Nusselt number values are produced. The reason for this was explained in the previous paragraph. Also as Rayleigh number increases, Nusselt number values increase and this was explained before for Figure (4.3).

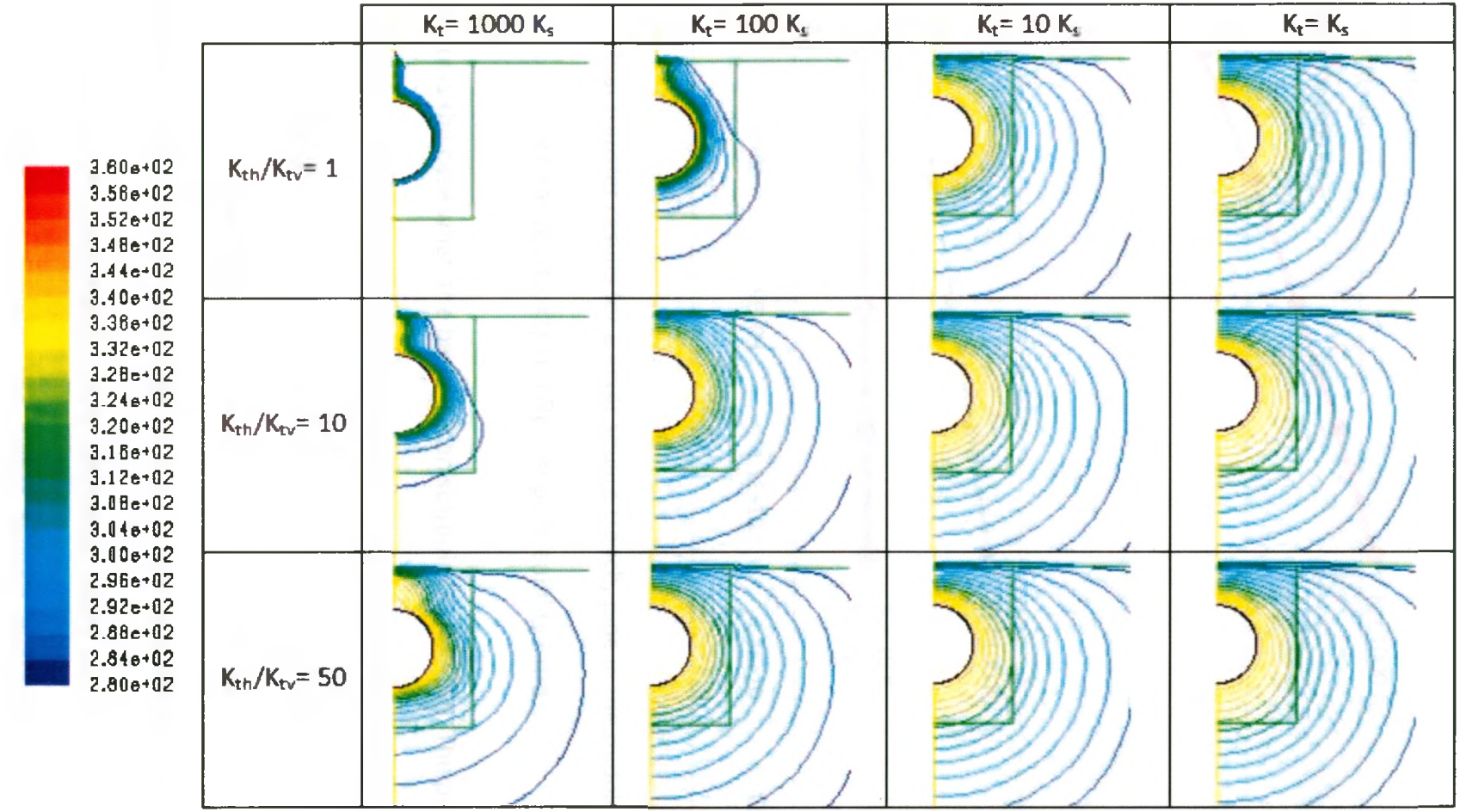


Figure 4.4 Isotherms for a 4rx4r square trench at different anisotropic ratios and permeability anisotropy ratios at $T_h$=340 K.

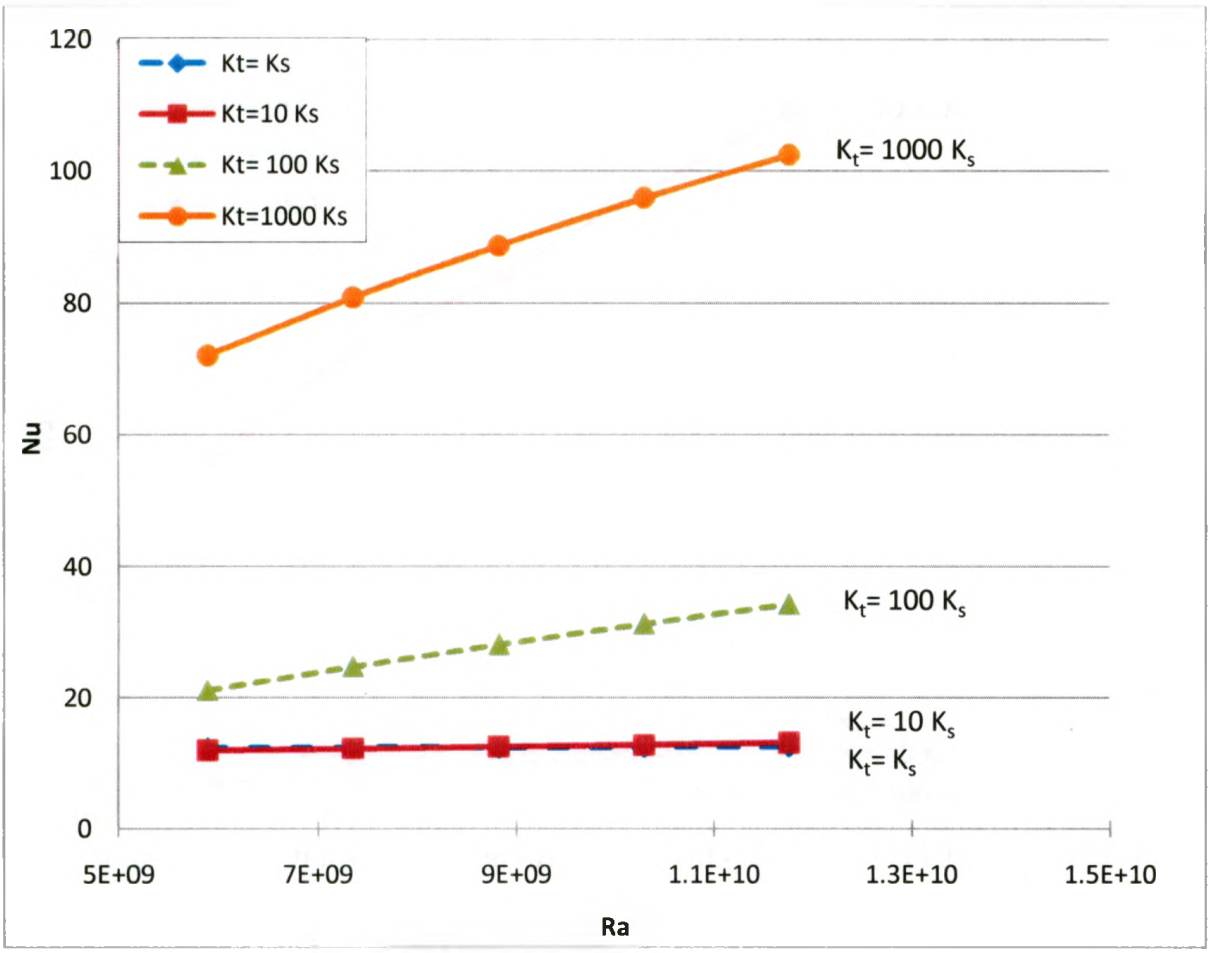


Figure 4.5 Heat transfer results for a 4rx4r square trench, pipe in the middle of the trench for ($K_{th}/K_{tv}$=1) at different permeability ratios.

Figure (4.6) shows the case when the backfill is anisotropic ($K_{th}/K_{tv}$=10). The permeability ratio of $K_t$= 1000 $K_s$ is still high enough for producing high convection heat transfer. As the permeability ratio decreases, the vertical permeability of the backfill becomes very low making it difficult for the fluid to carry heat away from the pipe and flow vertically. At low Rayleigh numbers, conduction heat transfer is the predominant heat transfer mode meaning that as the permeability ratio decreases, more soil solid is available to conduct heat, and thus this explains the higher Nusselt number values for lower permeability ratios.

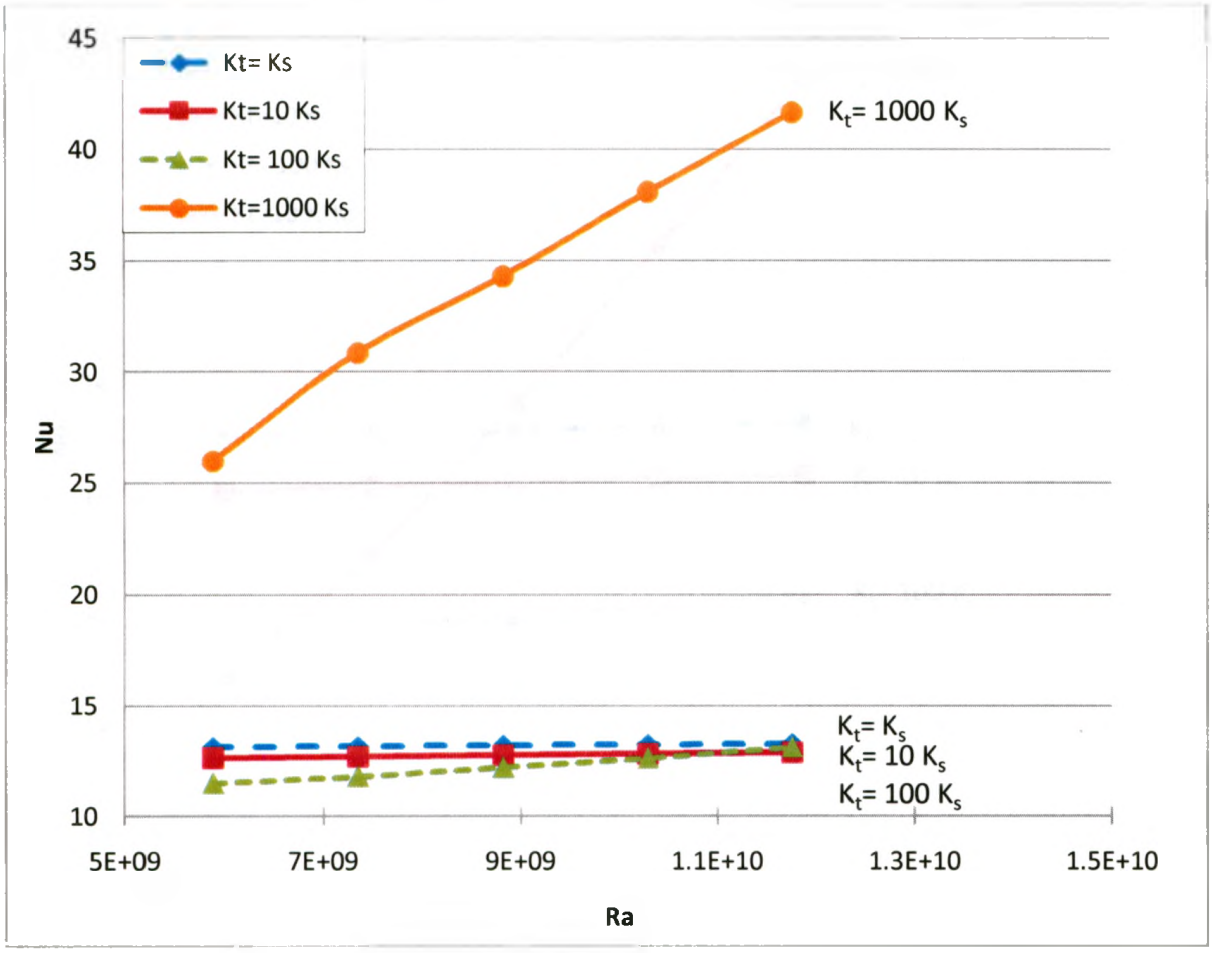


Figure 4.6 Heat transfer results for a 4rx4r square trench, pipe in the middle of the trench for ($K_{th}/K_{tv}$=10) at different permeability ratios.

Figure (4.7) shows the case when the backfill is anisotropic ($K_{th}/K_{tv}$=50). At low Rayleigh numbers, conduction is the only mode of heat transfer taking place. At high permeability ratio and high porosity, less soil solid is available to conduct heat and so less heat transfer and lower Nusselt number will be produced. Also as can be noticed from the same figure, as the Rayleigh number increases, the permeability ratio of $K_t$= 1000 $K_s$, starts producing higher Nusselt numbers as convection initiates and keeps increasing.

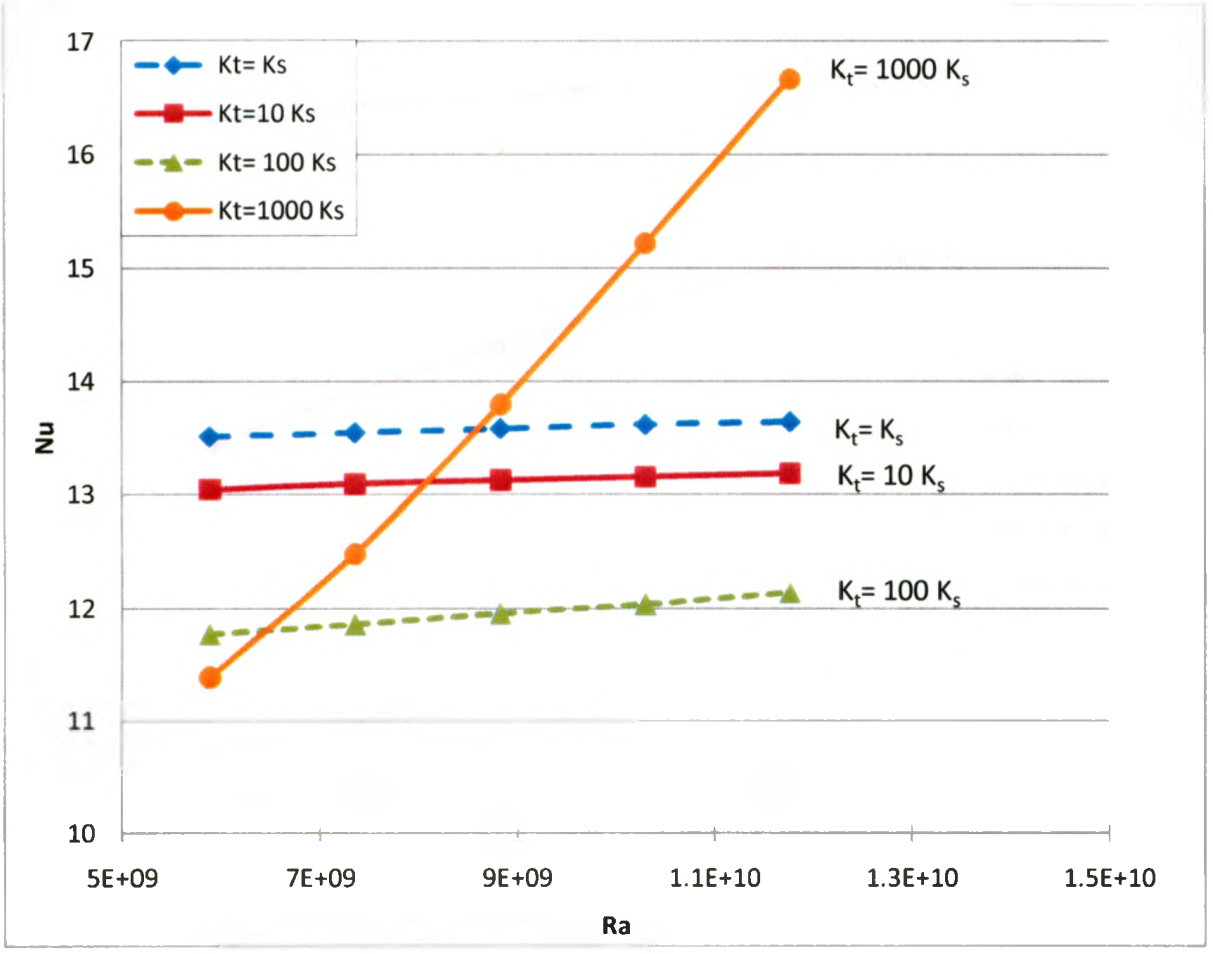


Figure 4.7 Heat transfer results for a 4rx4r square trench, pipe in the middle of the trench for ($K_{th}/K_{tv}$=50) at different permeability ratios.

Figure (4.8) shows the case where highest heat transfer takes place for each of the permeability ratios and this occurs as discussed before when the backfill is isotropic. It also shows the worst case scenario, when the pipe is not backfilled at all and sea water is completely free to carry heat away from the isothermal pipe and rise in the vertical direction. This is the case that gives the highest Nusselt numbers of all as it represents unrestricted free convection.

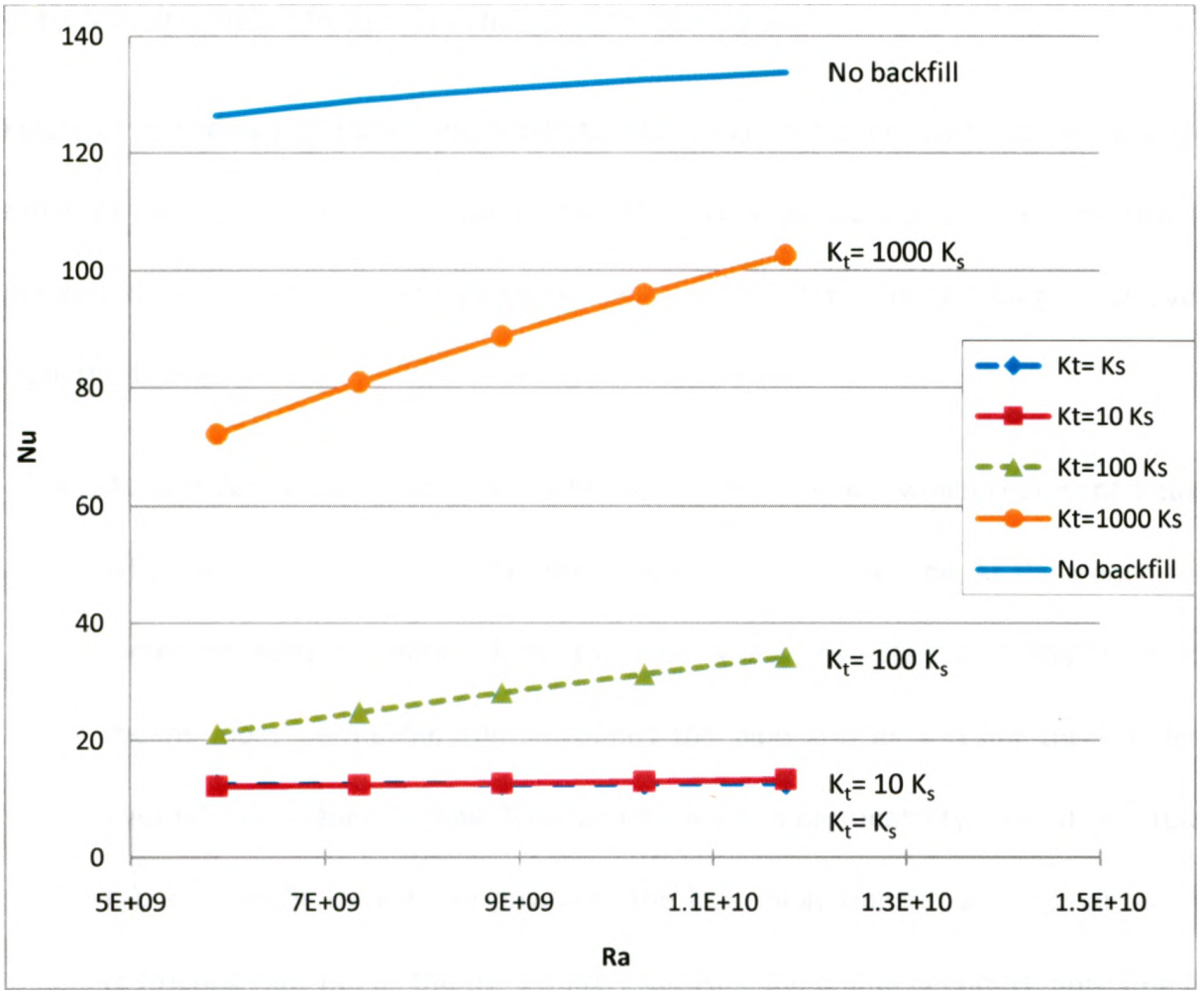


Figure 4.8 Heat transfer results for a 4rx4r square trench, pipe in the middle of the trench for ($K_{th}/K_{tv}$=1) at different permeability ratios and in the case of the pipe not backfilled.

As can be noticed from the graphs of all the previous cases, that the curve for ($K_t$= 1000 $K_s$) is always steep indicating that convection is predominant meaning as the Rayleigh number increases, higher Nusselt numbers are produced. But at lower permeability ratios, conduction is predominant and this is indicated by the near horizontal curves.

4.3.3.3 Heat transfer Results for Different Trench Sizes

Figure (4.9) shows the isotherms results for the range of trench sizes examined at the range of permeability ratios adopted when the soil is isotropic ($K_{th}/K_{tv}$=1). The results presented are for a pipe outer coating temperature of 340 K. The following is observed from the figure:

- At high permeability ratios ($K_t$= 1000 $K_s$) and ($K_t$= 100 $K_s$), which represent a case when soil is first poured in the trench as a backfill for the pipe, as the trench size increases, heat dissipation from the pipe is less restricted as a bigger trench means more permeable soil surrounds the pipe and as a result there is less hydraulic resistance to flow. This can be seen at a permeability ratio of ($K_t$= 1000 $K_s$), a 2.5rx2.5r trench size produces the least heat transfer as its small size is restricting flow but as the trench size increases, the plume becomes more free to form and more heat losses result, this trend is more clear in Figures (4.10) & (4.11).
- For a given trench size, as the permeability ratio decreases and the backfill soil permeability decreases, less heat is lost from the pipe as the hydraulic resistance increases. For the case representing when the pipe is first backfilled ($K_t$= 1000 $K_s$), the permeability of the backfill is high allowing for convective heat losses but for the case representing full settlement of the backfill soil ($K_t$= $K_s$), conduction becomes the predominant mode of heat transfer.

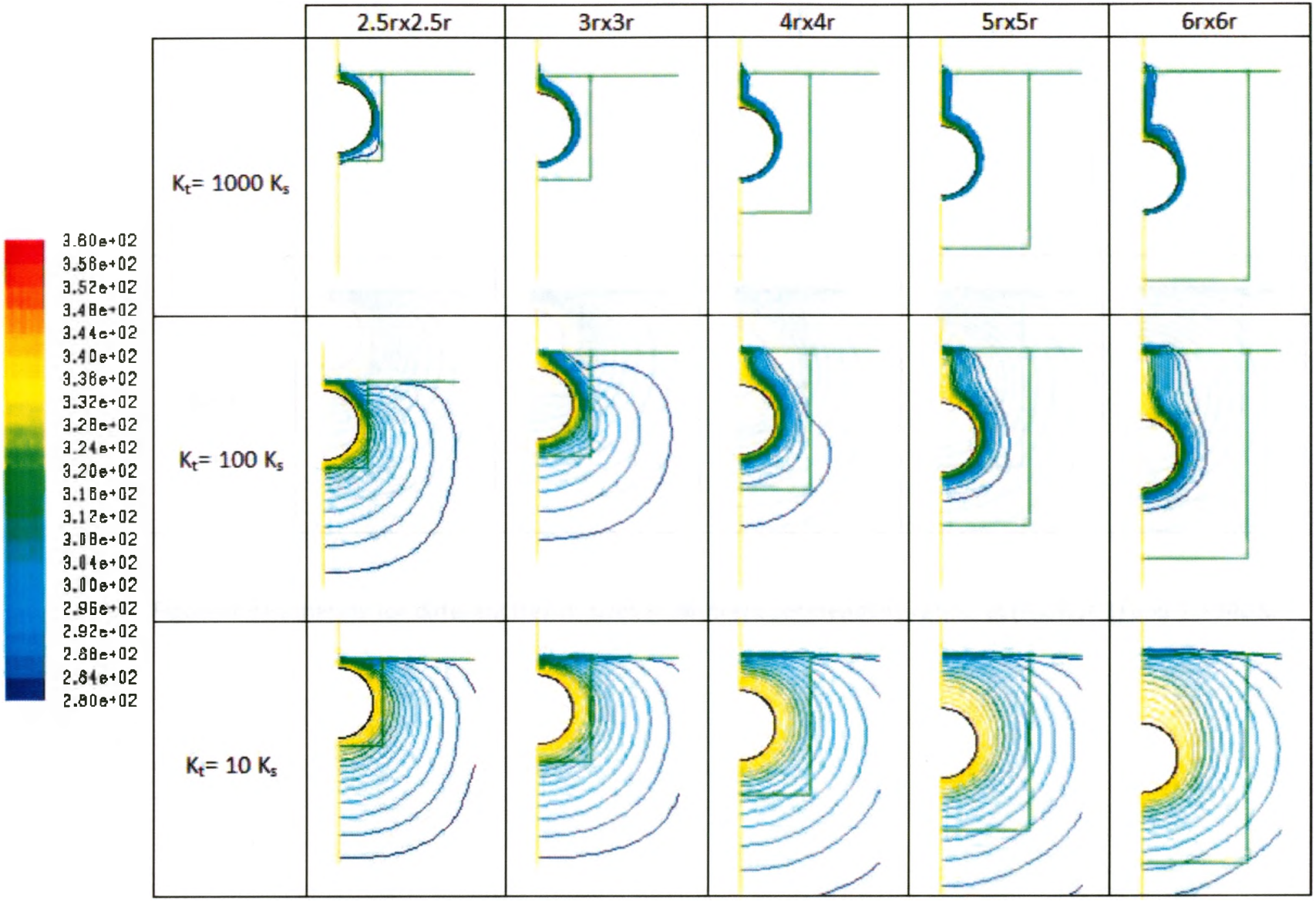
2.5rx2.5r
3rx3r
4rx4r
5rx5r
6rx6r
$K_t$= 1000 $K_s$
$K_t$= 100 $K_s$
$K_t$= 10 $K_s$
3.60e+02
3.56e+02
3.52e+02
3.48e+02
3.44e+02
3.40e+02
3.36e+02
3.32e+02
3.28e+02
3.24e+02
3.20e+02
3.16e+02
3.12e+02
3.08e+02
3.04e+02
3.00e+02
2.96e+02
2.92e+02
2.88e+02
2.84e+02
2.80e+02

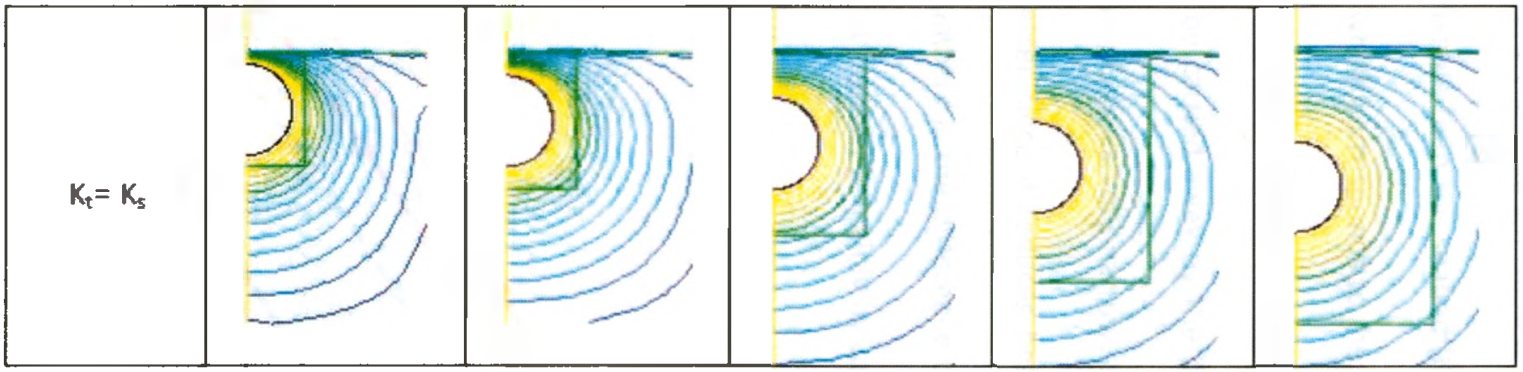


Figure 4.9 Isotherms for different trench sizes at different permeability ratios, at ($K_{th}/K_{tv}$= 1) and $T_h$=340 K.

Figures (4.10) and (4.11) show the Rayleigh-Nusselt relationship, for the case where the trench is much more permeable than the seabed ($K_t$=1000 $K_s$) and ($K_t$=100 $K_s$), and the soil is isotropic ($K_{th}/K_{tv}$=1), which corresponds to the case where the soil is first backfilled into the trench. As the trench size increases, the more permeable soil surrounding the pipe allows more heat to be carried away by the flowing fluid producing high Nusselt numbers. Since the thermal plume is very narrow, a large trench will have little effect, and a smaller trench is better since it reduces heat losses. Also noticeable in Figure (4.11), for low Rayleigh numbers is the difference between heat losses for a 2.5rx2.5r and 3rx3r is very low as heat transfer is mainly by conduction, thus showing a change in the heat transfer mechanism.

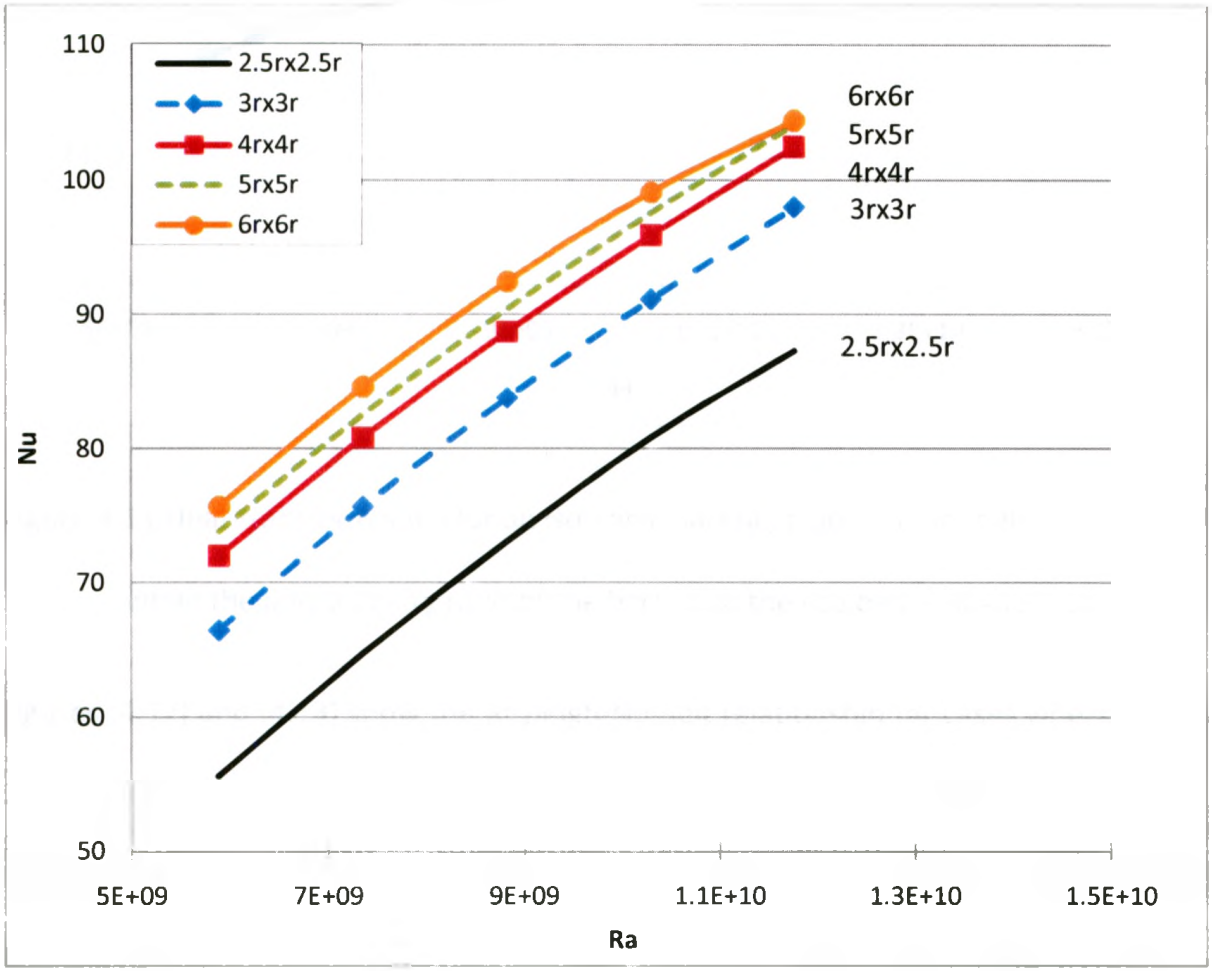

Figure 4.10 Heat transfer results for an isotropic backfill, pipe in the middle of the trench when the permeability ratio of the backfill to the sea bed is ($K_t$=1000 $K_s$).

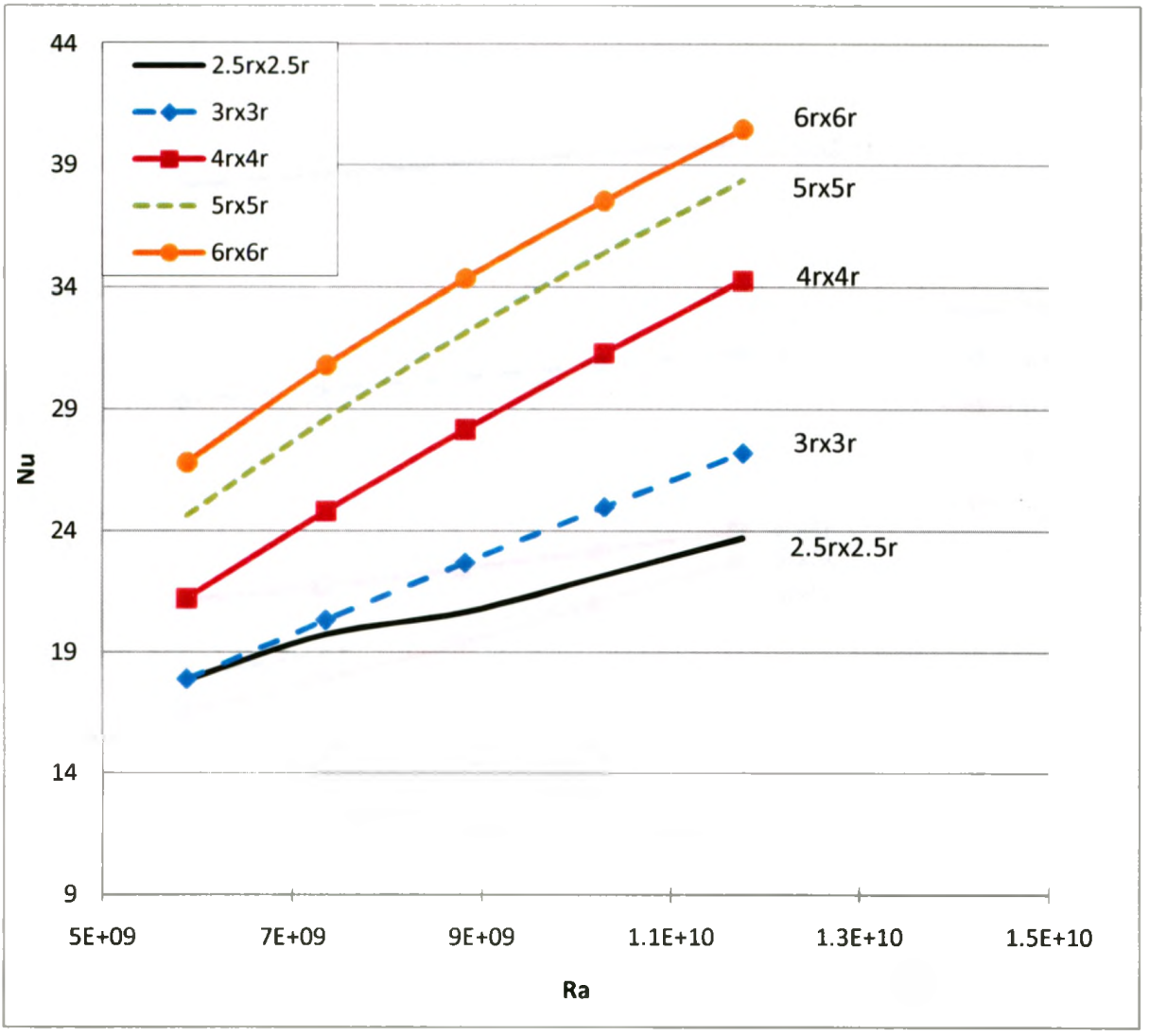


Figure 4.11 Heat transfer results for an isotropic backfill, pipe in the middle of the trench when the permeability ratio of the backfill to the sea bed is ($K_t$=100 $K_s$).

Figures (4.12) and (4.13) show the Rayleigh-Nusselt relationship for cases where the soil in the trench has completely settled i.e. at permeability ratios of ($K_t$=10 $K_s$) and ($K_t$=$K_s$) respectively. In these cases as the trench size increases, the water flow from the voids follow longer path to escape to the fluid layer as the pipe gets deeper in the trench as its

size increases and thus heat transfer is suppressed and this is expressed by the decreasing Nusselt number as the trench size increases.

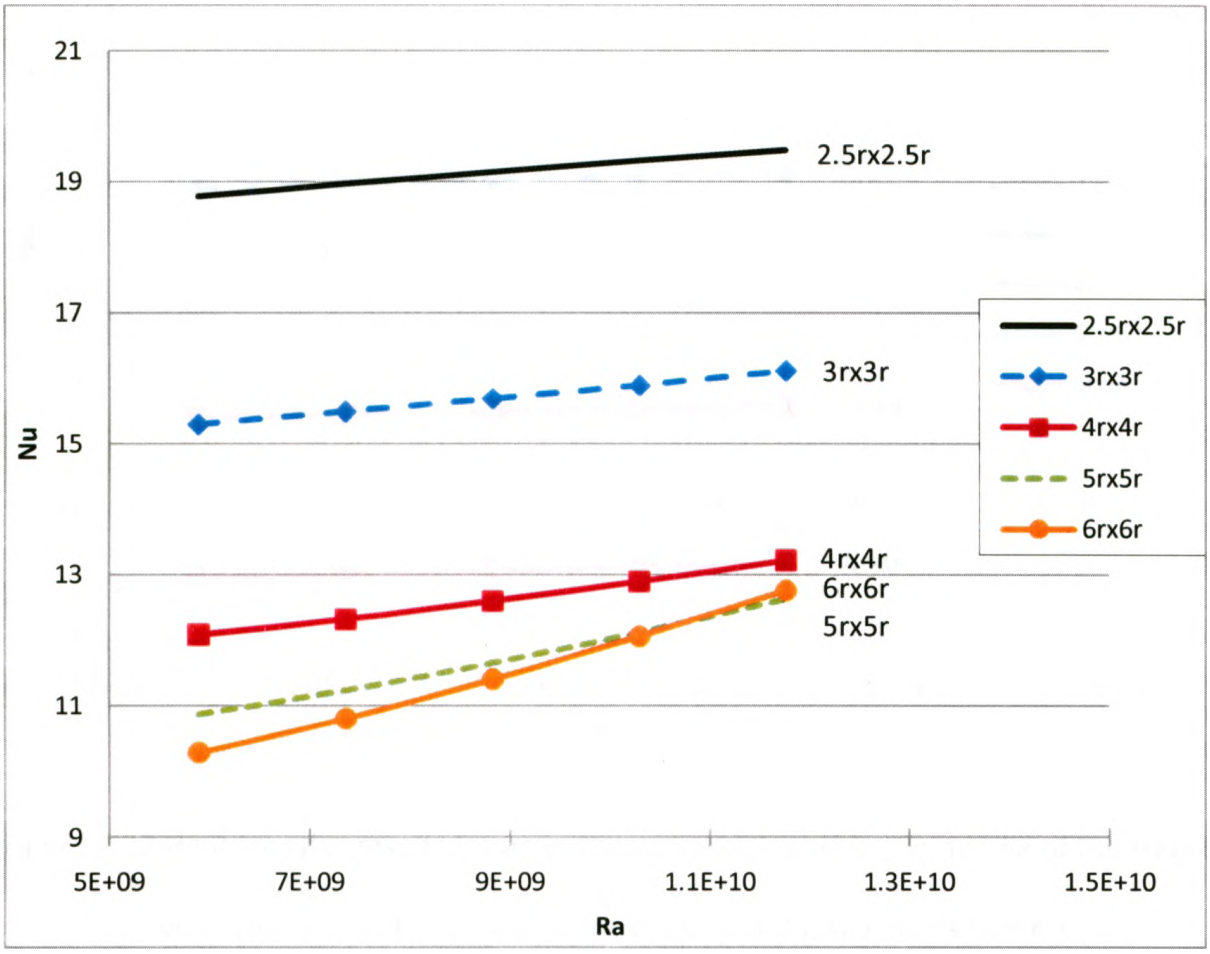


Figure 4.12 Heat transfer results for an isotropic backfill, pipe in the middle of the trench when the permeability ratio of the backfill to the sea bed is ($K_t$=10 $K_s$).

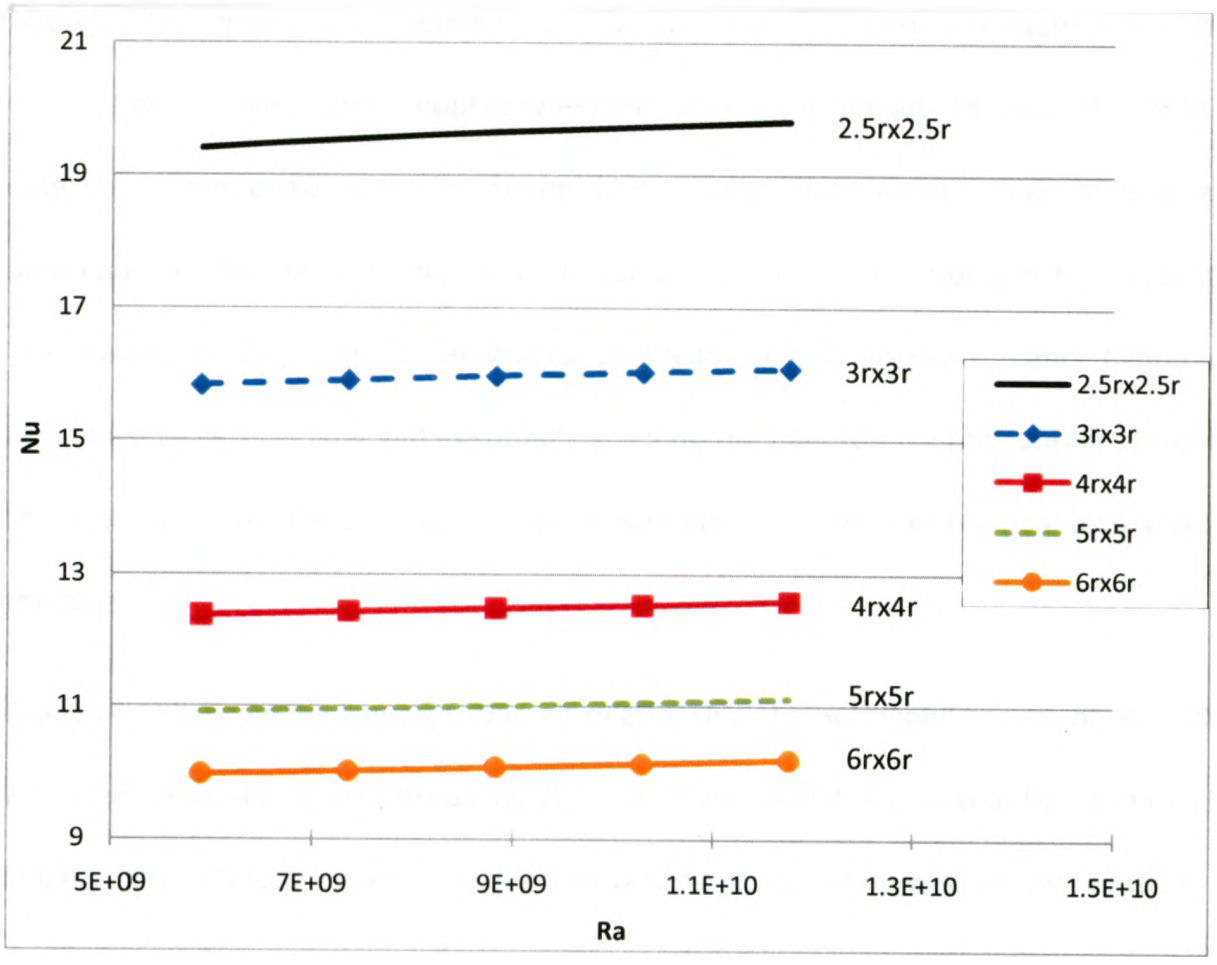


Figure 4.13 Heat transfer results for an isotropic backfill, pipe in the middle of the trench when the permeability ratio of the backfill to the sea bed is ($K_t$= $K_s$).

Figure (4.14) shows the isotherms results for the range of trench sizes examined at the range of permeability ratios adopted when the backfill is anisotropic ($K_{th}/K_{tv}$=10). For this case the same explanation for Figure (4.9) applies here except that, at a given permeability ratio the isotherms are more spread out than for the isotropic backfill case. The reason for this is the lower vertical permeability that results in higher hydraulic resistance to vertical flow and eventually allowing the fluid to flow horizontally carrying the heat away from the pipe forming wider isotherms. This reduces the heat losses from the pipe.

Figure (4.15) shows the Rayleigh- Nusselt relationship at a permeability ratio of ($K_t$=1000 $K_s$) when the backfill is anisotropic ($K_{th}/K_{tv}$=10). The permeability ratio of ($K_t$= 1000 $K_s$) is still high enough to overcome the effect of varying pipe position with respect to the top surface with increasing trench size, allowing for more heat to be lost and, thus, producing higher Nusselt number.

Figure (4.16) shows the Rayleigh- Nusselt relationship at a permeability ratios of ($K_t$=100 $K_s$) when the backfill is anisotropic ($K_{th}/K_{tv}$=10). In this case, the permeability ratio of ($K_t$= 100 $K_s$) follows the same trend followed by the lower permeability ratios ($K_2$= $K_1$) and ($K_2$= 10 $K_1$) in the isotropic case. In this case the vertical permeability becomes low to allow the fluid to flow vertically and overcome the effect of the varying pipe position.

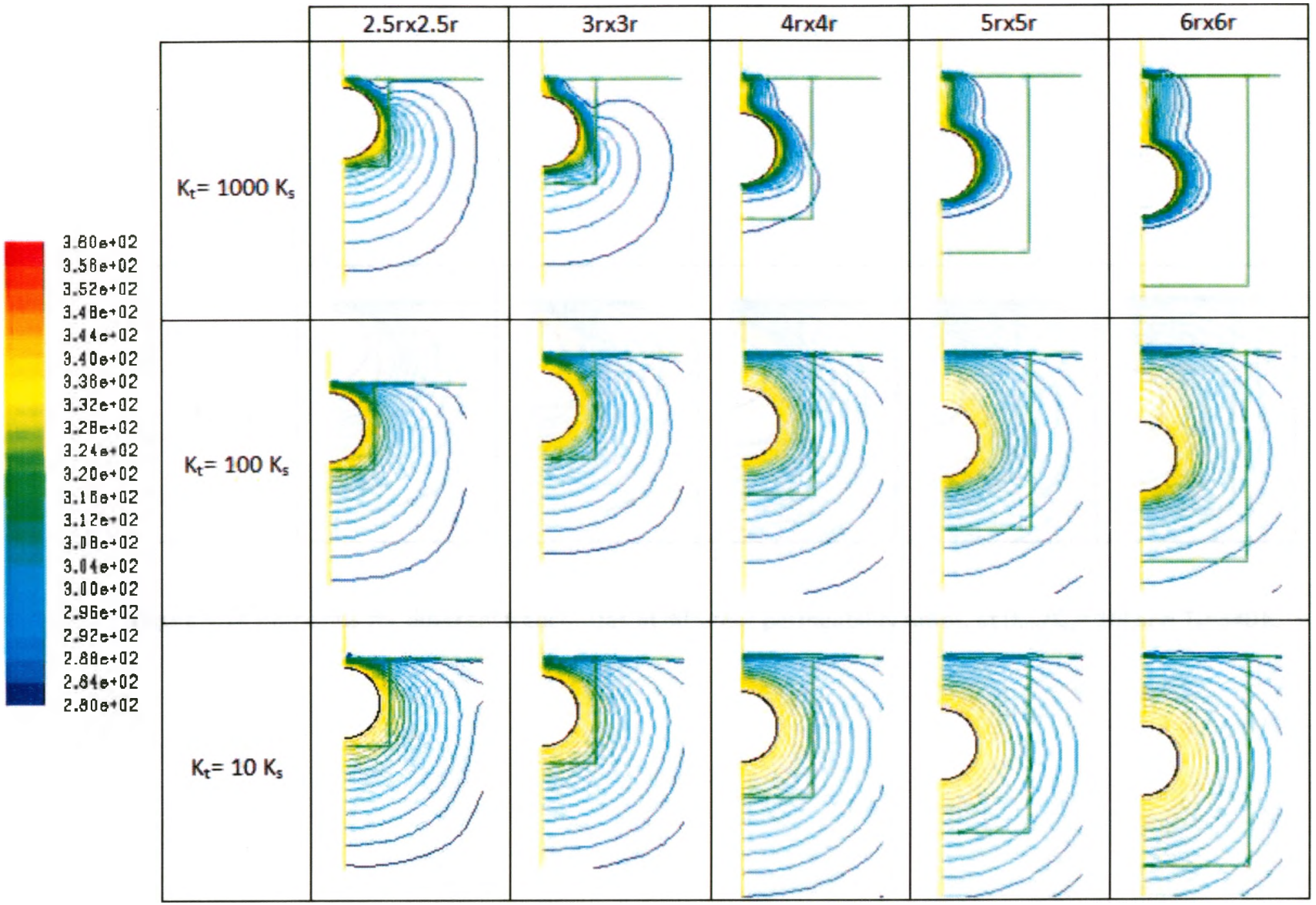
2.5rx2.5r
3rx3r
4rx4r
5rx5r
6rx6r
$K_t$= 1000 $K_s$
$K_t$= 100 $K_s$
$K_t$= 10 $K_s$
3.60e+02
3.56e+02
3.52e+02
3.48e+02
3.44e+02
3.40e+02
3.36e+02
3.32e+02
3.28e+02
3.24e+02
3.20e+02
3.16e+02
3.12e+02
3.08e+02
3.04e+02
3.00e+02
2.96e+02
2.92e+02
2.88e+02
2.84e+02
2.80e+02

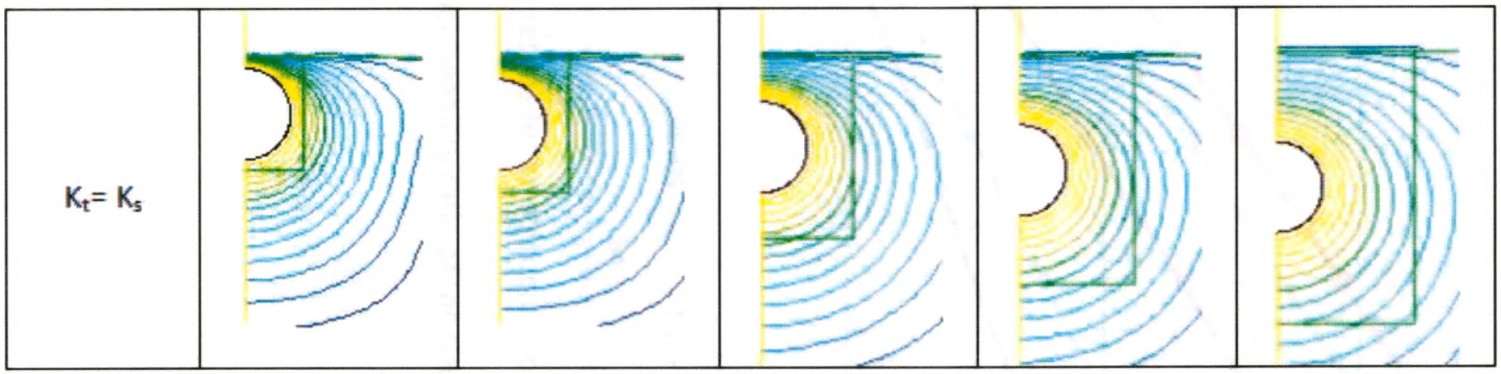


Figure 4.14 Isotherms for different trench sizes at different permeability ratios, at ($K_{th}/K_{tv}$= 10) and $T_h$=340 K.

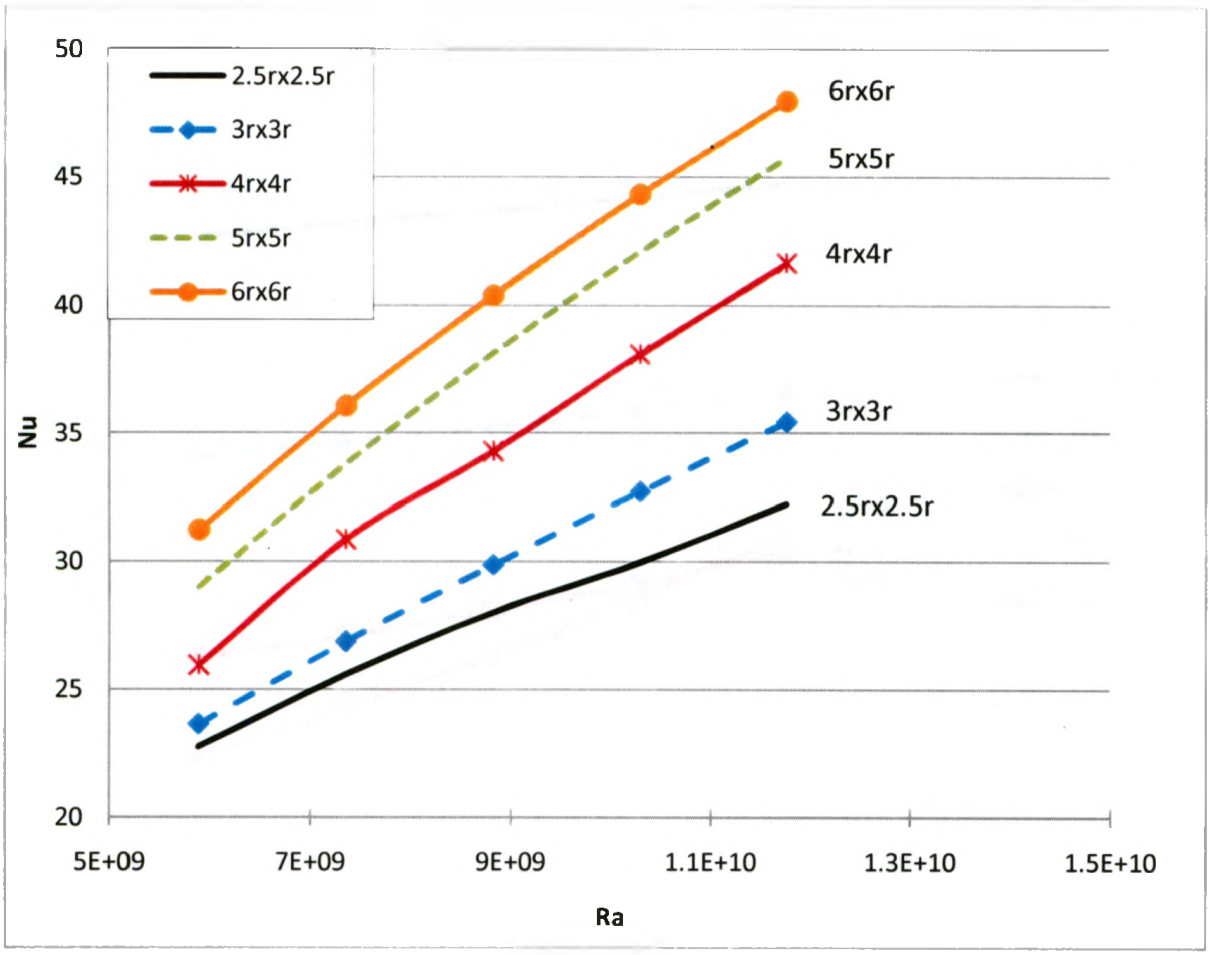


Figure 4.15 Heat transfer results for anisotropic backfill ($K_{th}/K_{tv}$=10), pipe in the middle of the trench when the permeability ratio of the backfill to the sea bed is ($K_t$=1000 $K_s$).

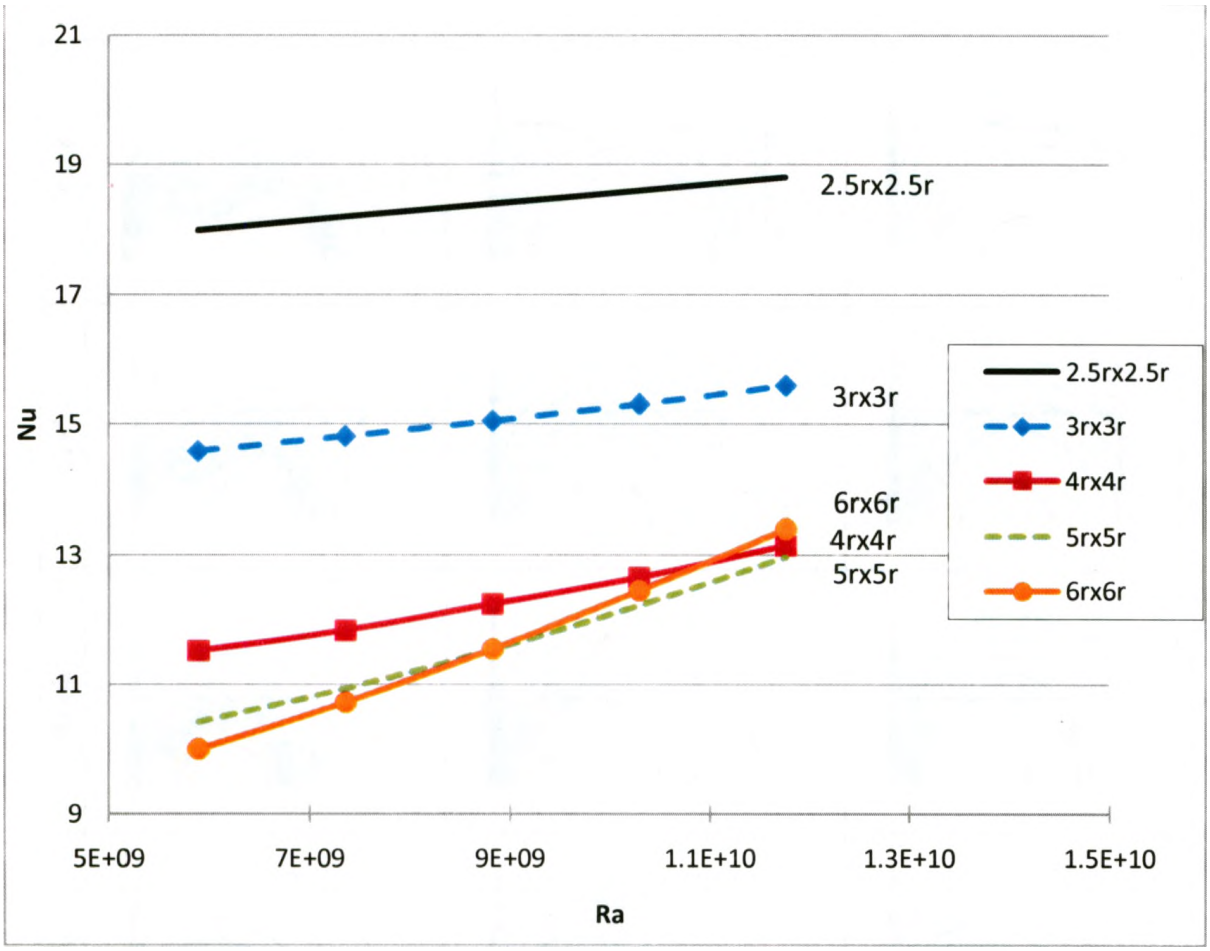


Figure 4.16 Heat transfer results for anisotropic backfill ($K_{th}/K_{tv}$=10), pipe in the middle of the trench when the permeability ratio of the backfill to the sea bed is ($K_t$=100 $K_s$).

Figure (4.17) shows the isotherms results for the range of trench sizes examined at the range of permeability ratios adopted when the backfill is anisotropic ($K_{th}/K_{tv}$=50). For this case at a given permeability ratio the isotherms are totally spread out in the porous regions than the two previous cases. The reason for this is that the vertical permeability gets to its lowest values making it difficult for the vertical dissipation of pore water and thus the pore water escapes laterally forming widely spread out isotherms.

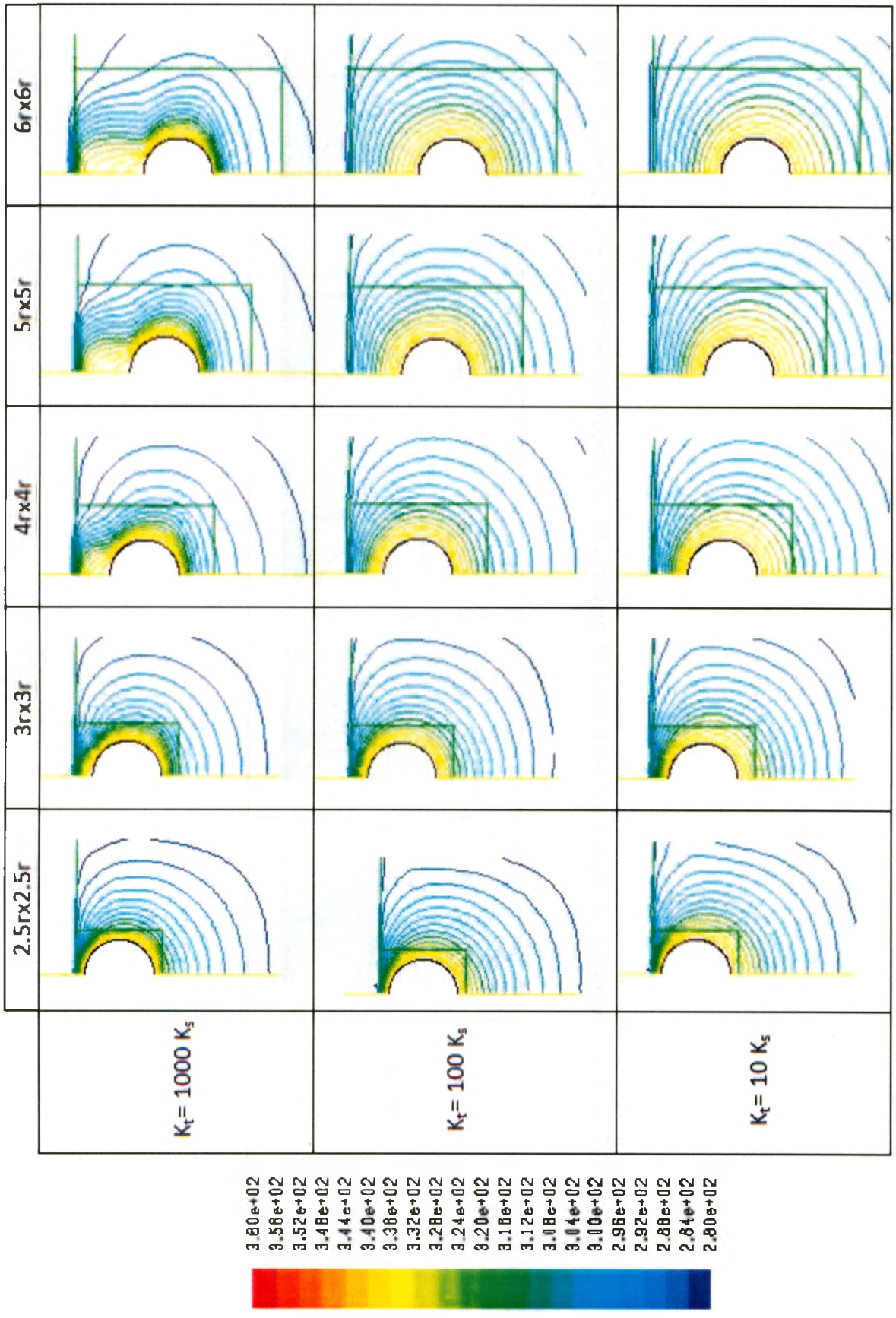
2.5rx2.5r
3rx3r
4rx4r
5rx5r
6rx6r
Kt= 1000 Ks
Kt= 100 Ks
Kt= 10 Ks
3.60e+02
3.56e+02
3.52e+02
3.48e+02
3.44e+02
3.40e+02
3.36e+02
3.32e+02
3.28e+02
3.24e+02
3.20e+02
3.16e+02
3.12e+02
3.08e+02
3.04e+02
3.00e+02
2.96e+02
2.92e+02
2.88e+02
2.84e+02
2.80e+02

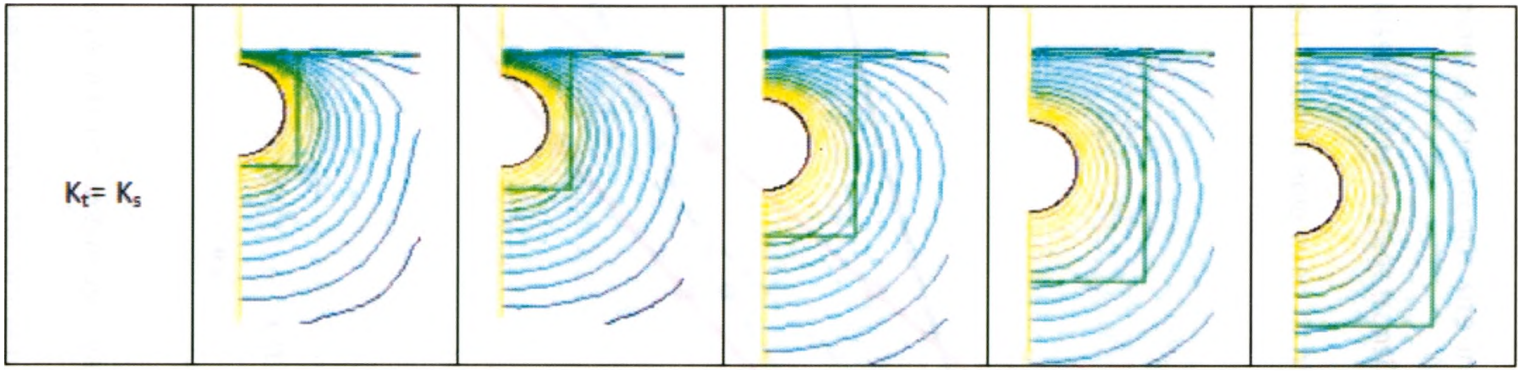


Figure 4.17 Isotherms for different trench sizes at different permeability ratios, at ($K_{th}/K_{tv}$= 50) and $T_h$=340 K.

The vertical permeability for all permeability ratios becomes too small to overcome the varying position of the pipe as the trench size increases. The bigger the trench, the deeper the pipe and the less convective heat transfer taking place, so producing a lower Nusselt number. This effect is applicable even at high permeability ratio of ($K_t$=1000 $K_s$) as shown in (4.18).

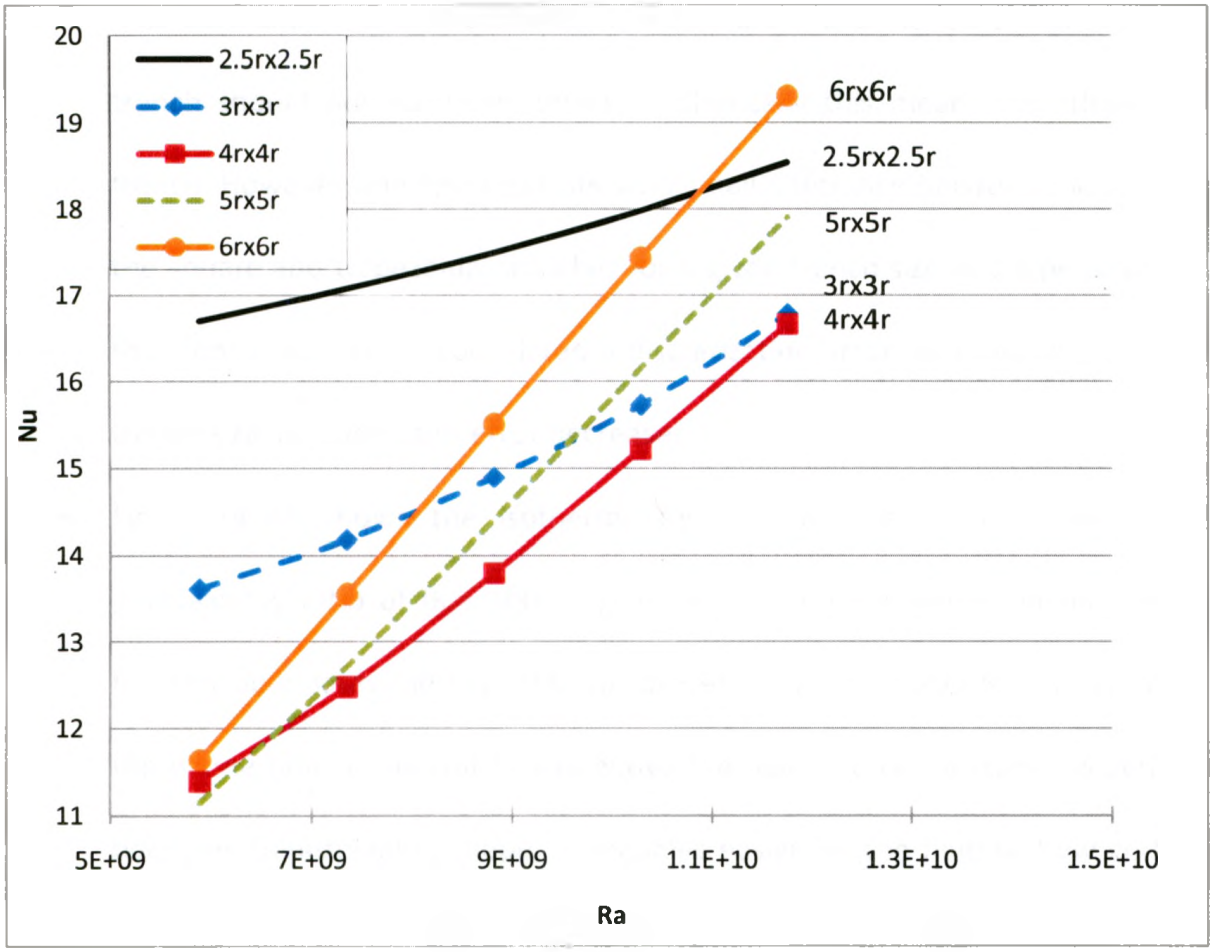


Figure 4.18 Heat transfer results for anisotropic backfill ($K_{th}/K_{tv}$=50), pipe in the middle of the trench when the permeability ratio of the backfill to the sea bed is ($K_t$=1000 $K_s$).

4.3.3.4 Heat Transfer Results for Different Trench Shapes

- Figure (4.19) shows the Nusselt number results for the smallest and biggest trench sizes, (2.5rx2.5r) & (6rx6r) respectively at each of the trench angles of 45° and 90° when the pipe is in the middle of the trench. These results are for permeability ratio of ($K_t$=$K_s$) and when the soil is isotropic ($K_{th}/K_{tv}$=1), meaning that both the seabed and the backfill soils are the same, so the shape of the trench should not have any effect as physically this means that there is no trench. However, the figure still shows a small difference between the results of the square and trapezoidal trenches for a given trench size and pipe position in the trench, and this is considered a discretization error. Also noted that as the trench size increases, this error decreases.
- Figure (4.20) shows the isotherms for the case of isotropic backfill and permeability ratio of ($K_t$= 1000 $K_s$), as this is the case where convection heat transfer dominates the heat transfer process. For the (2.5rx2.5r) square trench, the plume finds it difficult to rise above the pipe but as the trench widens and becomes trapezoidal in shape, it becomes easier for the fluid to flow vertically and form a plume. As the trench size increases, it becomes wider even in the case of square trenches and it becomes easier for the plume to escape.
- Figure (4.21) shows the Rayleigh-Nusselt results for the smallest and biggest trench sizes, (2.5rx2.5r) & (6rx6r) respectively at each of the trench angles of 45° and 90°. It shows that the difference in results between the square and the

trapezoidal trenches decreases when the trench size increases and thus the biggest difference in results occurs for a 2.5rx2.5r trench.

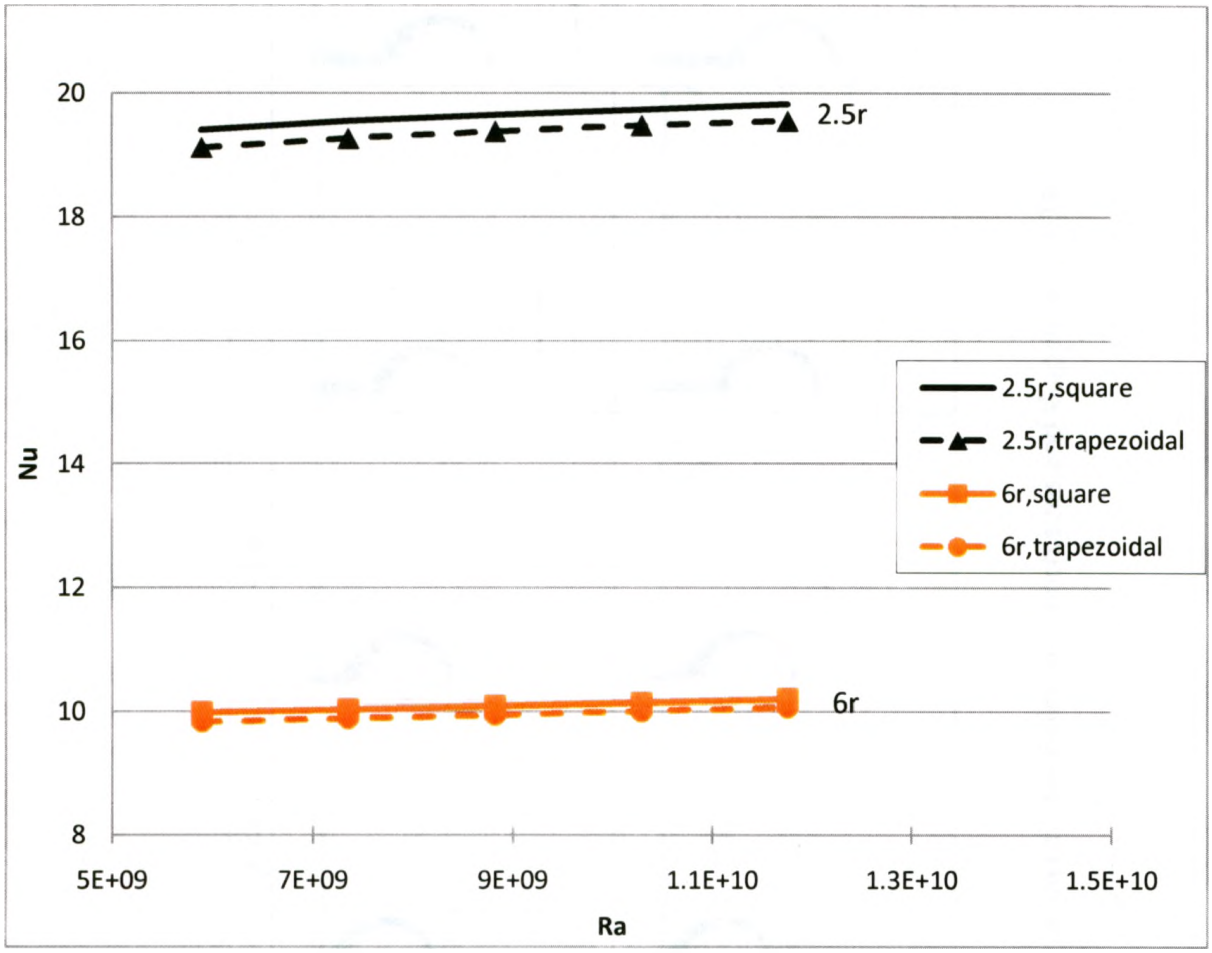


Figure 4.19 Discretization errors in the square and Trapezoidal trenches for the case of $(K_t=K_s)$ and $(K_{th}/K_{tv}=1)$.

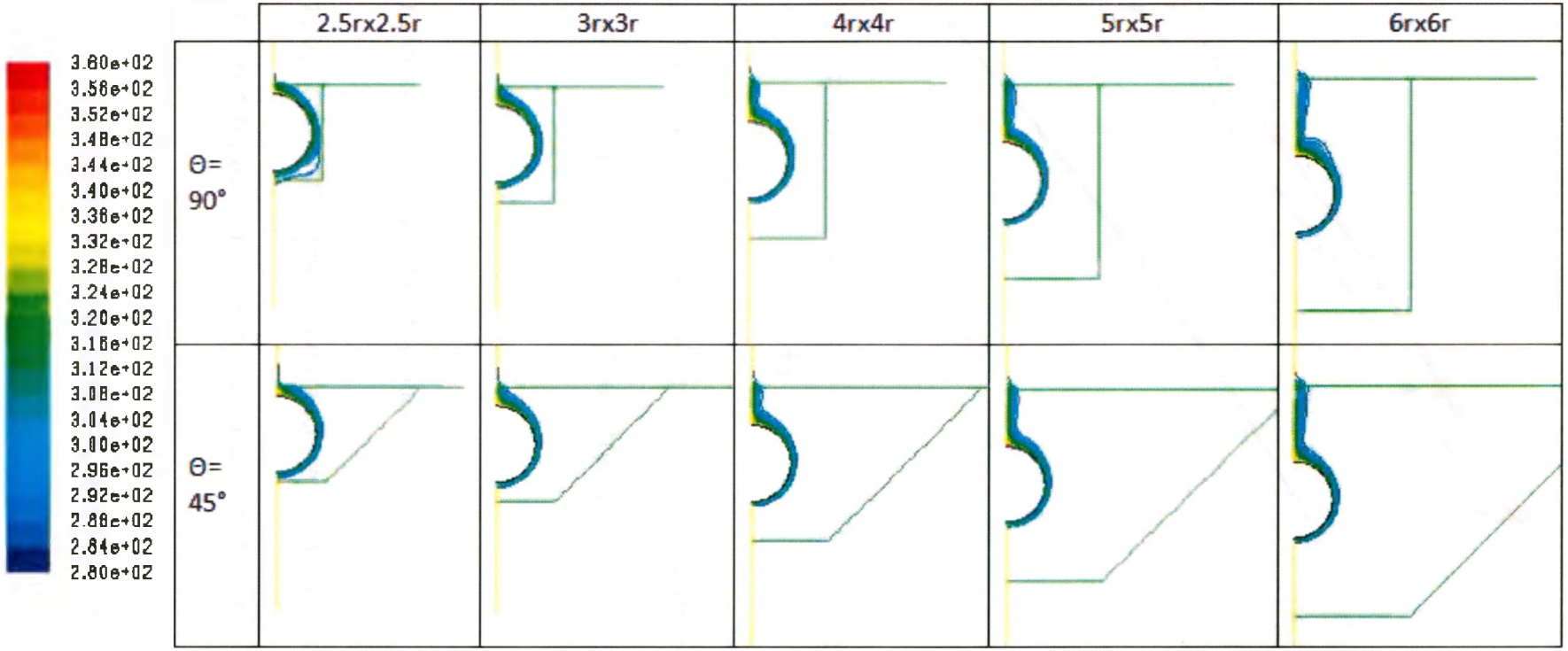


Figure 4.20 Isotherms for different trench sizes and shapes, at $T_h$= 340 K.

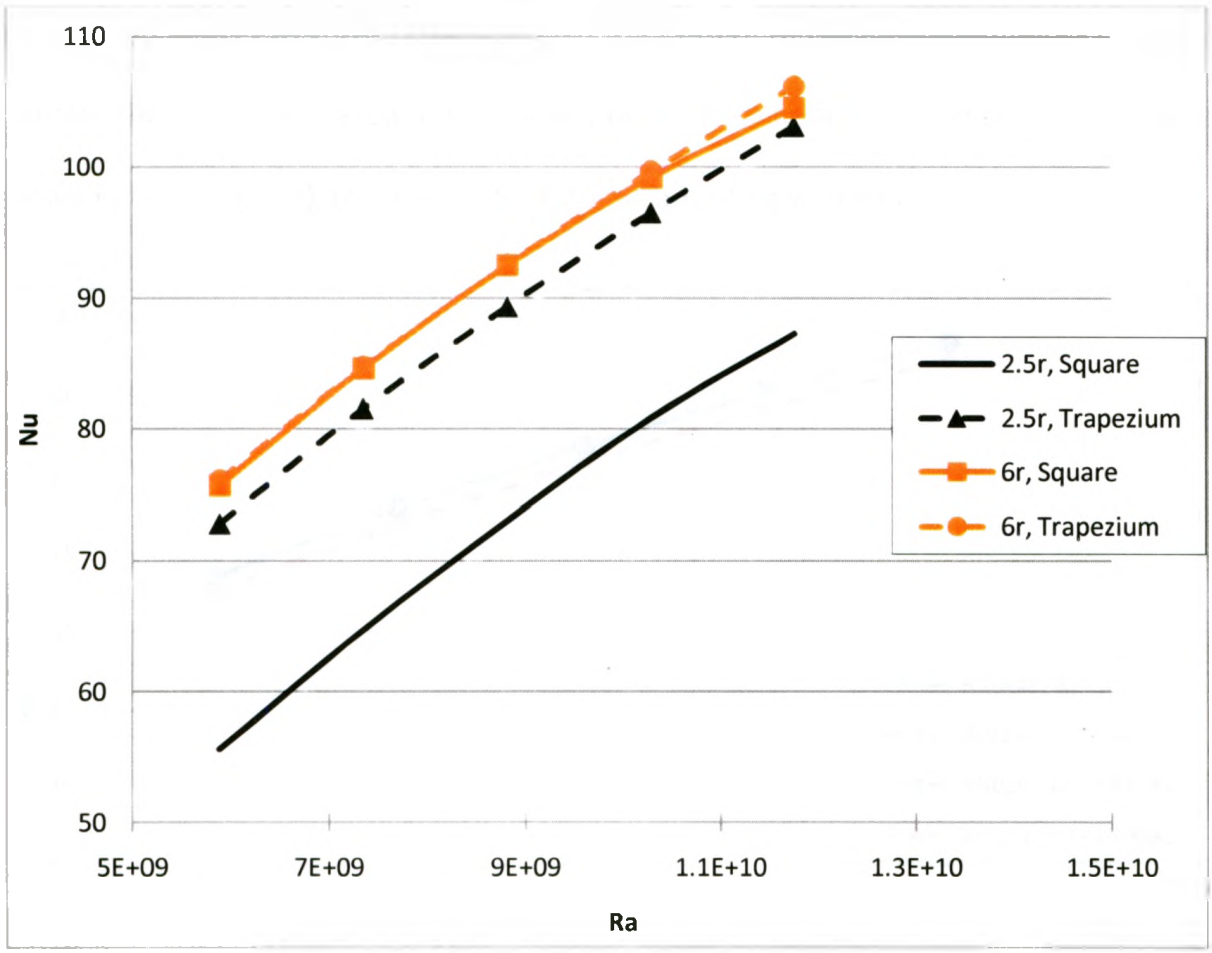


Figure 4.21 Difference in results between trenches with angles of 45° & 90° for (2.5rx2.5r) and (6rx6r) trenches.

### 4.3.3.5 Heat transfer results for varying the position of the pipe in the trench

In this study two positions for the pipe in the trench were investigated, these are middle and bottom of the trench positions. The investigation on the position of the pipe was carried out for all the range of flow and geometric parameters but only results for a (4rx4r) square trench at permeability ratios of ($K_t$= $K_s$) and ($K_t$= 1000 $K_s$) will be shown in this section, as it is representative of all results.

The current study has shown that a pipe in the bottom of the trench produces less heat transfer than the one placed in the middle of the trench, but this effect is negligible as shown in Figures (4.22), (4.23) and (4.24) for all anisotropy ratios.

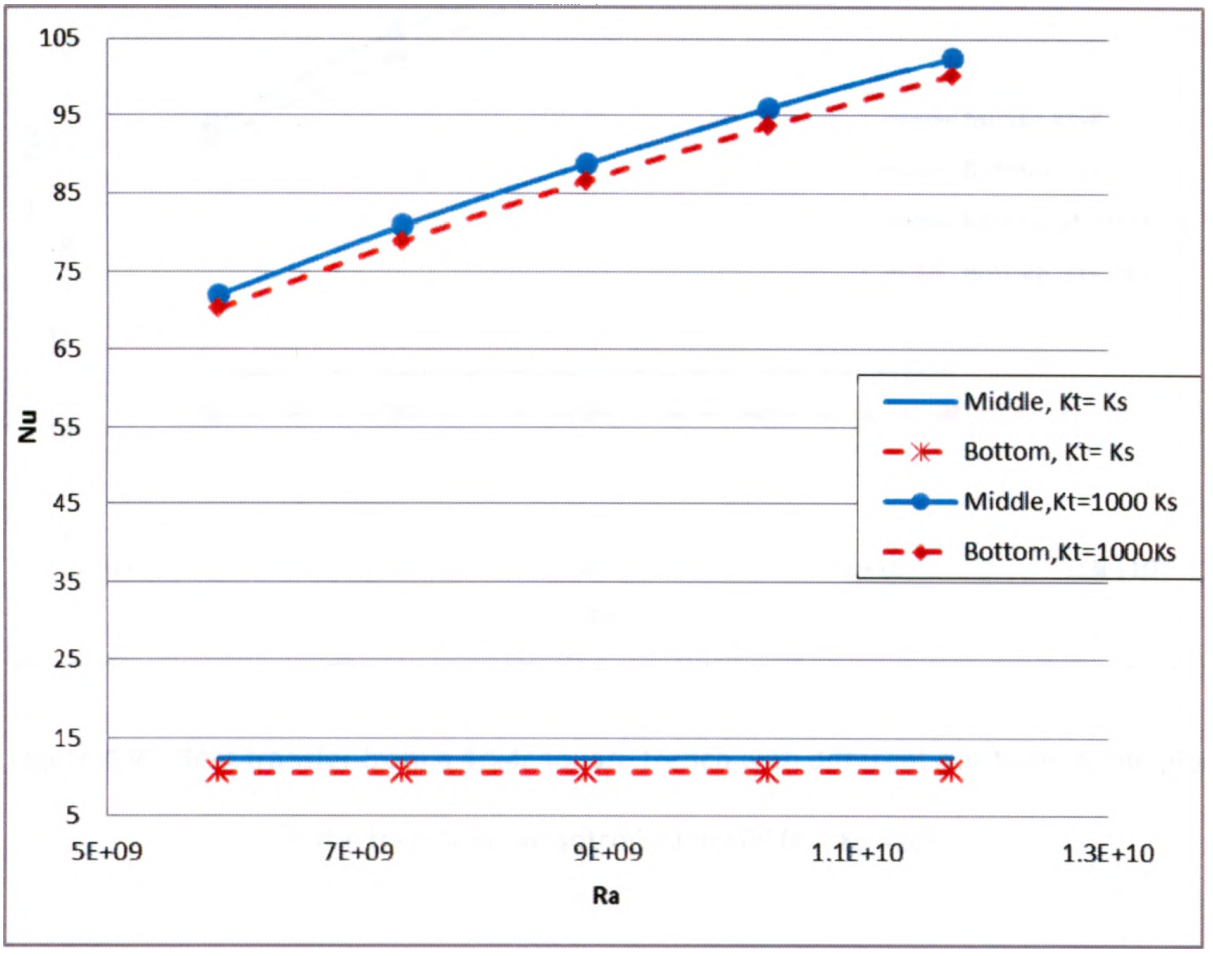


Figure 4.22 Heat transfer from a 4rx4r square trench with different positions of the pipe in the trench for isotropic backfill ($K_{th}/K_{tv}$=1).

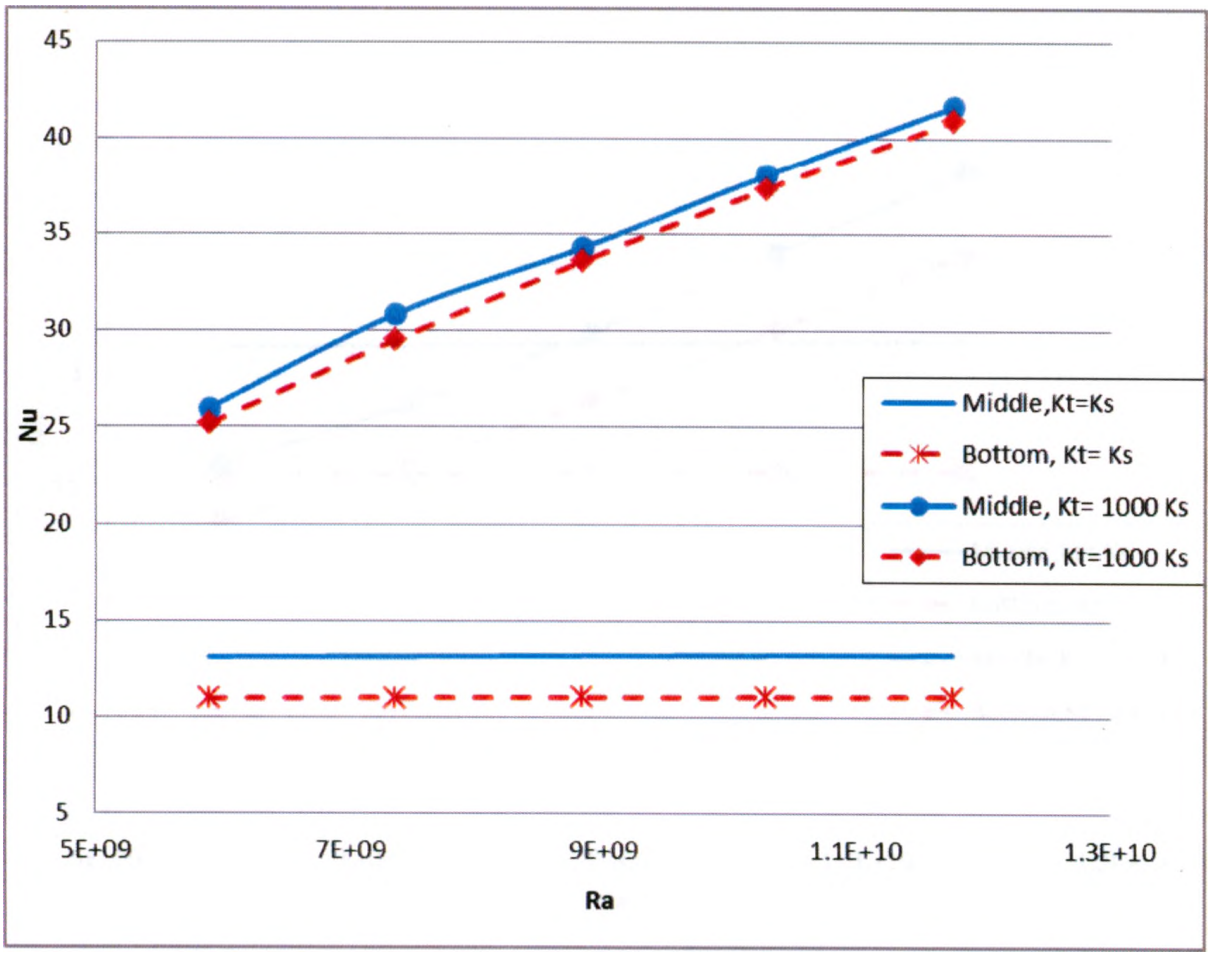


Figure 4.23 Heat transfer from a 4rx4r square trench with different positions of the pipe in the trench for anisotropic backfill ($K_{th}/K_{tv}$=10).

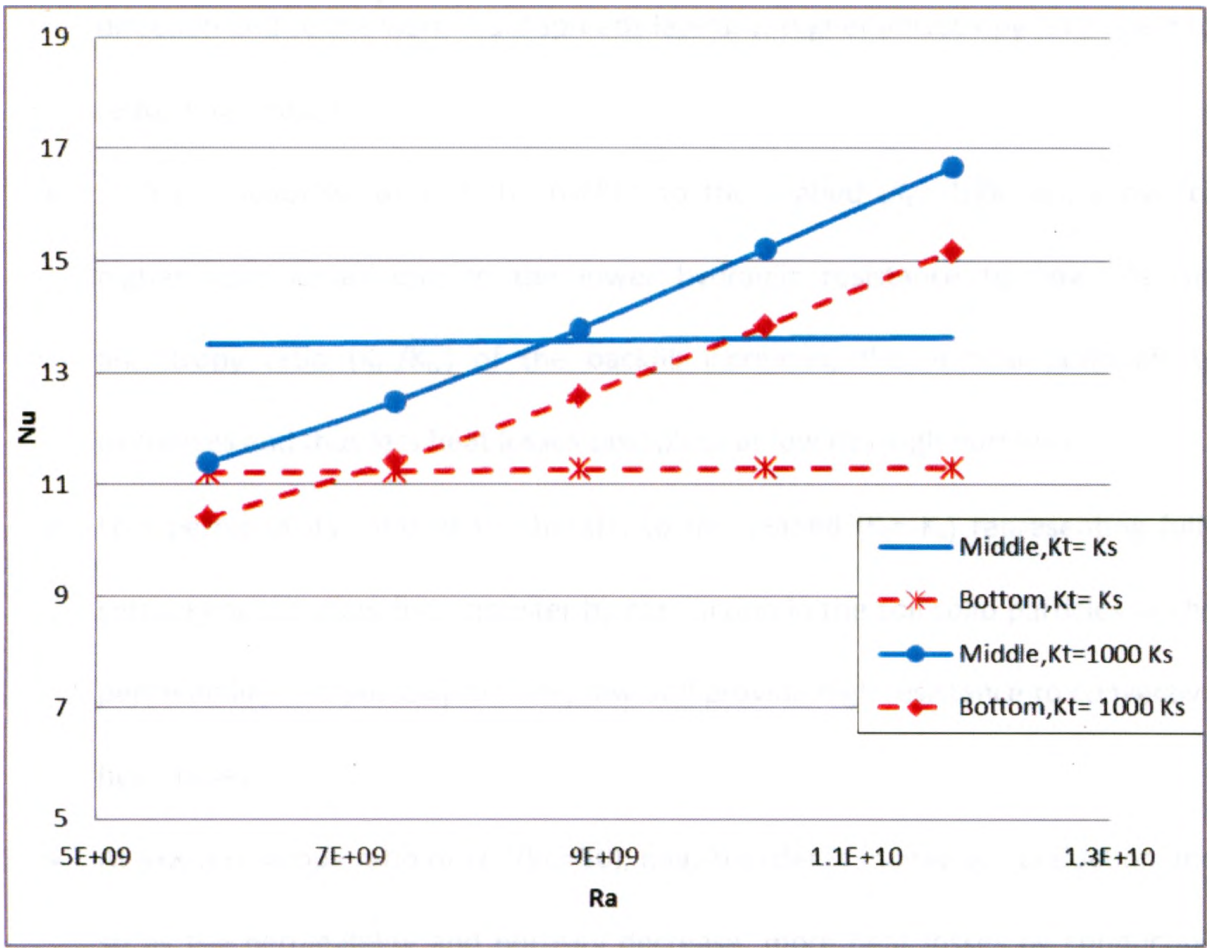


Figure 4.24 Heat transfer from a 4rx4r square trench with different positions of the pipe in the trench for anisotropic backfill ($K_{th}/K_{tv}$=50).

### 4.3.4 Summary for Sand

- An isotropic ($K_{th}/K_{tv}$=1) trench provides low hydraulic resistance to flow as the vertical component of permeability is high. Since the resistance to flow is fairly low, more heat losses from the pipe take place.
- As the anisotropy ratio of the backfill increases when the soil settles, the vertical permeability decreases providing higher resistance to flow in the vertical

direction and so the warm fluid spreads laterally. Higher anisotropy ratios help to reduce heat losses.

- High permeability ratio of the backfill to the seabed ($K_t$= 1000 $K_s$), allow for higher heat losses due to the lower hydraulic resistance to flow. As the anisotropy ratio ($K_{th}/K_{tv}$) of the backfill increases, the vertical permeability decreases and thus less heat losses take place at low Rayleigh numbers.
- Low permeability ratio of the backfill to the seabed ($K_t$= $K_s$) representing fully settled backfill allow heat transfer by conduction in the soil solid particles as the permeability and porosity are very low and provide high resistance to convective heat losses.
- At low anisotropy ratio of ($K_{th}/K_{tv}$=50), heat transfer is mainly by conduction and so as the permeability and porosity decrease, more heat losses by conduction take place. Lower permeability ratios of ($K_t$= $K_s$) and ($K_t$= 10 $K_s$) produce higher heat losses than higher permeability ratios.
- The general observation regarding varying trench sizes is, the bigger the trench size and thus the deeper the pipe gets into the trench, the less heat transfer take place.
- For small trench sizes e.g. (2.5rx2.5r) and (3rx3r), a trapezoidal trench allows for an easier formation of the plume and thus allow for higher heat losses than for a square trench.

- As the trench size increases, the difference in the results of the square and trapezoidal trenches become negligible as the plume is not restricted to form for both shapes.
- A pipe positioned in the bottom of the trench (d=H-r) always produces less heat losses than a pipe placed in the middle of the trench (d=H/2), as a longer path has to be followed by the fluid to escape to the fluid layer.

## 4.4 Heat Transfer from a Pipe Trenched in Clay and Overlain by a Fluid Layer

In this part of the study where clay seabed and backfill are studied, two cases were investigated. The first case is of a backfill consisting of slurry which is of a very low permeability and the second case is of a backfill consisting of big lumps of clay which is considered to be of a very high permeability and porosity. In this section only a (4rx4r) trench size was investigated.

### 4.4.1 Backfill of Clay Slurry

Clay slurry is considered to be fine grained soil that has very small pores and much lower permeability than for sand. The permeability of clay is orders of magnitude lower than that of sand as it consists of much smaller particles.

### 4.4.1.1 Parameters Considered in the Study

A clayey North Sea Sediment known as the Witch Formation consisting of illite, sand and carbonates was the material investigated in this part of the study, the properties of this material were found by Newson et al. (2002). The void ratio-permeability relation found in the previous reference was transformed to a porosity-intrinsic permeability relation as shown in Figure (4.25) using equation (4.1) and the aforementioned, Equation (1.3),

$$\varphi = \frac{e}{1+e} \tag{4.1}$$

$$K = \frac{k\mu}{\rho g}$$

Where $\varphi$ is the porosity;

e is the void ratio;

K is the intrinsic permeability ($m^2$);

k is the hydraulic permeability (m/s);

μ, ρ, g are the fluid properties.

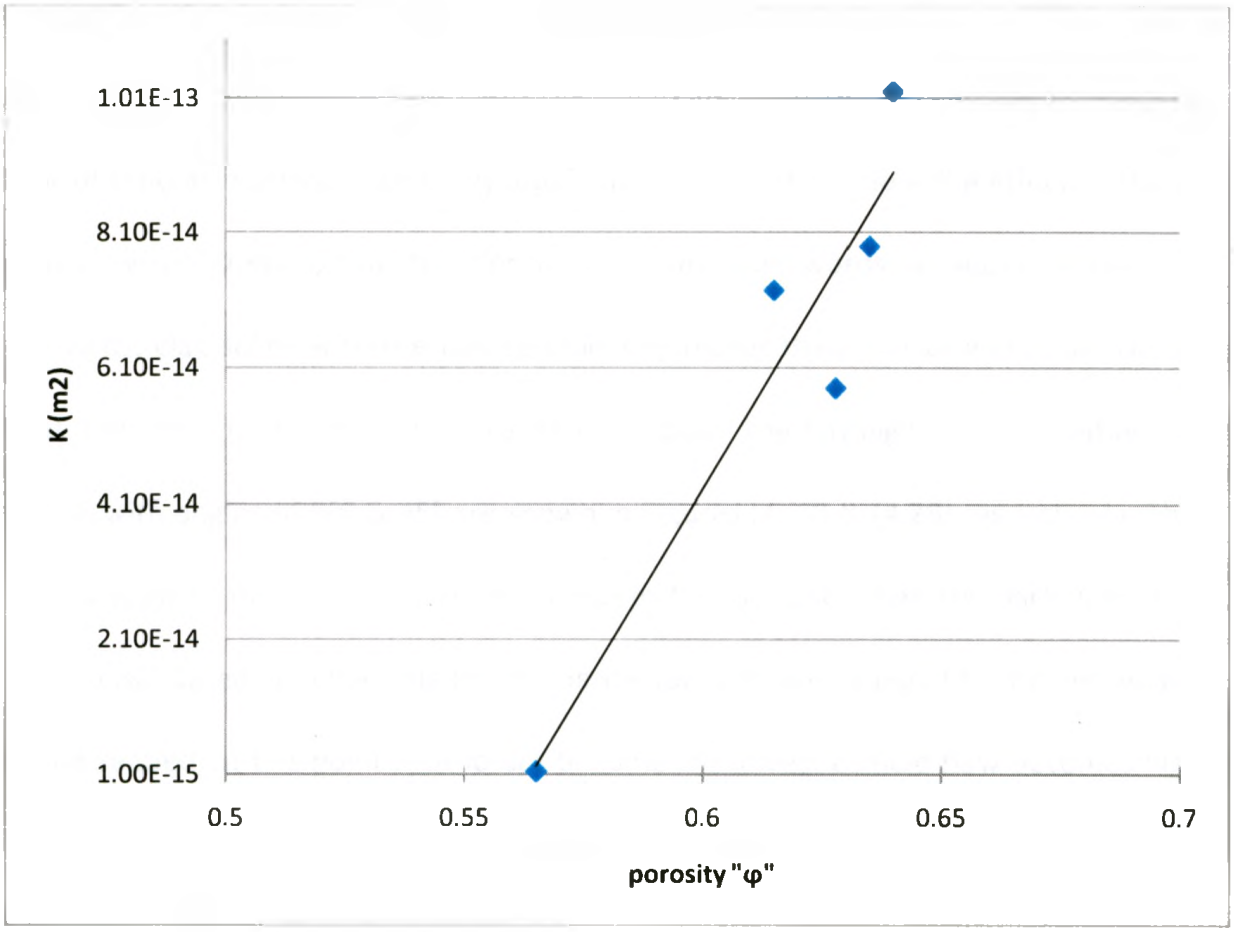


Figure 4.25 Clay slurry porosity-intrinsic permeability relation.

The seabed permeability was considered to be the lowest one obtained from the previous graph ($1.45*10^{-15}$ $m^2$) and the corresponding porosity was (0.565). A range of backfill permeabilities was studied and these are the points shown in the previous graph.

### 4.4.1.2 Results and Discussion

As the permeability of clay backfill is orders of magnitude lower than the sand backfill so all the results have shown only conduction heat transfer taking place as can be seen from the concentric isotherms in Figure (4.26). Since the mode of heat transfer is

predominantly conduction so this means that heat transfer depends on the effective thermal conductivity of the soil, also the permeability of the backfill allows moderate flow of fluid as it provides some hydraulic resistance to flow. So if the effective thermal conductivity increases, heat transfer increases. In other words, as water escapes from the voids, clay solids with thermal conductivity higher than that of water will conduct heat and allow for more heat losses from the pipe. The Rayleigh-Nusselt relation for a trench with angles of 90° & 45° are shown in Figures (4.27) & (4.28) respectively. These results support the previous discussion except for the case when the backfill becomes fully consolidated i.e. when the backfill permeability becomes equal to the permeability of the seabed, at this point heat losses become the lowest as fluid flow becomes highly restricted due to the very low permeability of the surrounding soil, providing high resistance to flow.

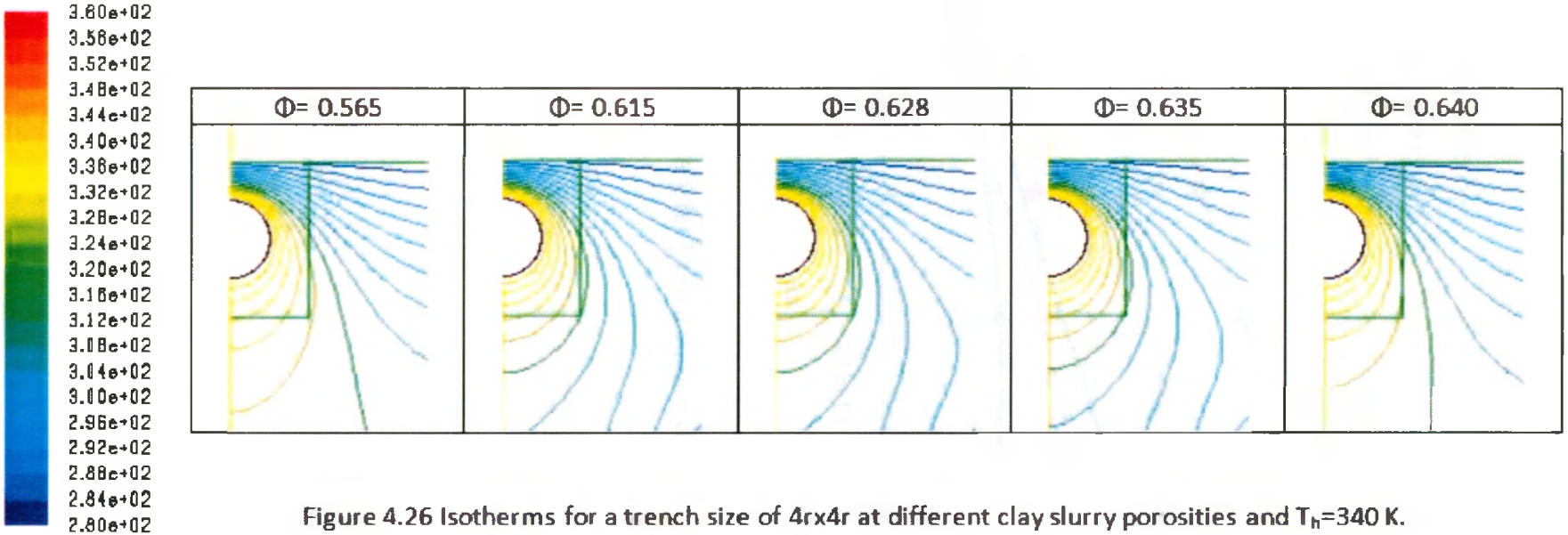


Figure 4.26 Isotherms for a trench size of 4rx4r at different clay slurry porosities and $T_h$=340 K.

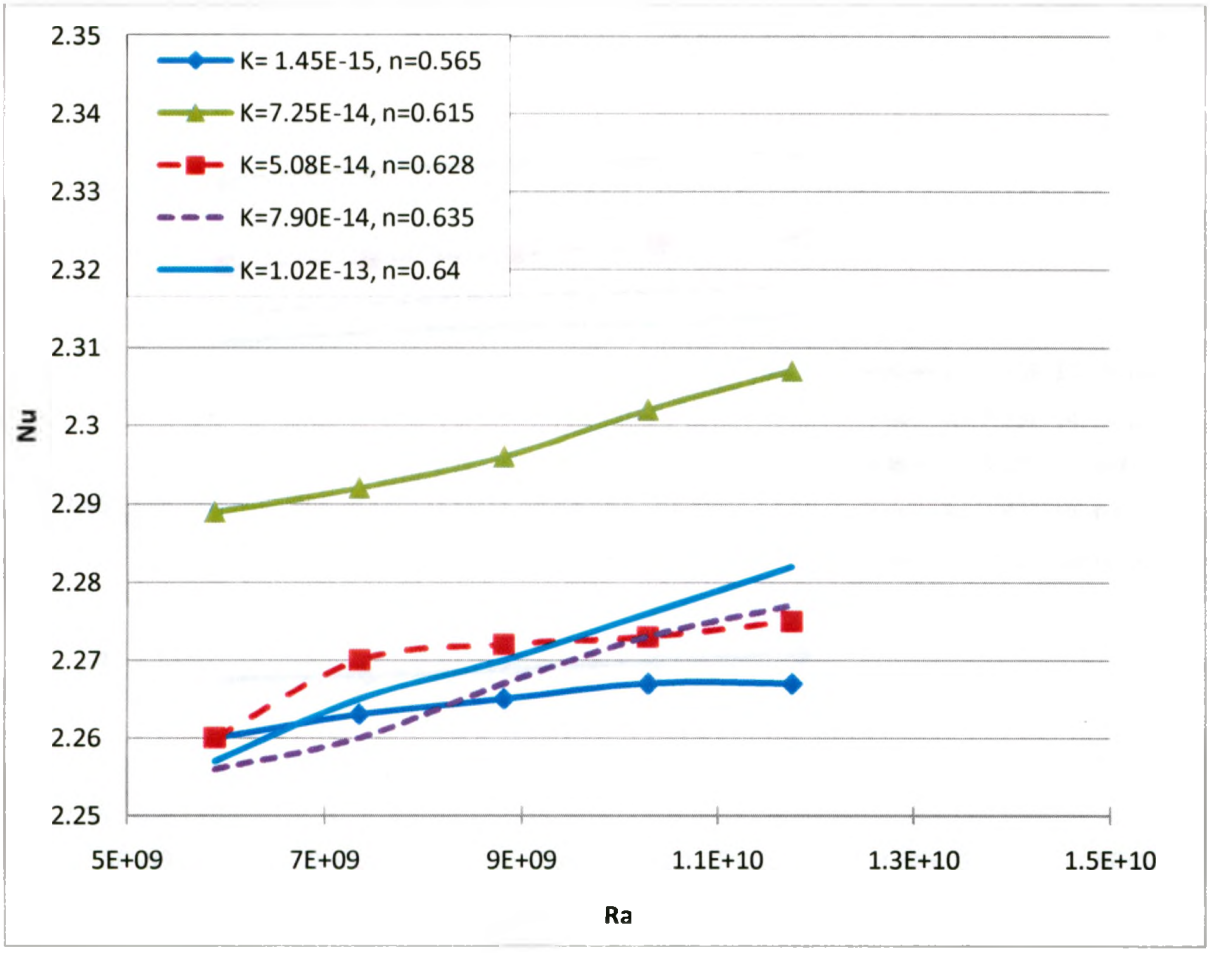


Figure 4.27 Heat transfer from a square clay slurry backfill.

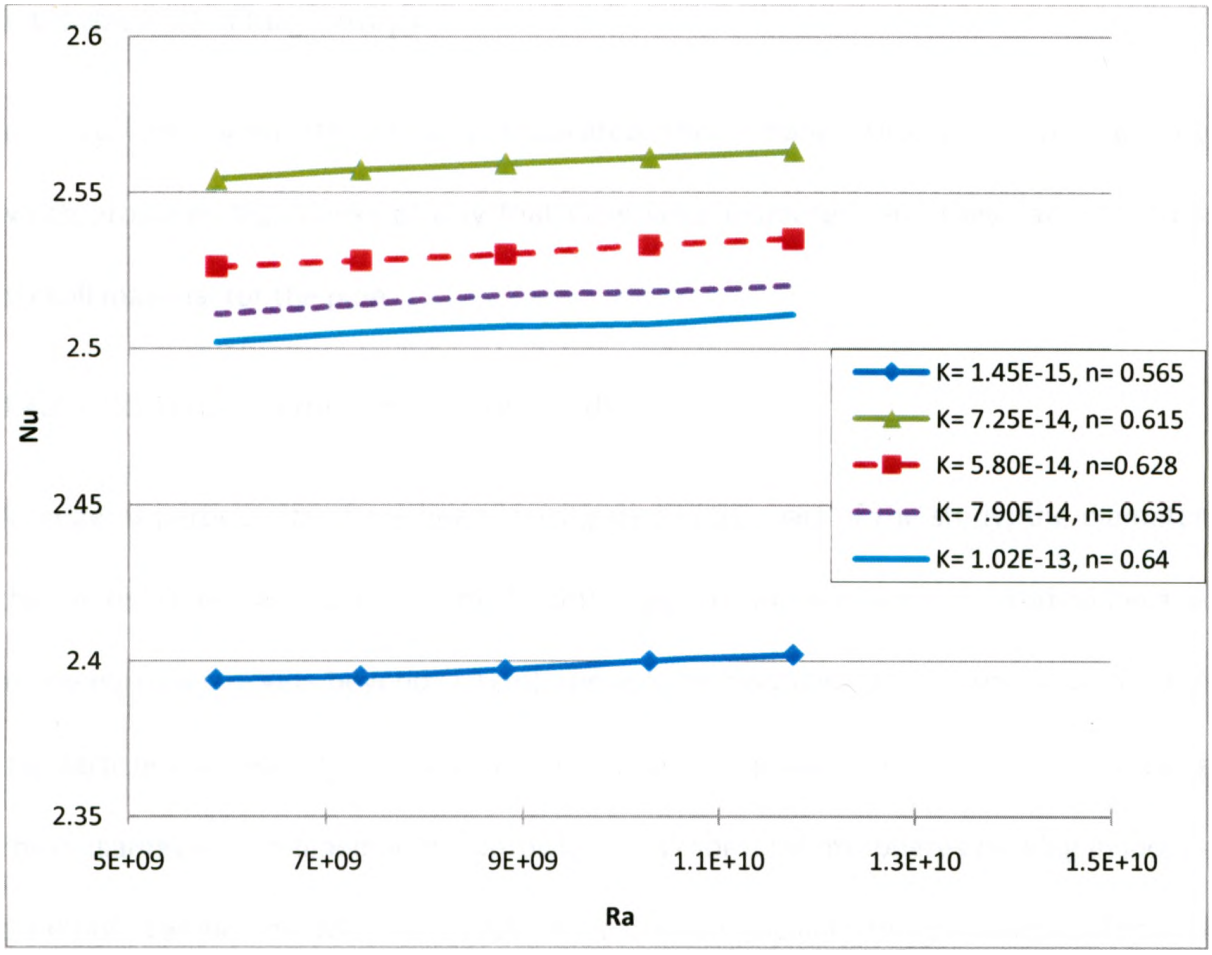


Figure 4.28 Heat transfer from a trapezoidal clay slurry backfill.

### 4.4.2 Backfill of Clay Lumps

In some cases when the trench is excavated, this is done using a ploughing process which produces big chunks of clay that have large diameters and these are reused as backfill material for the pipe.

#### 4.4.2.1 Parameters Considered in the Study

A range of particle sizes have been investigated in this part of the study; the diameters that were studied are (0.5, 1, 5 and 10 cm); bigger diameters were not studied because as the particle size gets beyond (10 cm), the volume averaging assumption is violated, as the particle size relative to the grid size becomes inappropriate for volume averaging. These diameters combined with a porosity of 0.47 for uniform spheres packing in loosest condition, Lambe and Whitman (1969) were used to calculate the permeability for each case using the Kozeny-Carman equation, (Equation 1.4). The results are shown in Table (4.6). The seabed properties were considered to be the same as for clay slurry.

| d (cm) | $\varphi$ | K ($m^2$) |
|---|---|---|
| 0.5 | 0.47 | 5.13E-08 |
| 1 | 0.47 | 2.05E-07 |
| 5 | 0.47 | 5.13E-06 |
| 10 | 0.47 | 2.05E-05 |

Table 4.6 Backfill permeabilities at different particle sizes of clay lumps.

#### 4.4.2.2 Results and Discussion

In case of large soil lumps, the backfill is considered highly permeable and so convective heat transfer is enhanced and more heat is lost from the pipe, as can be seen from Figure (4.29) which shows the results for a 4rx4r square trench. It is interesting to note that as the clay lump particle diameter reaches to 5cm and higher, convective heat transfer and so Nusselt number results exceed the worst-case scenario where the pipe is not backfilled at all. An explanation for this result is that the soil surrounding the pipe is now enhancing the heat transfer performance instead of suppressing it. The hypothesis for this action is that the porous medium now provides an increase in the effective surface area through which heat is convected to the fluid layer and in the meantime provides moderate resistance to fluid flow.

For larger clay lumps it is expected that the heat transfer results to decrease, as these larger lumps will have lower effective surface area to conduct heat from the pipe surface and so less fluid will be heated to be convected to the fluid layer. As the lump size keeps increasing, it is expected that the heat transfer results would converge to the no backfill case.

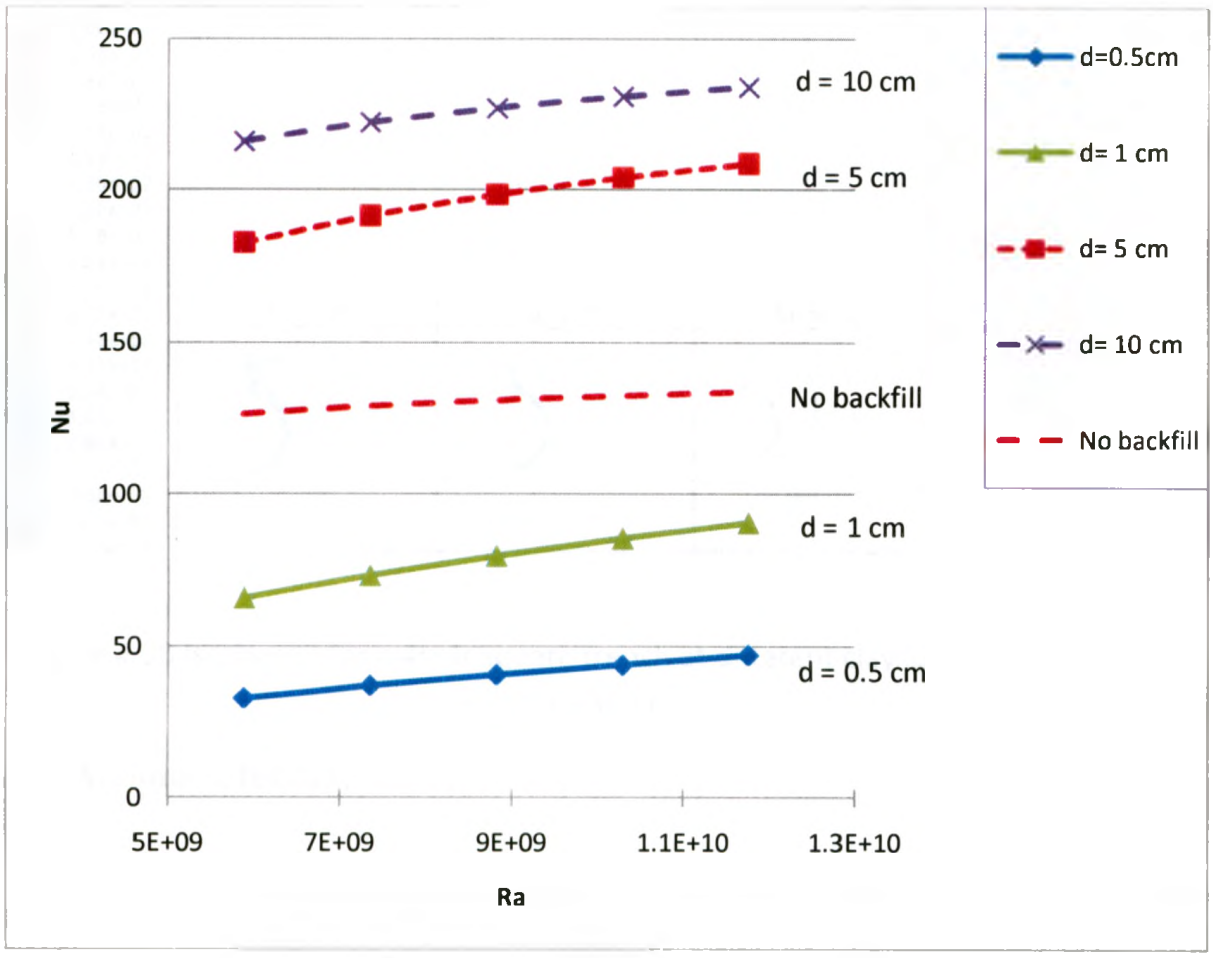


Figure 4.29 Heat transfer results for different clay lumps particle sizes.

Figure (4.30) shows the isotherms for a (4rx4r) square trench at a pipe temperature of 340 K, for a backfill consisting of clay lumps with different particle diameter and for the case of no backfill around the pipe. The isotherms for all cases show pure unrestricted convective heat transfer, as the isotherms are clustered near the heated pipe wall. The thermal plume for the (0.5 cm and 1 cm) clay particles is thicker than for the other cases indicating higher resistance to the flow.

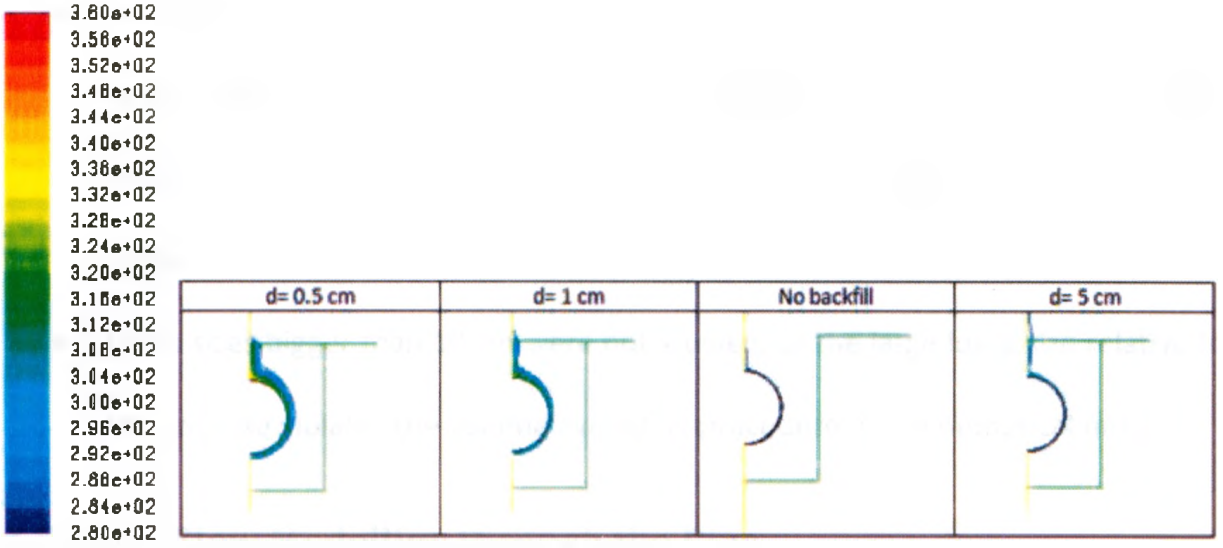


Figure 4.30 Isotherms for a 4rx4r square trench at different clay lumps diameters and $T_h$=340 K.

### 4.4.3 Summary for Clay

- For clay slurry backfill, since the permeability is very low, heat transfer is mainly by conduction. As the porosity of the clay slurry decreases, its effective thermal conductivity increases and as a result heat losses by conduction increase.
- Fully consolidated clay slurry backfill produces the lowest heat losses as the resistance to fluid flow is very high.
- For clay lumps, as the clay lumps size increases, heat losses increase due to the lower resistance to fluid flow occurring due to the increase in permeability.
- Lump sizes of 5 and 10 cm produced heat losses more than for the case of no backfill, since a larger lump size augments heat transfer instead of suppressing it, by providing a high effective surface area for heating the fluid (in addition to a moderate resistance to fluid flow) allowing for free convective heat transfer.

- It is expected that as the lump size increases, heat losses keep decreasing until approaching the no backfill case, as the effective surface area of the lumps decreases, even though the resistance to fluid flow becomes lower as the permeability increases.
- Lump sizes bigger than 10 cm were not studied, as the large lump size relative to the grid size violates the volume averaging procedure of the numerical model.

## 4.5 Fluid Flow Modelling through the Pipe

The change in thermal resistance due to trenching affects the total resistance for heat transfer from the inlet to the outlet of the pipe. This section describes the impact of using some of the trenching cases described previously on the thermodynamic aspects of fluid flow through the pipeline. This enables an assessment of the effect of changing in the properties of the fluid in the pipe due to heat losses as it flows through a length of a pipeline. The pumping power required to pump the fluid between pipeline pump stations is dependent on the viscosity of the fluid which is dependent on its temperature. Predictions of the costs can be made from this approach to help identify the optimum trenching conditions. The extreme case of a bare pipe embedded in different trenching conditions is examined here. Figure (4.31) shows the problem investigated in this section and Figure (4.32) shows the thermal circuit configuration of the pipeline for the described problem. The resistances ($R_1$, $R_2$ and $R_3$) are described as follows, Incropera & DeWitt (2002):

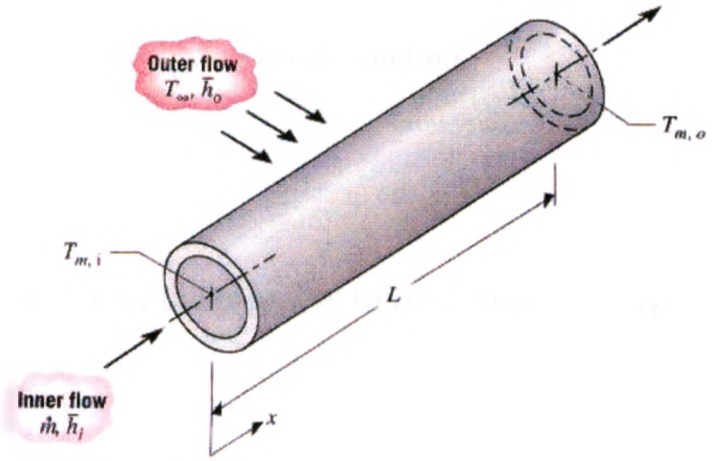


Figure 4.31 Heat transfer between fluid passing through the pipe and convective heat transfer from the pipe's surface (Incropera & DeWitt 2002).

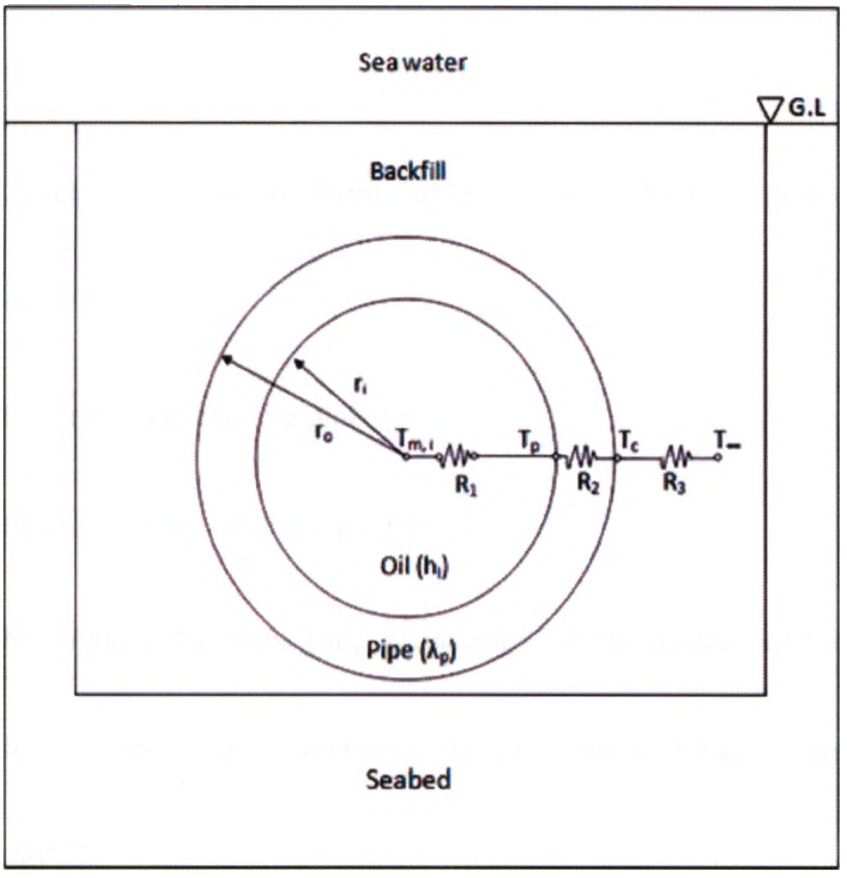


Figure 4.32 Thermal circuit for a pipe buried in porous media.

$R_1$ is the resistance due to convection heat transfer that occurs between the oil and the pipe's inner wall; it is given by the following equation;

$$R_1 = \frac{1}{(2\pi r_i L)h_i} \tag{4.2}$$

$R_2$ is the resistance offered by the pipe wall to conductive heat transfer; its equation is given by;

$$R_2 = \frac{\ln ({}^{r_o}/_{r_i})}{(2\pi L\, \lambda_{pipe})} \tag{4.3}$$

$R_3$ is the resistance to convective heat transfer from the pipe's surface to the surrounding soil; given by;

$$R_3 = \frac{1}{(2\pi r_o L)h_o} \tag{4.4}$$

The total resistance to heat transfer from the flowing oil to the soil is given by $R_{total}$;

$$R_{total} = R_1 + R_2 + R_3 \tag{4.5}$$

Where, $r_i$ is the inner radius of the pipe. (m);

$r_o$ is the outer radius of the pipe. (m);

$L$ is the length of the pipe. (m), calculations are performed per 1 km distance;

$h_i$ is the convective heat transfer coefficient of the oil flowing through the pipe. ($W/m^2.K$);

$h_o$ is the convective heat transfer coeffecient of the porous backfill. ($W/m^2.K$);

$\lambda_{pipe}$ is the thermal conductivity of the pipe. (W/m.K).

The total resistance ( $R_{total}$) to heat transfer is then utilised with the following equation (Incropera & DeWitt 2002) to find the temperature $T_{m,o}$ at the pipe outlet by knowledge of the other parameters;

$$\frac{T_\infty - T_{m,o}}{T_\infty - T_{m,i}} = exp\left(-\frac{1}{\dot{m}c_p R_{total}}\right) \quad (4.6)$$

Where, $T_\infty$ is the temperature of the free stream in the porous media (K);

$T_{m,o}$ is the bulk temperature at the outlet of the pipe (K);

$T_{m,i}$ is the bulk temperature at the inlet of the pipe (K);

$\dot{m}$ is the mass flow rate of the crude oil (kg/s.);

$c_p$ is the specific heat capacity of the crude oil (J/kg.K).

Using the obtained value of $T_{m,o}$ , the viscosity of the crude oil at a distance of 1 km from the inlet pump is obtained from Figure (4.33) assuming crude oil (specific gravity=0.93).

Using the obtained viscosity of the crude oil at a distance of 1 km, the Reynolds's number is calculated and the friction factor in the pipe is calculated using the following equation, Alexanderou (2001);

$$f = \frac{0.3164}{Re^{0.25}} \quad (4.7)$$

The pressure drop along the pipe length is then calculated using this equation, White (1986);

$$\Delta p = \frac{f\, v^2 L\, \rho}{2 D_i} \tag{4.8}$$

Where, $\Delta p$ is the pressure loss per 1 km of pipe length (Pa);

$f$ is the Darcy friction factor;

$v$ is the average velocity of the oil ($v = \frac{\dot{m}}{\rho A}$);

$A$ is the cross section area of the pipe $\left(\frac{\pi}{4} D_i^2\right)$;

$g$ is the gravitational acceleration (9.81 m/s$^2$);

$D_i$ is the inner diameter of the pipe. (m);

Using the pressure drop, the pumping power is finally calculated as;

$$P_p = Q \Delta p \tag{4.9}$$

Where, Q is the volumetric flow rate ($\frac{\dot{m}}{\rho}$). (m$^3$/s).

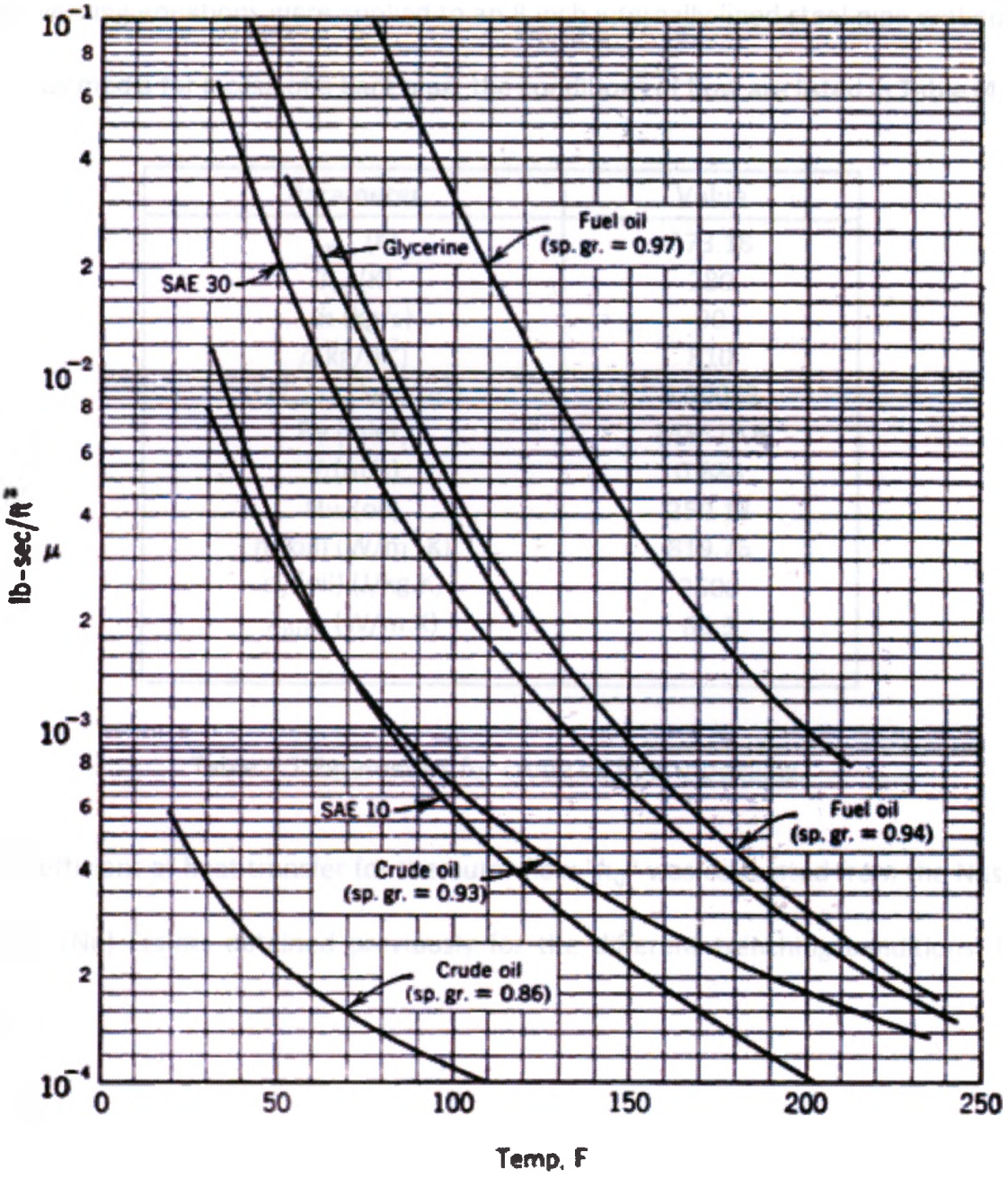


Figure 4.33 Dynamic viscosity versus temperature for typical grades of oil (Courtesy of Hunter Rouse, State University of Iowa, Iowa City 1990)

The governing equations were applied to an 8 inch internally lined steel pipe embedded in porous media for a case of a bare pipe; the conditions of flow are listed in Table (4.7).

| Parameter | Value |
|---|---|
| $T_{m,i}$ (K) | 373.18 |
| $T_{\infty}$ (K) | 280 |
| $\dot{m}$ (kg/s) | 90 |
| $\rho$(kg/m$^3$) | 810 |
| $\mu\,(T_{m,i})$ (kg.s/m$^2$) | 0.00083 |
| Re (inlet) | 345110.6 |
| $V_i$ (m/s) | 0.884 |
| $Nu_i$ (oil) | 250.13 |
| $h_i$ (oil) (W/m$^2$.K) | 819.76 |
| $c_p$ (oil) (J/kg.K) | 2500 |
| $\lambda_{pipe}$ (W/m.K) | 60.5 |

Table 4.7 Parameters for crude oil flow modelling.

The coefficient of heat transfer for the outer flow "$h_0$" was calculated from the Nusselt number (Nu) results obtained previously for the different trenching conditions. It is given by;

$$h_o = \frac{Nu\, k_f}{D_o} \tag{4.10}$$

The trenching conditions examined here and the corresponding coefficients of heat transfer are listed in Table (4.8). For sand, only the isotropic backfill ($K_{th}/K_{tv}$=1) was considered.

The resulting temperature at the outlet (after 1 km), corresponding viscosity, pressure loss and pumping power are listed in Table (4.9).

| soil | case | $h_o$ |
|---|---|---|
| sand | $K_t = K_s$ | 16.59 |
| | $K_t = 10K_s$ | 17.43 |
| | $K_t = 100K_s$ | 45.17 |
| | $K_t = 1000K_s$ | 135.13 |
| Clay Slurry | $\varphi = 0.565$ | 2.98 |
| | $\varphi = 0.64$ | 3.30 |
| Clay Lumps | d= 0.5 cm | 62.23 |
| | d= 10 cm | 308.44 |

Table 4.8 Heat transfer coefficient for the considered trenching conditions.

| soil | case | $T_{m,o}$ (K) | $\mu$ (kg.s/m$^2$) | $\Delta p$ (Pa) | $P_p$ (KW) |
|---|---|---|---|---|---|
| sand | $K_t = K_s$ | 364.35 | 0.00927 | 37770.7 | 4.196 |
| | $K_t = 10K_s$ | 363.94 | 0.00942 | 37922.6 | 4.213 |
| | $K_t = 100K_s$ | 351.96 | 0.0117 | 40034.2 | 4.448 |
| | $K_t = 1000K_s$ | 327.33 | 0.02148 | 46600.8 | 5.177 |
| Clay Slurry | $\varphi = 0.565$ | 371.47 | 0.00079 | 20407.6 | 2.267 |
| | $\varphi = 0.64$ | 371.29 | 0.0008 | 20471.9 | 2.274 |
| Clay Lumps | d= 0.5 cm | 345.88 | 0.0132 | 41259.9 | 4.584 |
| | d= 10 cm | 306.73 | 0.0391 | 54128.9 | 6.014 |

Table 4.9 Pumping power required for each trenching condition.

The following is noticed from the results;

- For the sand, when the backfill permeability increases, more heat is lost from the pipe thus lowering the oil's outlet temperature and making it more viscid, so the pressure gradient increases, thereby requiring higher pumping power.

- Clay slurry gave the lowest heat losses, and thus lowest pumping power required. This is due to its very low permeability as discussed before in section (4.4.1).
- Clay lumps with sizes of 10 cm produced the highest heat losses and lowest temperature after 1 km from the inlet pump and required the highest pumping power, as these lumps augmented heat losses as described before in section (4.4.2).
- The results have shown that the backfill properties have significant effect on heat transfer from the pipe. Burying a pipe in porous media in addition to coating it can provide thermal insulation to the pipe similar to pipe in pipe technology, Loch (2000). The required pumping power for transporting the oil will be lower if a coating is used to insulate the pipe in addition to the insulation provided by the porous media as it will provide an additional resistance for heat loss from the flowing fluid in the pipe.

## 4.6 Summary

Heat transfer from an isothermal pipe trenched in porous media and overlain by a fluid layer has been studied under different flow and geometric conditions. Two types of porous media have been investigated, sand and clay. The results show that in the case where the pipe is embedded in sand, the optimum conditions to reduce heat losses are a combination of a permeability ratio of the backfill to the seabed of 100 ($K_t$= 100 $K_s$) and an anisotropy ratio of the backfill of 50 ($K_{th}/K_{tv}$=50). This is applicable for all the trench

sizes and angles studied, because at this low vertical permeability, heat transfer is mainly due to conduction and so a more permeable backfill will also have a higher porosity. Hence less particle solid is available to conduct heat, giving the lowest values for heat transfer. A higher permeability ratio ($K_t$= 1000 $K_s$) initiates convection at higher Rayleigh numbers. Also when the pipe is placed in the bottom of the trench it produces less heat than when it is in the middle of the trench.

For the case of clay slurry which is considered to be highly impermeable, the higher the permeability and, thus, the porosity, the lower the heat losses that can take place as the only heat transfer mode available is conduction. However, for a backfill consisting of lumps of clay which have a high intergranular porosity (porosity between the grains) then the predominant mode of heat transfer is convection. Hence for smaller lump sizes (and intergranular porosity), less heat losses can take place.

Modelling of fluid flow in the pipe has approved the parametric study results by showing that for backfill conditions producing high heat losses due to their lower resistance to heat transfer, the temperature of the fluid at the outlet pump decreases and the fluid becomes more viscid thus requiring high pumping power. In contrast, for backfill conditions that produced low heat transfer due to their high resistance to heat transfer, the pressure drop between the pumps was lower and thus lower pumping power was required. This approves that a backfill with the right conditions can provide good insulation in combination to thermal coatings for the pipe.

# CHAPTER 5

# SUMMARY & RECOMMENDATIONS

## 5.1 Summary

The focus of this thesis was the investigation of heat and mass transfer from an isothermal pipe buried within a heterogeneous porous media, superimposed by a fluid layer. This problem is applicable to a number of offshore engineering problems such as offshore pipes, canisters and cables. The approach adopted for performing this study was to use the computational fluid dynamics (CFD) software FLUENT for numerical modelling.

In the field, different flow and geometric conditions can exist and have an impact on the heat transfer process. When the seabed is trenched, the pipe is placed in the base of the trench and then backfilled with the spoil resulting from the trenching process; the backfill soil becomes modified from its original state and therefore its permeability and porosity change. Also as time passes, the backfill soil settles and the vertical permeability can decrease making the backfill permeability anisotropic. The effect of these two different fluid flow conditions (a) different permeabilities of the backfill and the seabed and (b) permeability anisotropy of the backfill, on the heat transfer process were studied in this dissertation. Different geometric conditions were also considered in the study, such as trench size and angle, as well as varying the position of the pipe in the trench.

To assess the effect of soil type on the behaviour, the system response for two different soils were investigated namely sand and clay. The flow and geometric conditions mentioned previously were investigated in a sandy soil. However, for a clayey soil the effect of varying the size of the clay lumps filling the trench was investigated, as well as varying the permeability of a clay slurry backfill. Finally, the results of the current parametric study for different backfill conditions were used in estimating the pumping power required for pumping the oil flowing in the pipe as its properties change due to the heat losses from the pipe.

The following is noticed from the parametric study:

### 5.1.1 Sand Medium

- For all cases, as the Rayleigh number increased, heat losses were higher. The reason for this is that higher heating of the surrounding fluid produced a higher buoyancy force, which induced more fluid motion and thus higher convective heat losses.
- For all cases when the vertical component of permeability was reduced thereby increasing the permeability anisotropy ratio ($K_{th}/K_{tv}$), the heat losses decreased. This is because a lower vertical permeability increases the fluid flow resistance in the vertical direction.
- When the trench is isotropic ($K_{th}/K_{tv}=1$), more heat is lost from the pipe as the hydraulic resistance to vertical flow is low, allowing warm water to rise vertically carrying heat away from the pipe.

- For the case when the backfill is much more permeable than the seabed ($K_t$= 1000 $K_s$) and the soil is isotropic ($K_{th}/K_{tv}$=1), which corresponds to the case when the soil is first backfilled into the trench, high heat losses by convection take place. This is because at this high permeability and porosity, little hydraulic resistance in the backfill provides the opportunity for the warm water to escape from the voids to the fluid layer.
- For the cases representing sand backfill of very low permeability as in the case of slurried sand used for backfilling the trench or when the sand backfill has completely settled in the trench ($K_t$= 10 $K_s$) and ($K_t$= $K_s$), heat losses from the pipe are very low compared to higher permeability ratios ($K_t$= 100 $K_s$) and ($K_t$= 1000 $K_s$). The reason for this is that the lower permeability and porosity of the backfill introduce high resistance to the flow of the warm fluid.
- For low permeability ratios such as ($K_t$= $K_s$), ($K_t$= 10 $K_s$) and ($K_t$= 100 $K_s$), as the anisotropic permeability ratio ($K_{th}/K_{tv}$) of the backfill increases, and therefore the vertical permeability decreases, heat transfer by conduction becomes predominant. The lower the porosity and permeability of the backfill, the more soil solid is available to conduct heat, and thus higher heat losses take place as the permeability and porosity are further reduced.
- A very high permeability ratio of ($K_t$= 1000 $K_s$) follows the trend stated in the previous point at high anisotropy ratio of ($K_{th}/K_{tv}$= 50), but as the Rayleigh number increases, convective heat transfer initiates and continues increasing.

- The highest heat losses from the pipe take place when there is no backfill in the trench, as the sea water becomes completely free to carry heat away from the pipe, thus representing unrestricted free convection.
- Since the pipe was always placed in the middle of the trench (d=H/2) or at the bottom of the trench (d=H-r), for the different trench sizes, as the trench size increased, the pipe depth increases. For the low permeability ratios of ($K_t$=$K_s$) and ($K_t$= 10 $K_s$), heat losses decrease since a longer path is followed by the flowing fluid to escape to the fluid layer.
- In contrast, at high permeability ratios of ($K_t$= 100 $K_s$) and ($K_t$= 1000 $K_s$), since the permeability of the backfill is very high and convection heat transfer is dominating the heat transfer process, producing a narrow plume that was not affected by the trench size and the varying position of the pipe in the trench.
- A trapezoidal trench shape generally produced more heat losses than a square one, as it provided higher effective surface area for fluid motion. The effect of varying the shape of the trench was highest for small trench sizes and this effect decreased as the trench size increased. For small trenches, a square trench restricted the formation of the plume, while a trapezoidal trench allowed for free formation of the plume.
- A pipe placed in the bottom of the trench always produced less heat losses than a pipe placed in the middle of the trench, as the deeper the pipe gets in the trench, the more heat losses are suppressed due to the longer path being followed by the escaping fluid flow.

- Modelling of oil flow in the pipe has shown that the case of ($K_t$= 1000 $K_s$) required the highest pumping power. For this case, highest heat losses took place, lowering the temperature of the oil at the outlet pump and making it more viscid thus requiring higher pumping power and thereby higher cost of transportation. In contrast, the case of ($K_t$= $K_s$) which gave the lowest Nusselt number results and thus higher resistance to heat transfer, has given the lowest pressure loss and thus required lowest pumping power for the transportation of oil.

### 5.1.2 Clay Medium

- Fully consolidated clay slurry backfill, i.e. with permeability and porosity equal to those of the seabed, produced the lowest heat losses from the pipe, since the very low permeability provided very high resistance to the fluid flow.
- The heat transfer mode for the clay slurry backfill was mainly by conduction, as observed from the concentric isotherms.
- For conductive heat transfer, more heat losses resulted when the porosity of the backfill decreased, as more soil solid was available to conduct heat. The effective thermal conductivity of the soil increases when its porosity decreases allowing for more heat losses by conduction.
- In contrast, a backfill consisting of clay lumps always produced convective heat transfer due to its relatively high permeability and intergranular porosity.
- Clay lumps of sizes of 5 and 10 cm produced greater heat losses than for a pipe with no backfill. The reason for this is that heat transfer from the pipe was

augmented rather than suppressed by the porous medium, as the clay lumps provided a high effective surface area to warm the fluid and also the permeability was relatively high to allow for the escaping of the warmed fluid to the fluid layer.

- The volume averaging procedure was not applicable for particle sizes higher than 10 cm, as the particle size would be high relative to the grid size and thus would violate the volume averaging phenomenon.
- Modelling of oil flow in the pipe has shown lowest pressure drop for a pipe backfilled with clay slurry. Clay slurry has a very low permeability providing high resistance to heat transfer and thus less heat is lost from the pipe, keeping the oil temperature high and keeping it less viscid. This means low pumping power is required for the transportation of the oil.
- For the case of a backfill consisting of clay lumps, 10 cm lumps size required the highest pumping power for the transportation of oil as the highest heat losses took place for this case making the oil highly viscous.

## 5.2 Recommendations

- Since the present study was investigated numerically, an experimental study is required for verification of the results.
- Since this study considered the problem in 2-dimensional form, application of a 3-dimensional model would help increase the efficiency of the results.

- Laboratory or in-situ measurement of the permeability anisotropy, thermal conductivity and other properties of actual offshore or analog soils would give more accurate results.
- Considering the effect of a rock backfill as usually crushed rock is deposited in large quantities to cover the trenched pipe.
- Heating changes the properties of clay and thus this should be considered.
- Studying other boundary conditions for the pipe surface, such as non-isothermal pipe, or asymmetric heating.

# APPENDIX A

Comparison between the experimental, analytical and numerical results collected by Morgan (1997) and the validation test performed using the boundary conditions adopted by the current study.

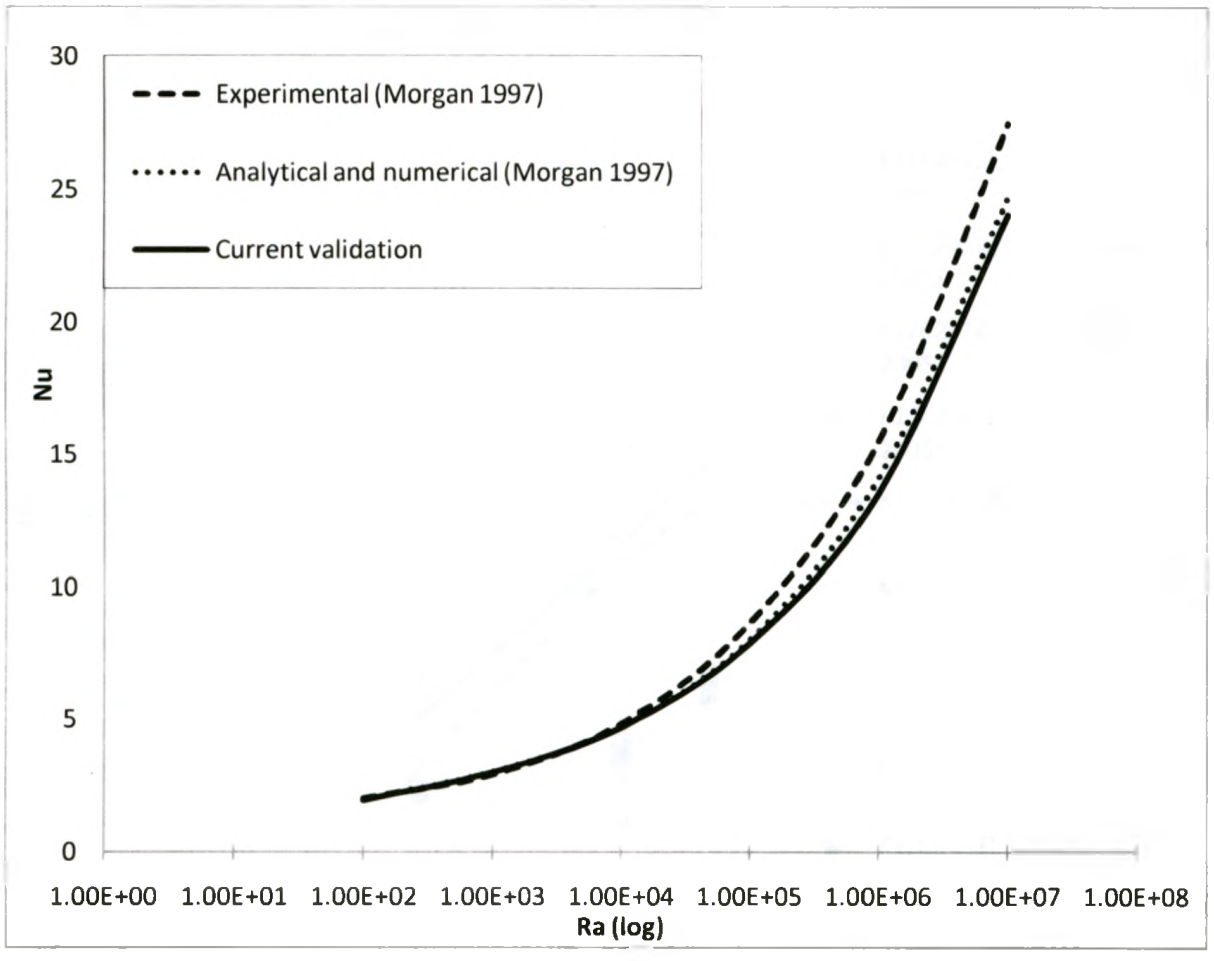


Figure A.1 Validation results for convective heat transfer from an isothermal cylinder in air (Morgan 1997).

Comparison between the results obtained by Ngo & Lai (2005) and the validation test results obtained using the same boundary conditions employed by the authors, for permeability ratios of, $K_1$= 0.1 $K_2$, $K_1$= 10 $K_2$ and $K_1$= $K_2$ and backfill thickness t/r of, 0.5, 1 and 2

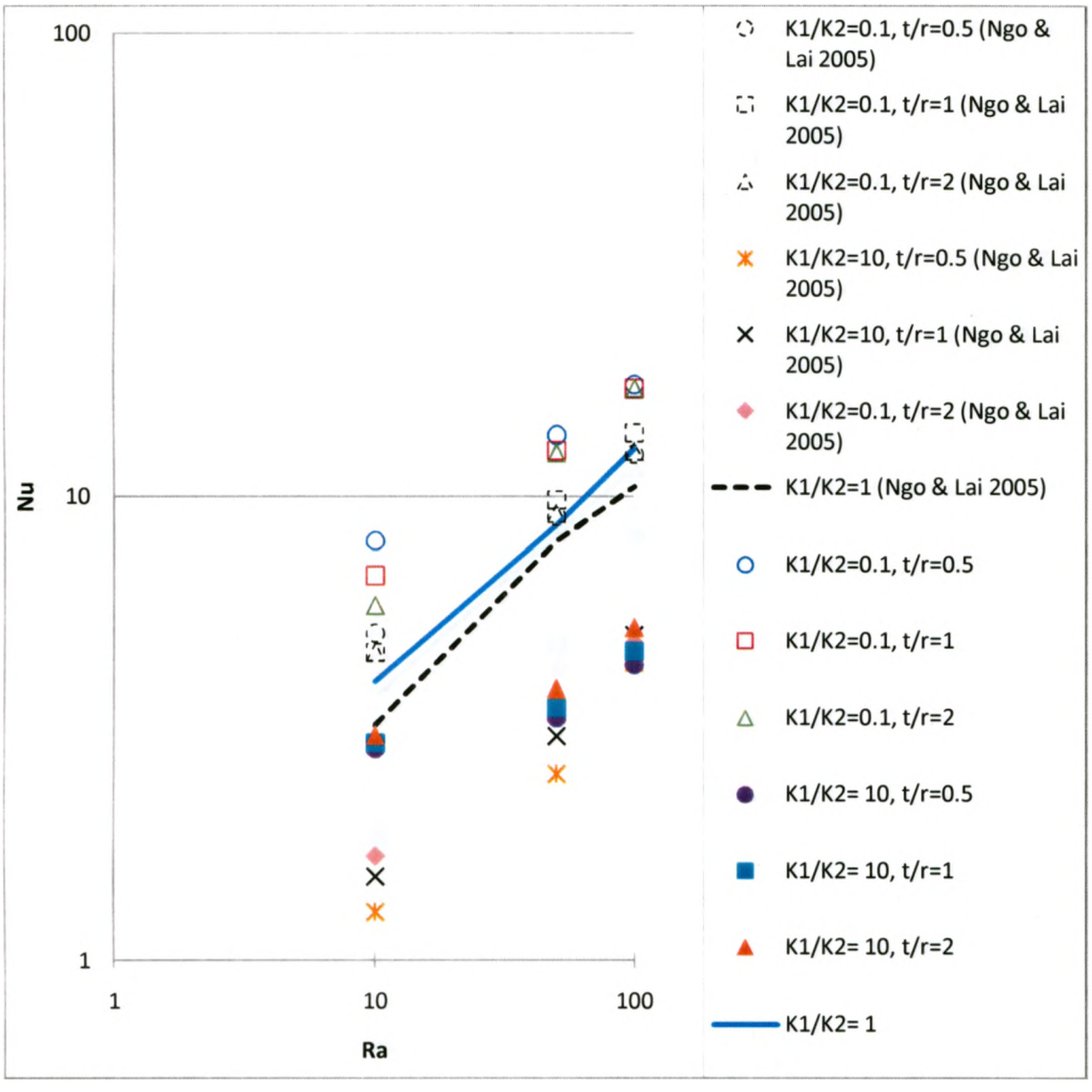


Figure A.2 Validation results for heat transfer from a pipe buried in porous media (Ngo & Lai 2005) using the same boundary conditions employed by the authors.

Comparison between the results obtained by Ngo & Lai (2005) and the validation test results obtained using the boundary conditions adopted by the current study, for permeability ratios of, $K_1$= 0.1 $K_2$, $K_1$= 10 $K_2$ and $K_1$= $K_2$ and backfill thickness t/r of, 0.5, 1 and 2.

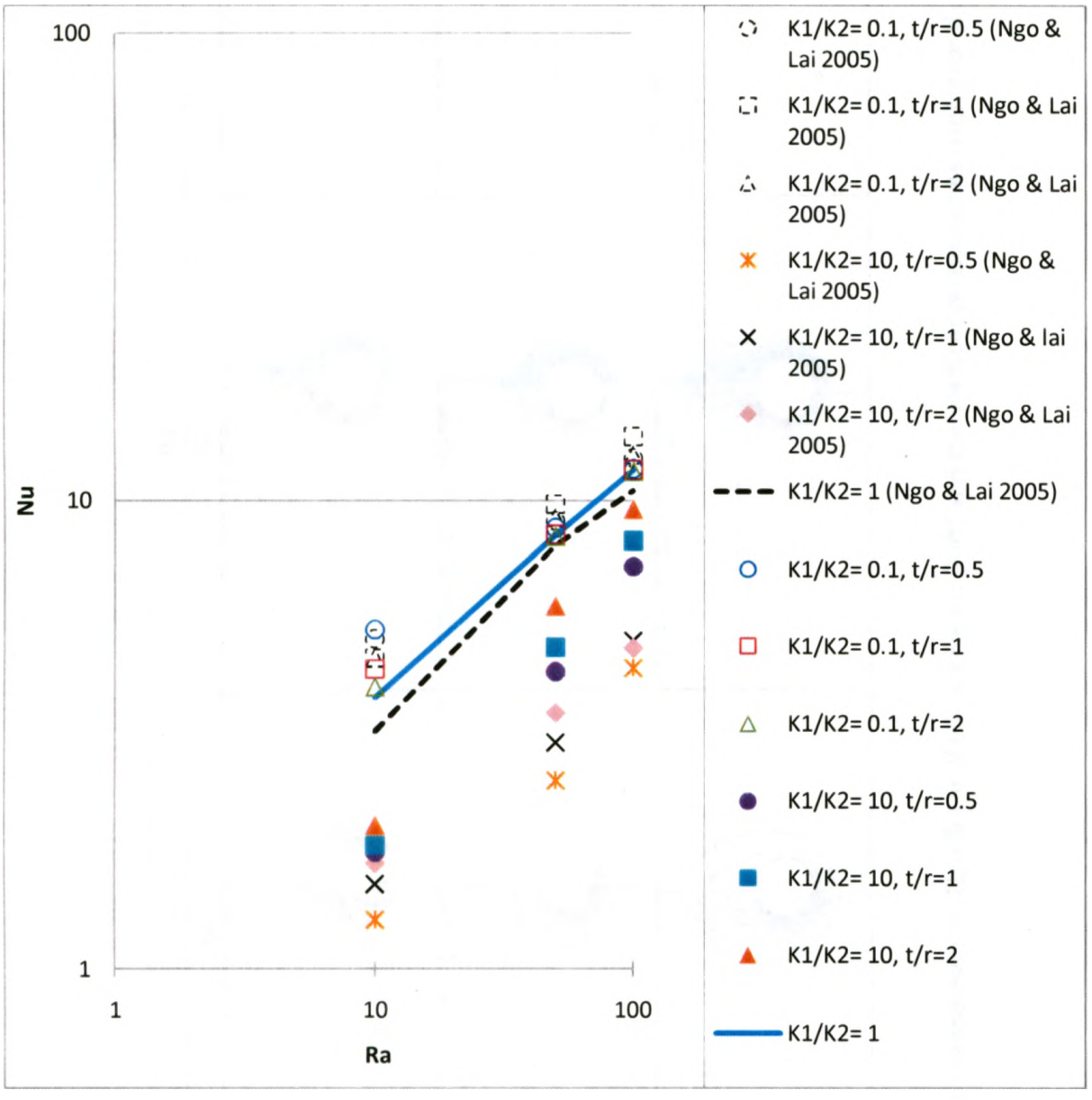


Figure A.3 Validation results for heat transfer from a pipe buried in porous media (Ngo & Lai 2005) using the boundary conditions adopted in the current study.

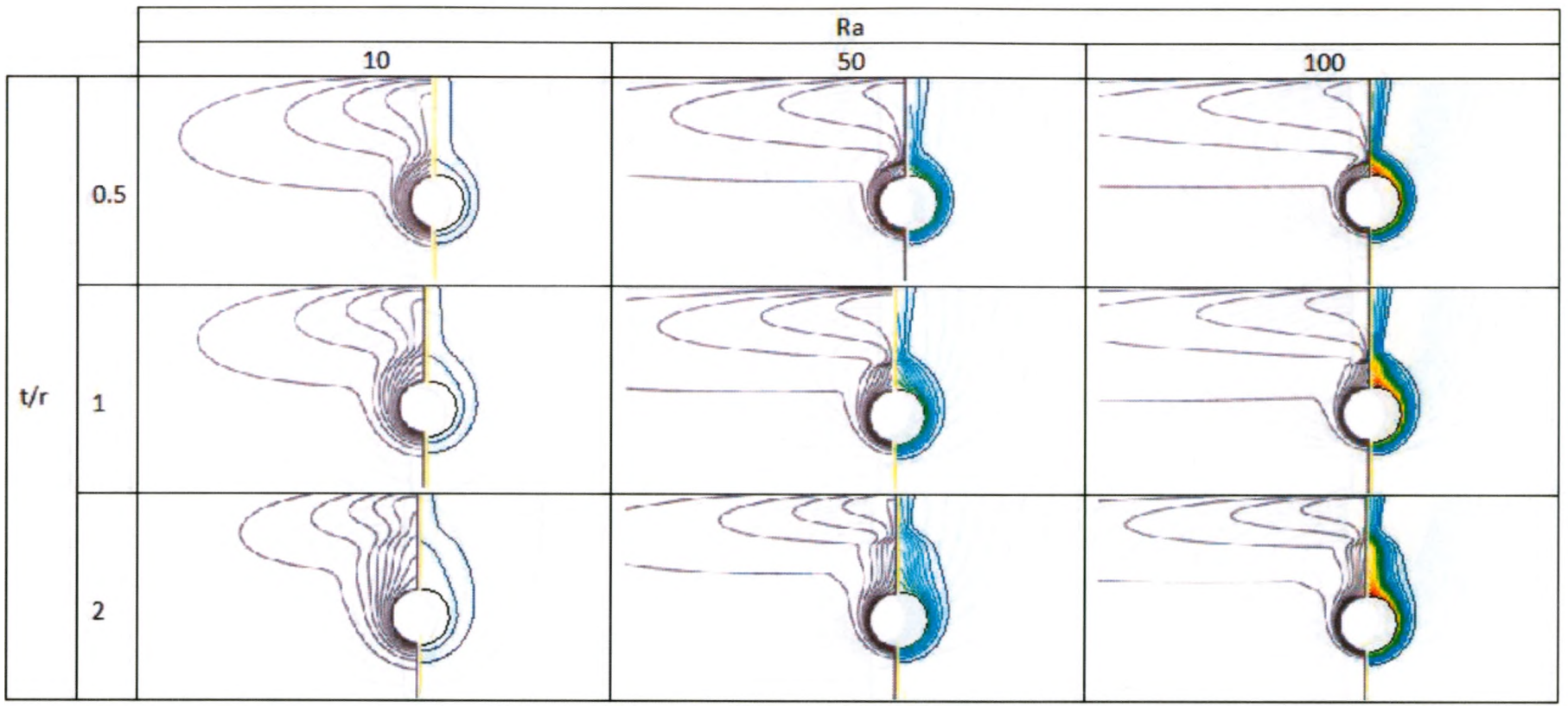


Figure A.4 Comparison of (Ngo & Lai 2005) isotherms (left) and the verification isotherms (right) for the case of $K_1 = 0.1\ K_2$.

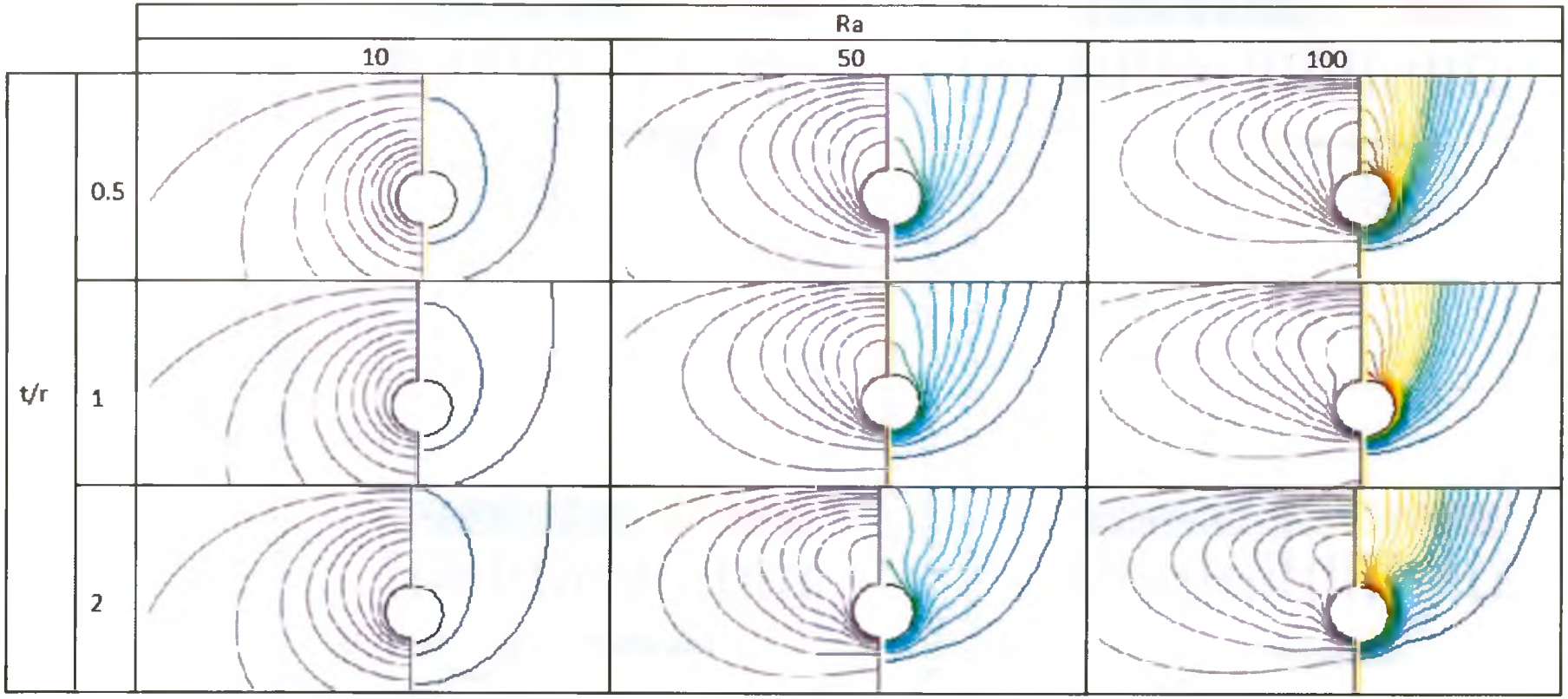


Figure A.5 Comparison of (Ngo & Lai 2005) isotherms (left) and the verification isotherms (right) for the case of $K_1$= 10 $K_2$.

# APPENDIX B

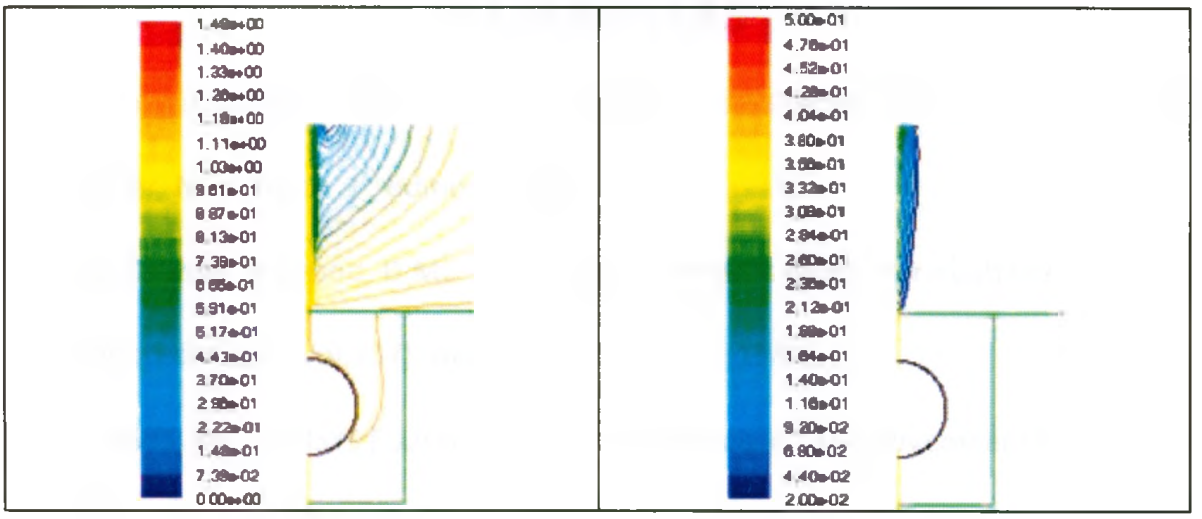

(a) (b)

Figure B.1 (a) Streamlines (Kg/s) and (b) pressure contours (Pa) for a 4rx4r square trench in a sand medium at a permeability ratio of ($K_t$=1000 $K_s$) and permeability anisotropy ratio of ($K_{th}/K_{tv}$=1).

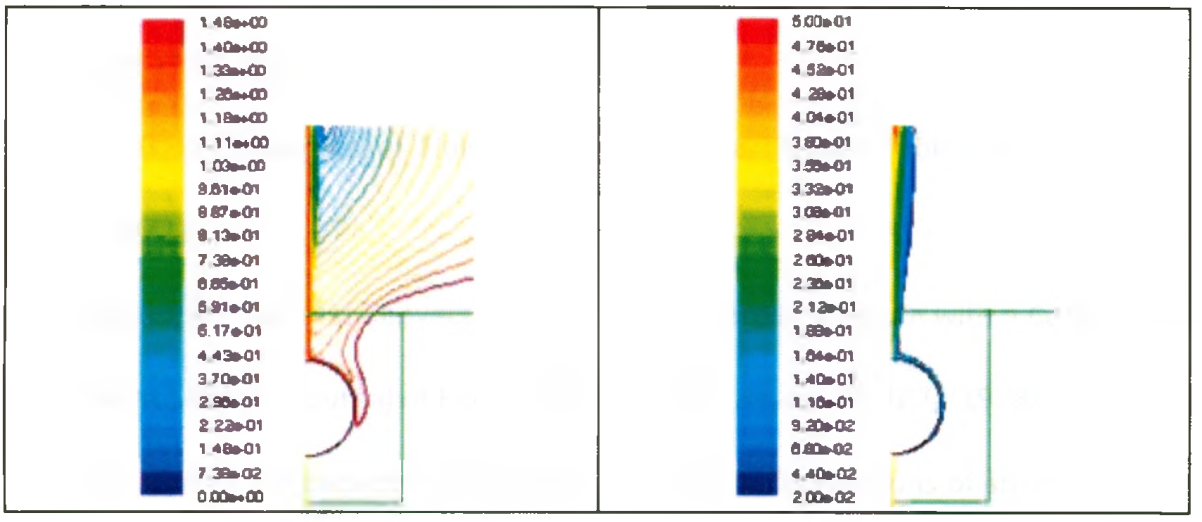

(a) (b)

Figure B.1 (a) Streamlines (Kg/s) and (b) pressure contours (Pa) for a 4rx4r square trench in a clayey medium for a trench consisting of clay lumps with diameter of 10 cm.

# REFERENCES


- Alexandrou, A.: "Principles of Fluid Mechanics." Prentice hall Inc., Upper Saddle River, New Jersey, 1st edition, (2001).
- Al-Tabbaa, A.,Wood, D.M.: "Some Measurements of the Permeability of Kaolin." Geotechnique, Vol. (37), No. (4), pp. 499–503, (1987).
- ANSYS, Inc.: "ANSYS FLUENT User's Guide" Release 13.0, November (2010).
- Bai, Y.: "Pipelines and Risers." Elsevier Ocean Engineering Book Series, Vol. (3), (2001).
- Bai, Y. and Bai, Q.: "Subsea Pipelines and Risers." 1st edition, (2005).
- Basak, P.: "Soil Structure and its Effects on Hydraulic Conductivity." Soil Science, Vol. (114), No. (6), pp. 417-422, (1971).
- Bear J.: "Dynamics of Fluids in Porous Media." Dover Publications: New York, (1972).
- Bejan, A., "Natural Convection in an Infinite Porous Medium with a Concentrated Heat Source," Journal of Fluid Mechanics, Vol. 89, pp. 97-107, (1978).
- Bjerrum, L.: "Geotechnical problems involved in foundations of structures in the North Sea." Geotechnique, Vol. 23, No. (3), pp. 319-358, (1973).
- Bouma, J. and Dekker, L.W.: "A Method for Measuring the Vertical and Horizontal $K_{sat}$ of Clay Soils with Macropores." Soil Science Society of American Journal 45, pp. 65-62, (1981).

- Bradean, R., Ingham, D.B., Heggs, P.J. and Pop, I.: "Unsteady Free Convection Adjacent to an Impulsively Heated Horizontal Circular Cylinder in Porous Media." Numerical Heat Transfer, Part A, Vol. 31, pp. 325-346, (1997).
- Braestrup, M.W., Andersen, J.B., Andersen, L.W., Bryndum, M.B., Christensen, J.B. and Nielsen, N.J.R.: "Design and Installation of Marine Pipelines." Wiley-Blackwell, 1st edition, (2005).
- Brereton, N.R.: "Physical Property Relationships from Sites 765 and 766." Proceedings of the Ocean Drilling Program, Scientific Results, Vol. (123), pp. 453-465, (1992).
- Carman, P.C.: "Fluid Flow through Granular Beds." Transactions of the Institution of Chemical Engineers 15, 150, (1937).
- Carman, P.C.: "Flow of Gases through Porous Media." Butterworths Scientific Publications, London, (1956).
- Cedergren H.R.: "Drainage of Highway and Airfield Pavements." John Wiley and Sons, NY, (1974).
- Chan, H.T. and Kenny, T.C.: "Laboratory Investigation of Permeability Ratio of New Liskeard Varved Clay." Canadian Geotechnical Journal, Vol. (10), No. (3), (1973).
- Chapuis, R.P., Gill,D.E., Baass, K.: "Laboratory Permeability Tests on Sand: Influence of the Compaction Method on Anisotropy." Canadian Geotechnical Journal Vol. (26), No. (4), pp. 614–622, (1989).

- Chapuis, R.P., Gill, D.E.: "Hydraulic Anisotropy of Homogeneous Soils and Rocks: Influence of the Densification Process." Bulletin of the International Association of Engineering Geology 39, pp. 75–86, (1989).
- Chapuis, R.P. and Aubertin, M.: "Predicting the Coefficient of Permeability of Soils Using the Kozeny-Carman Equation." EPM-RT-2003-03.
- Chason, D.B. and Siegel, D.I.: "Hydraulic Conductivity and Related Physical Properties of Peat, Lost River Peatlans, Northern Minnesota." Soil Science, Vol. (142), No. (2), pp. 91-99, (1986).
- Childs, E.C.: "The Measurement of the Hydraulic Permeability of Saturated Soil in Situ." I. Principles of a Proposed Method. Proceedings of the Royal Society London, A215, pp. 525-535, (1957).
- Childs, E.C., Collis-George, N. and Holmes, J.W.: "Permeability Measurements in the Field as Assessment of Anisotropy and Structure Development." Journal of Soil Science, Vol. (8), No. (1), pp. 27-41, (1957).
- Christopher, D.M. and Wang, B.X.: "Non-Darcy Natural Convection around a Horizontal Cylinder Buried Near the Surface of a Fluid-Saturated Porous Medium." International Journal of Heat and Mass Transfer, Vol. 36, pp. 3663-3669, (1993).
- Clayton, S.A., Scholes, O.N., Hoadley, A.F.A., Wheeler, R.A., McIntosh, M.J., Huynh, and D.Q.: "Dewatering of Biomaterials by Mechanical Thermal Expression." Drying Technology, Vol. (24), No. (27), pp. 819-834. (2006).

- Collins, R.E.: "Flow of Fluids through Porous Materials." Reinhold, New York, (1961).
- Dean, E.T.R.: "Offshore Geotechnical Engineering." 1st edition, (2010).
- De Boodt, M.F. and Kirkham, D.: "Anisotropy and Measurement of Air Permeability of Soil Clods." Soil Science, pp. 127-133, (1952).
- Eckert, E.R.G. and Drake, R.M.: "Analysis of Heat and Mass Transfer." Mc.Graw-Hill Book Company, (1972).
- Farouk, B. and Shayer, H.: "Natural Convection around a Heated Cylinder in a Saturated Porous Medium." Journal of Heat Transfer, Vol. 110, pp. 642-648, (1988).
- Farouki, O.T.: "Thermal Properties of Soils." US Army Corps of Engineers, Cold Regions Research and Engineering Laboratory, Hanover, NH, (1981).
- Fand, R.M., Steinberger, T.E. and Cheng, P.: "Natural Convection Heat Transfer from a Horizontal Cylinder Embedded in a Porous Medium." International Journal of Heat and Mass Transfer, Vol. 29, pp. 119-133, (1986).
- Fontugne, D.: "Permeability Measurement in Anisotropic Media." M.S. Thesis, Department of Chemical Engineering and Metallurgy, Syracuse University. (1969).
- Forster, S., Bobertz, B. and Bohling, B.: "Permeability of Sands in the Coastal Areas of the Southern Baltic Sea: Mapping a Grain Size Related Sediment Property." Aquatic Geochemistry, 9, pp. 171-190, (2003).

- Garga, V.K.: "Effect of Sample Size on Consolidation of a Fissured Clay." Canadian Geotechnical Journal, 25, pp. 76-84, (1988).
- Guo, B., Song, S., Chacko, J. and Ghalambor, A.: "Offshore Pipelines." Elsevier Science and Technology, (2005).
- Hadley, G.R., McVey, D.F. and Morin, R." "Thermophysical Properties of Deep Ocean Sediments." Marine Geotechnology, Vol. (5), No. (3-4), pp. 257-295, (1984).
- Hazen, A.: "Discussion: Dams on Sand Foundations." Transactions of the American Society of Civil Engineers 73, 199, (1911).
- Hickox, C.E. and Watts, H.A.: "Steady Thermal Convection from a Concentrated Source in a Porous Medium," Journal of Heat Transfer, Vol. 102, pp. 248-253, (1980).
- Himasekhar, K. and Bau, H.H.: "Thermal Convection around a Heat Source Embedded in a Box Containing a Saturated Porous Medium." Journal of Heat Transfer, Vol. 110, pp. 649-654, (1988).
- Howard, A.: "Pipeline Installation." Lakewood, Colorado, USA. 1st edition, (1996).
- Incropera, F.P., and De Witt, D.P.: "Introduction to Heat Transfer." John Wiley and Sons, New York, 4th edition, (2002).
- Ingham, D.B. and Pop, I., "Natural Convection about a Heated Horizontal Cylinder in a Porous Medium," Journal of Fluid Mechanics, Vol. 184, pp. 157-181, (1987).
- Johansen, O.: "Thermal Conductivity of Soils." PhD Thesis, Trondheim, Norway. (1975).

- Kaviany, M.: "Principles of Heat Transfer in Porous Media." Springer-Verlag, NY, 2nd edition, (1995).
- Kenny, T.C. and Chan, H.T.: "Field Investigation of Permeability Ratio of New Liskeard Varved Clay." Canadian Geotechnical Journal, Vol. (10) No. (473), pp. 473-488, (1973).
- Kersten, M.S.: "Laboratory research for the determination of the thermal properties of soils." Research Laboratory Investigations, Engineering Experiment Station, University of Minnesota, Minneapolis, Minn. Technical Report 23, (1949).
- Kirkham, D.: "Proposed Method for Field Measurement of Permeability of Soil below the Water Table." Soil Science Society of American Proceeding 10, pp. 58-68, (1945).
- Kiyama, T.,Kita, H., Ishijima,Y.,Yanagidani, T., Aoki,K., Sato, T.: "Permeability in Anisotropic Granite under hydrostatic Compression and Triaxial Compression Including Post-Failure Region." Rock Mechanics 2, pp. 1643–1650, (1996).
- Kozeny, J.: "Uber kapillare Leitung desWassers in Boden." Sitzungsberichte der Heidelberger Akademie der Wissenschaften, Mathematisch Naturwissenschaftliche Klasse. Abt 2a (136), pp. 271–306, (1927).
- Krumbein, W.C., Monk, G.D.: "Permeability as a Function of the Size Parameters of Unconsolidated Sand." Technical Publications. American Institute of Mining, Metallurgical, and Petroleum Engineers, 11, (1942).

- Kuehn, T.H. and Goldstein, R.J.: "Correlating Equations for Natural Convection Heat Transfer between Horizontal Circular Cylinders." Int. J. Heat Mass Transfer, Vol. 19, pp. 1127-1134, (1976).
- Lambe, T.W. and Whitman, R.V.: "Soil mechanics." New York, Wiley, (1969).
- Latini, R.G.: "Measurement of Directional Permeabilities." M.S. Thesis, Department of Chemical Engineering and Metallurgy, Syracuse University. (1967).
- Leroueil, S., Bouclin, G., Tavenas, F., Bergeron, L., La Rochelle, P.: "Permeability Anisotropy of Natural Clays as a Function of Strain." Canadian Geotechnical Journal Vol. (27), No. (5), pp. 568–579, (1990).
- Loch, K.: "Flowline Burial: An Economic Alternative to Pipe-in-Pipe." Offshore Technology Conference, Houston, Texas, (2000).
- Mansur, C.I. and Kaufman, R.I.: "Dewatering." Foundation Engineering, McGraw-Hill, New York, (1962).
- Mansur, C.I. and Dietrich, R.S.: "Pumping Tests to Determine permeability Ratio." ASCE Journal of the Soil Mechanics and Foundation Division, 91 (SM4), pp. 151-183, (1965).
- Matsuda, J.I. and Von Herzen, R.P.: "Thermal Conductivity Variation in a Deep-sea Sediment core and its Relation to $H_2O$ and Si Content" Deep-Sea Research, Vol. (33), No. (2), pp. 165-175, (1985).
- Maxwell, J.B.: "Data Book on Hydrocarbons." D. Van Nostrand Company Inc., $8^{th}$ edition, (1965).

- Millham, N.P. and Howes, B.L.: "A Comparison of Methods to Determine K in a Shallow Coastal Aquifer." Ground Water, Vol. (33), No. (1), pp. 49-57, (1995).
- Mitchell, J.K.: "Fundamentals of Soil Behaviour." John Wiley and Sons Inc., N.Y, (1993).
- Morgan, V.T.: "Heat Transfer by Natural Convection from a Horizontal Isothermal Circular Cylinder in Air". Heat Transfer Engineering. Vol. (18), No. (1), pp. 25-33, (1997).
- Muralidhar, K., Baunchalk, R.A., and Kulacki, F.A.: "Natural Convection in a Horizontal Porous Annulus with a Step Distribution in Permeability." Journal of Heat Transfer, Vol. 108, pp. 889-893, (1986).
- Muskat, M.: "Physical Principles of Oil Production." McGraw-Hill, New York, (1949).
- Newson, T.A., Brunning, P. and Stewart, G.: "Thermal Conductivity of Consolidated Offshore Clayey Backfill." Proceedings of OMAE's 21st international conference on Offshore Mechanics and Arctic Engineering, (2002).
- Ngo, C.C. and Lai, F.C.: "Effects of Backfill on Heat Transfer from a Buried Pipe." Journal Heat Transfer 127 pp. 780–784, (2005).
- Ngo, C.C.: "Buoyancy Induced Heat and Mass Transport in a porous Medium near a Buried Pipe." PhD thesis, University of Okalahoma, (2006).
- Ngo, C.C. and Lai, F.C.: "Heat Transfer Analysis of Soil Heating System." International Journal of Heat and Mass Transfer, Vol. 52, pp. 6021-6027, (2009).

- Nield, D. A. and Bejan, A.: "Convection in Porous Media." Springer- Verlag, New York, 2nd edition, (1999).
- Nielsen, D.R., Van Genuchten, M.Th. and Biggar, J.W.: "Water Flow and Solute Transport Processes in the Unsaturated Zone." Water Resources Research, Vol. (22), No. (9), pp. 89S-108S, (1986).
- Olsen, H. W.: "Hydraulic Flow through Saturated Clays." Proceedings of the 9th National Conference on Clay and Clay Minerals, pp. 131-161, (1962).
- Oosthuizen, P.H. and Naylor, D.: "Natural Convective Heat Transfer from a Cylinder in an Enclosure Partly Filled with a Porous Medium." International Journal of Numerical Methods for Heat and Fluid Flow, Vol. 6, pp. 51-63, (1996).
- Poulos, H.G.: "Marine Geotechnics." Unwin Hyman Ltd, London, (1988).
- Pop, I., Ingham, D.B. and Cheng, P.: "Transient Free Convection about a Horizontal Circular Cylinder in a Porous Medium." Fluid Dynamics Research, Vol. 12, pp. 295-305, (1993).
- Pop, I., Ingham, D.B. and Bradean, R.: "Transient Free Convection about a Horizontal Circular Cylinder in a Porous Medium with Constant Surface Flux Heating." Acta Mechanica, Vol. 119, pp. 79-91, (1996).
- Quenelle, A. and Gunaltun, M.: "Comparisons between Thermal Insulation Coatings for Underwater Pipelines." Offshore Technology Conference, (1987).
- Ratcliffe, E.H.: "The Thermal Conductivity of Ocean Sediments." Journal of Geophysical Research, Vol. (65), No. (5), pp. 1535-1541, (1960).

- Scheidegger, A.E.: "The Physics of Flow through Porous Media." University of Toronto Press, (1974).
- Schlichting, H.: "Boundary Layer Theory." McGraw Hill, New York, 4th edition, (1960).
- Schock, S.G.: "A Method for Estimating the Physical and Acoustic Properties of the Sea Bed using Chirp Sonar Data." Journal of Oceanic Engineering, Vol. (29), No. (4), pp. 1200-1217, (2004).
- Scholes, O.N., Clayton, S.A., Hoadley, A. F. A.: "Permeability Anisotropy due to Consolidation of Compressible Porous Media." Transportation in Porous Medium (2007) 68, pp. 365-387, (2006).
- Selim, H. M.: "Water Seepage through Multi-layered Anisotropic Hillside." Soil Science Society of American Journal 51, pp. 9-16, (1987).
- Sharkawy, M.H., Lienhard, J.H. and Zubair, S.M.: "Thermophysical Properties of Seawater: A Review of Existing Correlations and Data." Desalination and Water Treatment, (2010).
- Slattery, J. C.: "Flow of Viscoelastic Fluids through Porous Media," American Inistute of Chemical Engineers Journal, Vol. 13, No. 6, pp. 1066–1071, (1967).
- Tavenas, F., Jean, P., Leblond, P. and Leroueil, S.: "The Permeability of Natural Soft Clays. Part 2: Permeability Characteristics." Canadian Geotechnical Journal. 20, pp. 645-660, (1983).
- Terzaghi, K., Peck, R.B.: "Soil Mechanics in Engineering Practice." 2nd edition. John Wiley and Sons Inc.,New York, (1967).

- Whitaker, S.: "Diffusion and dispersion in porous media," American Inistute of Chemical Engineers Journal, Vol. 13, No. 3, pp. 420–427, (1967).
- White, F.M.: "Fluid Mechanics." Mc-Graw Hill Inc., (1986).
- Willson, A.M., Huettel, M. and Klein, S.: "Grain Size and Depositional Environment as Predictors of Permeability in Coastal Marine Sands." Coastal and Shelf Science, 80, pp. 193-199, (2008).
- Witt, K.J., Brauns, J.: "Permeability Anisotropy due to Particle Shape." Journal of Geotechnical Engineering, Vol. (109), No. (9), pp. 1181–1187, (1983).
- Wong, R.C.K.: "A Model for Strain-induced Permeability Anisotropy in Deformable Granular Media." Canadian Geotechnical Journal, Vol. (40), No. (1), pp. 95–106, (2003b).
- Vafai, K.: "Handbook of Porous Media." 2nd edition, Taylor & Francis, Boca Raton, Fla, USA, (2005).
- Zaslavsky, D. and Rogwski, A.S.: "Hydrologic and Morphologic Implications of Anisotropy and Infiltration in Soil Profile Development." Soil Science Society of American Proceedings, 33, pp. 594-599, (1969).
- Znidarcic, D. and Aiban S.A.: "Discussion to: Some Measurements of the Permeability of Kaolin by Al-Tabaa and Wood." Geotechnique, 38, pp. 453-454, (1988).